**Ana Isabel Araújo Manuel Machado de Sousa**

Licenciatura em Ciências da Engenharia Biomédica

# Chitosan-based drug delivery systems – optimization and modelling

Dissertação para obtenção do Grau de Mestre em

Engenharia Biomédica

Orientador: Prof. Doutor João Paulo Borges, Professor Auxiliar, DCM – FCT/UNL

Co-orientador: Mestre Paula Soares, DCM-FCT/UNL

Júri:

Presidente: Prof. Doutora Carla Maria Quintão Pereira

Arguente: Doutora Teresa Maria Alves Casimiro Ribeiro

Orientador: Prof. Doutor João Paulo Miranda Ribeiro Borges

FACULDADE DE CIÊNCIAS E TECNOLOGIA
UNIVERSIDADE NOVA DE LISBOA

**Julho, 2015**

**Ana Isabel Araújo Manuel Machado de Sousa**

Licenciatura em Ciências da Engenharia Biomédica

# Chitosan-based drug delivery systems – optimization and modelling

Dissertação para a obtenção do Grau de Mestre

em Engenharia Biomédica

Orientador: Prof. Doutor João Paulo Borges, Professor Auxiliar, DCM-FCT/UNL

Co-orientador: Mestre Paula Soares, DCM-FCT/UNL

Composição do júri:

Presidente: Prof. Doutora Carla Maria Quintão Pereira

Arguente: Doutora Teresa Maria Alves Casimiro Ribeiro

Orientador: Prof. Doutor João Paulo Miranda Ribeiro Borges

Faculdade de Ciências e Tecnologia da Universidade Nova de Lisboa

Departamento de Física

**Julho, 2015**

**Chitosan-based drug delivery systems – optimization and modelling**

# Agradecimentos

Agradeço desde já a Deus, que mesmo nos momentos mais críticos e em que me senti com pouca fé, me mostrou a sua presença na minha vida das mais variadas formas.

Este trabalho não poderia ter sido desenvolvido sem a ajuda e o apoio de várias pessoas que me acompanharam neste processo e fizeram parte do meu percurso nestes últimos anos. Não posso deixar de agradecer a todos eles, que de uma maneira ou de outra me fizeram caminhar na direção certa.

Ao professor João Paulo Borges, por ter aceite orientar a minha tese, por todas as ideias e sugestões que me foi dando ao longo do trabalho, que me ajudaram a melhor estruturar esta investigação, e ainda pela disponibilidade demonstrada para resolver algumas situações burocráticas que foram surgindo.

À Paula Soares, por tudo! Pela enorme disponibilidade, por tudo o que me ensinaste, por sempre me apoiares e me impedires de desistir, mesmo quando tudo parecia correr mal. Agradeço-te ainda a companhia, a boa disposição e o optimismo que sempre me transmitiste. Obrigada, do fundo do meu coração! Foste, sem dúvida, a melhor co-orientadora que poderia ter!

Agradeço ainda ao professor Jorge Silva, por ter disponibilizado o seu laboratório de células para poder desenvolver os ensaios de citotoxicidade, necessários para que este trabalho fosse concluído, e pela paciência connosco, principalmente em detectar as fontes das contaminações.

À minha colega, parceira e, acima de tudo, amiga Diana, um muito obrigado! Foste essencial ao longo desta tese, com o teu companheirismo e boa disposição. A minha companhia nas maratonas no laboratório, nas sessões do espectrofotómetro, quando tínhamos infinita loiça para lavar, no desespero da escrita ou nos nossos telefonemas intermináveis com dúvidas e risos. Foi muito bom partilhar esta fase contigo; foste uma boa descoberta na minha vida!

Às minhas amigas do laboratório, Diana, Inês, Mariana e Tânia, que proporcionaram o melhor ambiente que poderia ter para trabalhar, com as partilhas de músicas e vídeos malucos, pelas risadas, pelos almoços, pela companhia e pelo apoio, obrigada!

Agradeço ao restante pessoal do laboratório de Polímeros, em particular à Augusta, pelas suas conversas, à Susete, por tudo o que me ensinou, e à Coro, pela sua animação e boa disposição, animando sempre qualquer sala (ah e pelas boleias também..)!

À Luísa, que para além de todos os momentos ao longo do curso e da tese, ainda partilhou comigo os melhores 5 anos da minha vida, quando fizemos Erasmus em Pisa. Ficaste para sempre no meu coração, és uma grande amiga! Obrigada por tudo!

Aos centípedes – Luísa, Inês, Andreia, Joana, Alex, João, Rui, Bruno, Edgar e Manel – obrigada por estes anos de curso. A vossa companhia e amizade foi essencial nesta caminhada! Agradeço em particular à Joana, ao Rui e ao João, que, cada um à sua maneira, estiveram bem presentes nesta etapa da tese e me deram todo o apoio que podia precisar.

Ao Ricardo, o meu padrinho académico, que sempre esteve presente e até a viver em Inglaterra me ajuda nos meus deveres académicos. Nunca falhas padrinho!

À Su e à Grega, por serem desde há muitos anos um apoio muito grande na minha vida e por acreditarem sempre nas minhas capacidades.

Aos amigos Pisanos, particularmente Carolina, Nuno e João, pelo vosso apoio e animação constantes.

Ao pessoal dos Olivais que me ajudaram a caminhar sempre na melhor direção e sempre me apoiaram em todos os momentos da minha vida. Um especial agradecimento à Maria Campos, ao Davide Raposo, à Sofia Cavaco e ao Ricardo Gomes. Vocês são especiais e realmente importantes; obrigada por me aturarem!

À Rita, que me conhece desde a infância e mesmo distante esteve sempre comigo em todos os momentos, e me ajudou a desanuviar da tese com os nossos cafés e saídas para dançar!

Finalmente, e não menos importantes, agradeço a todos os da minha família, que sempre me apoiaram e me ajudaram a ter forças para ultrapassar todos os obstáculos que o curso e a tese me foram trazendo. À minha mãe, agradeço toda a paciência e todos os conselhos que me deu, principalmente ao longo desta tese; ao meu pai, por me aturar e ir constantemente perguntando qual o estado do trabalho, sempre te interessaste pelo meu percurso académico. Obrigada pais, por me ajudarem a tornar os meus sonhos possíveis. Ao meu irmão, que sempre foi um exemplo para mim e me foi dando o apoio e a ajuda que eu precisava. À Leonor, que me acompanha desde que entrei para a faculdade. Aos meus avós e aos meus tios, por toda a preocupação e carinho e por me receberem sempre tão bem nas suas casas, quando vou de visita. E por fim aos meus priminhos, Leonardo e Inês, que, com a inocência própria de uma criança, sempre me deram alegria e me encheram o coração!

# Abstract

The increase of cancer incidence on the last decades and the non-existence of totally efficient therapies, leads to an urgent need to develop new cures or enhance the therapies already in use. Chemotherapy has been one of the most used therapies for cancer disease, and although it is very efficient in destroying malignant cells, it also comes with many disadvantages for the patients, especially due to its lack of specificity to tumour cells. In this work, all studies were made using doxorubicin (DOX), a drug commonly used in chemotherapy that apart from destroying cancer cells, also lead to future cardiotoxicity problems to the patients. A targeted drug delivery system was studied in this work, using two biopolymers, chitosan and one of its derivatives, *o*-HTCC, taking advantage of their pH-sensitivity.

Doxorubicin was encapsulated in both chitosan and *o*-HTCC nanoparticles and also in superparamagnetic iron oxide nanoparticles (SPION's) coated with both chitosan and *o*-HTCC. DOX release experiments were performed for different pH mediums, representing different *in-vivo* situations: bloodstream (7.4), tumour cells environment (6.5) and endosomal/lysosomal compartments (4.5). It was verified that an initial burst effect occurs, especially in more acidic medium, and a controlled release was then achieved. A higher drug release was observed in pH 4.5 in all nanocarriers in study. Mathematical models were applied to the data, finding that Weibull and Korsmeyer-Peppas models are the best fit in describing DOX release mechanism. It was concluded that DOX release happened through a complex and anomalous mechanism for almost all the samples, probably due to the swelling behaviour of the polymers.

A study of the influence of polymer molecular weight was also performed and it was concluded that this parameter only has influence in nanoparticles' size.

This work indicates that these nanocarriers can be further developed for targeted drug delivery systems, especially with doxorubicin.

***Keywords:*** chitosan nanoparticles; coated superparamagnetic iron oxide nanoparticles; doxorubicin; drug release; mathematical modelling; *o*-HTCC nanoparticles; targeted drug delivery.

# Resumo

Com o aumento da incidência de cancro nas últimas décadas e com a falta de terapias totalmente eficientes para este tipo de doença, é urgente desenvolver novas curas ou melhorar as terapias já utilizadas. A quimioterapia é uma das terapias mais usadas para o tratamento de cancro e, apesar de ser muito eficiente na destruição das células malignas, tem enormes desvantagens para os pacientes, especialmente devido à sua pouca especificidade para as células tumorais. Neste trabalho, todos os estudos foram efectuados utilizando a doxorrubicina (DOX), um fármaco frequentemente usado nos tratamentos de quimioterapia que, apesar de matar as células cancerígenas, leva ainda a problemas cardíacos para o paciente, no futuro. Nesta dissertação, foi estudado um sistema de libertação localizada de fármaco, utilizando dois biopolímeros, o quitosano e um dos seus derivados, *o*-HTCC, tirando partido da sua sensibilidade ao pH.

A doxorrubicina foi encapsulada em nanopartículas tanto de quitosano como de *o*-HTCC e ainda em nanopartículas superparamagnéticas de magnetite (SPION's) revestidas com ambos os polímeros. Os ensaios de libertação do fármaco foram realizados em meios com diferentes pH, representando várias situações *in-vivo*: corrente sanguínea (7,4), meio envolvente das células tumorais (pH 6,5) e os compartimentos endossomais/lisossomais (4,5). Verificou-se uma libertação inicial muito acentuada, principalmente no caso do pH mais ácido, e depois foi atingida uma libertação mais controlada. Foi ainda verificado que a maior percentagem de libertação ocorre para o pH de 4,5 para todos os nano-transportadores em estudo. Os modelos matemáticos foram aplicados a estes dados e os que melhor descrevem este tipo de mecanismo de libertação são os de Korsmeyer-Peppas e de Weibull. Concluiu-se que a libertação ocorre por mecanismo complexo e anómalo para a maioria das amostras, provavelmente devido ao inchamento dos polímeros. Foi ainda efectuado um estudo da influência do peso molecular dos polímeros e concluiu-se que influencia apenas o tamanho das nanopartículas.

Este trabalho demonstra então que estes nano-transportadores podem ser desenvolvidos para sistemas de entrega localizada de fármaco, particularmente para a doxorrubicina.

***Palavras-chave:*** doxorrubicina; libertação localizada de fármaco; modelação matemática; nanopartículas de *o*-HTCC; nanopartículas de quitosano; nanopartículas superparamagnéticas de magnetite com revestimento.

# Table of Contents

# List of Tables

# List of Figures

# Abbreviations and acronyms

Cs – Chitosan

Cs NP's – chitosan nanoparticles

Cs SPION's – Chitosan coated superparamagnetic iron oxide nanoparticles

DA – Deacetylation degree

DOX - Doxorubicin

EE – Encapsulation efficiency

EPR effect – Enhanced permeability and retention effect

HCl - hydrochloric acid

Mw – Molecular weight

*o*-HTCC - *o*-(2-hydroxyl) propyl-3-trimethyl ammonium chitosan chloride

*o*-HTCC NP's – *o*-HTCC nanoparticles

*o*-HTCC SPION's - *o*-(2-hydroxyl) propyl-3-trimethyl ammonium chitosan chloride coated superparamagnetic iron oxide nanoparticles

PBS – Phosphate buffer saline

SPION's – Superparamagnetic iron oxide nanoparticles

TPP – Sodium Tripolyphosphate

TREG – Triethylene glycol

# 1 Introduction

According to the World Health Organization (WHO) cancer incidence has been increasing in the last years and it is expected to more than duplicate until 2030 [1]. Current therapies are not completely efficient, having different outcomes and causing side effects to patients. It is not yet available any standard and ideal treatment. For example chemotherapy successfully destroys cancer cells, but also tend to affect other body parts, the healthy ones, increasing the toxicity of this therapy [1]. In this way, it's very important to find other methods that will reduce chemotherapy toxicity and increase the specificity of this treatment to tumour cells.

Through all drugs that are being used in chemotherapy today, this study was based on Doxorubicin (DOX) (Figure 1.1), one of the most used anticancer drugs in chemotherapy. This drug is used in a range of tumour such as acute leukaemia, osteogenic sarcomas, lymphomas and solid tumours, such as breast and lung cancer, and it belongs to the anthracycline family [2].

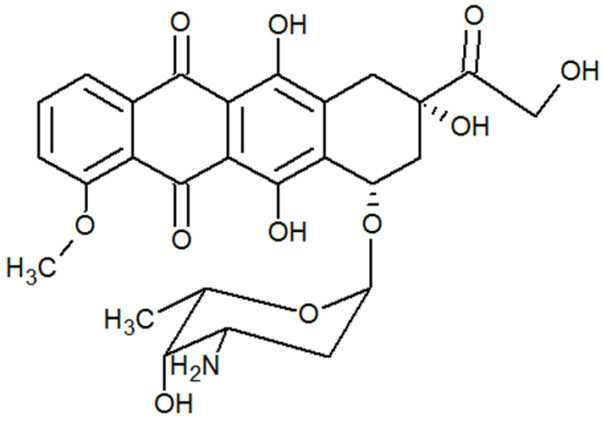


**Figure 1.1 - Chemical structure of doxorubicin.**

DOX affects the DNA double helix, interfering with the synthesis of nucleic acid. Therefore, DOX is more effective when the cells are on S phase, also interfering through enzyme inhibition. Even with all its effectiveness and benefits, DOX develops multidrug resistance and cardiotoxicity for the patient when it's administered in the traditional way [2]. It is not fully understood the mechanism that leads to this cardiac toxicity but the truth is that 5-23% of patients develop anthracycline-induced secondary cardiotoxicity [3]. This drug also has a slow terminal clearance, being metabolised by the liver and only about 40% of doxorubicin are excreted. Consequently only a reduced quantity of DOX really reaches the tumour area [2].

In order to achieve a controlled release of DOX and therefore avoid its cardiotoxicity, this drug has been microencapsulated in several systems, such as Doxil ® and Caelyx® [3]. However, this kind of particles (within the micron range of diameter) is only viable to accessible

tumours, because its increased size does not enable the circulation in the bloodstream. Therefore, smaller systems have been investigated on the last years to overcome those problems and become reachable to the tumour area [4].

Different pH are detectable in our body and it is possible to take great advantage of this fact to design smart passive targeted systems. Blood has a neutral pH (nearly 7.4) whereas tumour microenvironment presents an acidic pH (approximately 6.5) due to the lactic acid as a result of anaerobic glucose metabolism of cancer cells. Additionally, some organelles, such as endosomes or lysosomes, can achieve lower pH values, between 3.5 and 5.5 [5, 6]. Thus, a drug delivery system that exploits these differences and that has pH-sensitivity is of interest as a drug carrier for oncology treatments.

Nanotechnology and nanomedicine are helping the development of successful targeted transporting systems, which deliver the chemical drug directly to the region of the tumour. Using nanoparticles as a drug delivery system is very advantageous as they can circulate in the bloodstream for longer time, are able to accumulate in the tumour area and allow a controlled release of the drug. These advantages and properties result essentially from their nano-size, which allow these nanoparticles to leave the bloodstream and to pass through tumour microvasculature [7].

Although there is no clear line dividing these categories, targeted drug delivery can be grouped into active and passive targeting. Active targeting requires the use of some targeting molecule specific for cancer cells, such as ligands or antibodies. On the other hand, passive targeting takes advantage of tumour's microenvironment, involving the use of carriers that take benefit of physiological and natural properties of cancer tissues [7, 8]. This passive targeting usually exploit the enhanced permeability and retention (EPR) effect as a mechanism for localization and accumulation of the nanocarrier at the tumour area, due to an inefficient lymphatic drainage [7, 9]. It is the nanoparticles size that allows this passive behaviour, as they can pass through tumour vasculature. In order to accumulate in the tumour area, nanoparticles must have their size between 100 and 200 nm [7, 8].

Several nanoparticles are being studied and used as targeted drug delivery systems [10], such as liposomes [11], nanospheres [12, 13], magnetic nanoparticles [9, 14, 15], polymeric micelles [16] or aquasomes [17, 18]. Nanoparticles can either be composed of natural materials, as lipids, biopolymers or proteins, or synthetic, such as gold, silver or magnetite. Each of these nanoparticles differs in their properties, stability, drug release rates and targeted delivery ability. It is important that the chosen system suits the drug and its therapeutic proposes [2].

Chitosan is a biopolymer widely used in drug delivery systems because of its biocompatibility, biodegradability, low toxicity, among others [19]. In this dissertation, the main system for targeted drug delivery in study is composed of chitosan nanoparticles. This is a passive tar-

geting system because drug release is conditioned by the different physiological properties of chitosan, such as pH or temperature.

## 1.1 Aim and Objectives

The main purpose of this thesis is to study DOX controlled release profile from chitosan nanoparticles in different pH at physiological temperature (37ºC) and modelling this release through the application of mathematical models used to describe these types of mechanisms. Finding the models that best describe the experimental data allow the understanding of what happens on the DOX-nanoparticles system that allows DOX release. Another objective is to do the same study but using a chitosan derivative, *o*-(2-hydroxyl) propyl-3-trimethyl ammonium chitosan chloride (*o*-HTCC), which has different solubility characteristics, allowing a comparison between these two nanocarriers. An additional purpose is to study and model DOX release from coated superparamagnetic iron oxide nanoparticles, with either chitosan or *o*-HTCC. Figure 1.2 has a representative scheme of the systems in study in this work: (a) polymeric nanoparticles with doxorubicin and (b) polymer coating superparamagnetic iron oxide nanoparticles with doxorubicin.

Apart from these main goals, this thesis also has some partial objectives:

- Study the influence of polymer molecular weight, chitosan or *o*-HTCC, in these nanocarriers systems, in terms of nanoparticle dimension and DOX encapsulation and release.
- Analysis of chitosan, *o*-HTCC and coated superparamagnetic nanoparticles cytotoxicity.

It is important to refer that this thesis is a continuation of some other thesis still in development, and some materials used here were prepared in that work. For example, chitosan with different molecular weights and chitosan derivative, *o*-HTCC, were produced in this other work.

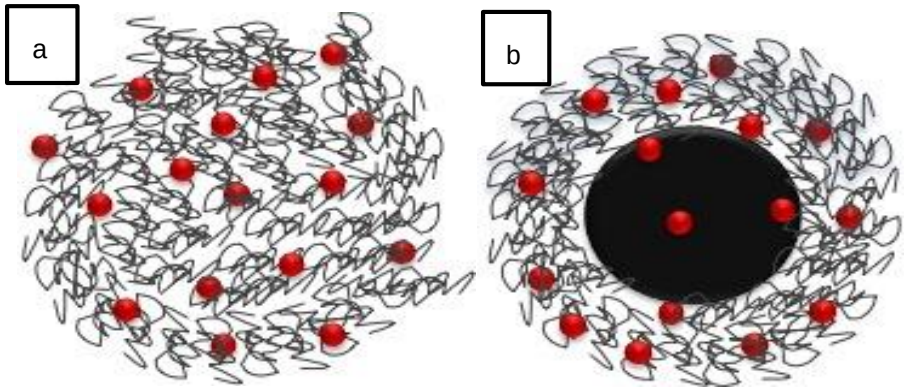


**Figure 1.2 - Schematic representation of (a) DOX (red) loaded chitosan/o-HTCC nanoparticles and (b) DOX loaded chitosan/o-HTCC coated SPION's.**

This manuscript is structured in eight different chapters. Chapter 1 is the introduction, where a contextualization of this work is given. Chapters 2, 3 and 4 are theoretical ones, giving some notions of the main subjects of this thesis, taking literature references into account. In this way, in chapter 2, chitosan nanoparticles are presented, given some focus to its structure and properties as a biomaterial, preparation methods, applications and state of the art as a nanocarrier for doxorubicin. It is also in this chapter that is presented the chitosan derivative, *o*-HTCC, and its properties. Chapter 3 covers the superparamagnetic iron oxide nanoparticles, their structure and properties and production methods. Finally, in chapter 4 are explained the existing mathematical models for drug delivery systems, with a separation from mechanistic realistic and empirical/semi-empirical theories. Materials and methods used in this thesis are described in chapter 5. Chapter 6 presents and discusses all the obtained results, including the comparison between the different nanocarriers studied. Conclusions and perspectives on future developments are presented in chapter 7. And finally, chapter 8 contains all literature references that support this research.

# 2 Chitosan Nanoparticles

## 2.1 Structure and properties of chitosan

Chitosan (Figure 2.1) is a cationic polysaccharide, being the second most abundant polymer present in nature [20]. It results from the deacetylation of chitin present in crustaceans shells [21]. The main difference between chitosan and chitin is the deacetylation degree: chitosan occurs when the deacetylation degree (DA) is more than 50% [22]. This polymer is used for a diversity of biomedical applications due to its biocompatibility, low toxicity, good biodegradability [19], high hydrophilicity, high mechanical strength [23], cost-effectiveness [24] and polyelectrolyte property [25]. Chitosan is also able to reside for prolonged time in the gastrointestinal tract and increases cellular permeability, amplifying absorption, gaining potential as a composition of oral drug forms [21]. Chitosan can have different molecular weights depending on the conditions of its harvesting [2].

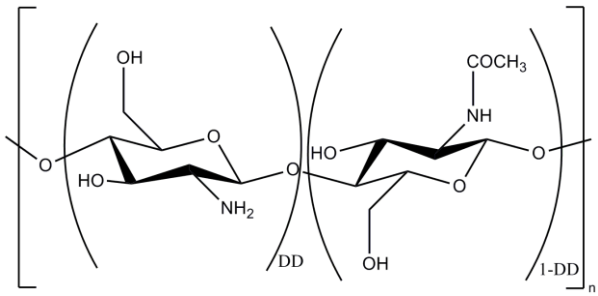


**Figure 2.1 - Chitosan chemical structure.**

This biopolymer presents strong intra- and intermolecular hydrogen bonds, showing low solubility and reactivity in aqueous medium. Chitosan is insoluble at neutral and alkaline pH [21] and shows almost neutral charge [19], but it assumes a positive charge and becomes soluble at acidic pH [21]. This pH-sensitivity happens due to a large quantity of amino groups on chitosan chains. As a consequence of these solubility issues and its pH sensitive behaviour, chitosan nanoparticles present a swelling behaviour [5].

## 2.2 Preparation of chitosan nanoparticles

To prepare chitosan nanoparticles there are some used techniques such as ionic gelation, reverse micelle formation, precipitation self-assembly and spray drying [7].

Ionic gelation method presumes the use of polyanions such as sodium tripolyphosphate (TPP), which crosslinks with chitosan through electrostatic interactions [25]. Tripolyphosphate is mostly used because of its non-toxicity and quick gelling property [26]. TPP is an anion with three phosphate groups with negative charge ($P_3O_{10}^{5-}$) that interacts with the positively charged

ammonium groups ($NH_3^+$) of chitosan when dissolved in acetic acid, which allows the crosslinking of the absorbed chitosan molecules to each other, forming spherical particles [25, 27]. A scheme of this interaction is shown in Figure 2.2. Chitosan nanoparticles formation through this method is dependent of the ratio between TPP and chitosan. Rampino *et al*. [28] verified that increasing the quantity of TPP also increase the amount of chitosan nanoparticles and that for high quantity of available TPP, nanoparticles suspension becomes more turbid, with the disadvantage of forming larger nanoparticles and aggregates.

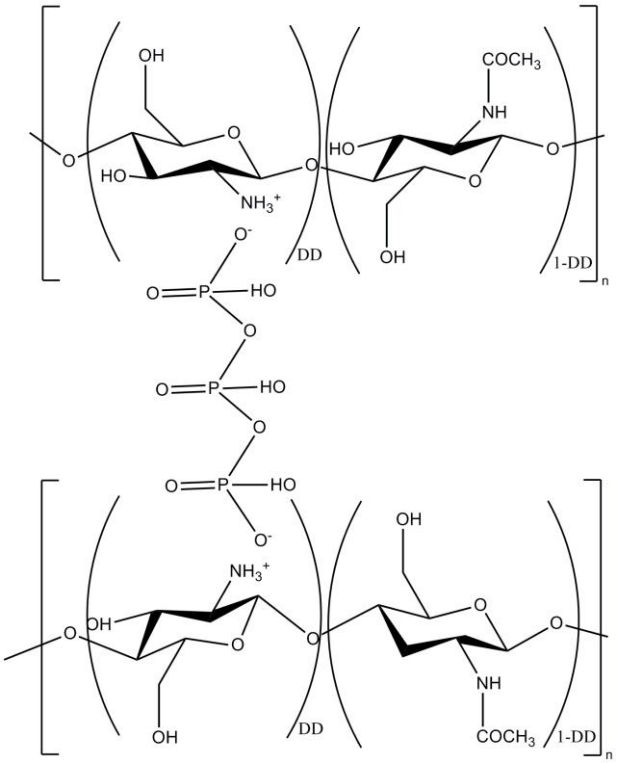


**Figure 2.2 – Scheme of chitosan and TPP molecules interaction.**

This is a simple method, which allows the production of chitosan nanoparticles without using high temperatures or organic solvents [28]. Other advantage is that this method does not need auxiliary molecules, such as catalysts, which is a benefit for biomedical and pharmaceutical applications. Moreover, chitosan nanoparticles prepared by ionic crosslinking usually show pH-sensitive swelling, a main reason for their usage in drug delivery applications [29].

## 2.3 Applications of chitosan and chitosan nanoparticles

Additionally to chitosan huge potential as a biomaterial, this biopolymer is also getting attention not only in biomedicine and nanotechnology, but also in textiles, industry, food or ecology [21].

One of chitosan applications in biomedicine is in medical imaging. To be used as an image contrast agent it should incorporate some inorganic material, such as metals, becoming a composite with better characteristics for this purpose. For example, magnetite ($Fe_3O_4$) coated with chitosan is being studied to be used in Magnetic Resonance Imaging (MRI) and was proven to work as a contrast imaging agent in this technique [21].

Chitosan has also been studied as an organic coating to magnetic nanoparticles as it decreases aggregation and offers more stability to the nanoparticles, increases targeting and biocompatibility and decreases chemotherapy side effects [24, 30, 31].

As a drug delivery system, chitosan has been studied for gene delivery, implants and nasal, oral, parenteral and transdermal administration [22]. For example, Quan Gan *et al.* [26] studied chitosan nanoparticles as carriers for BSA protein, analysing all preparation conditions of chitosan nanoparticles such as chitosan molecular weight or concentration of each component of the system. They verified that the best encapsulation efficiency occurred for higher molecular weight of chitosan and protein concentration and lower chitosan/TPP ratio and chitosan concentration. Also Aydin and his research group [5] studied chitosan nanoparticles as a localized delivery system to tumour cells for 5-fluorouracil. In this case was taken advantage of chitosan pH sensitivity, concluding that for acidic pH there was higher release ratio. It also showed a controlled release profile for this drug.

### 2.4 Chitosan swelling behaviour

Drug release from chitosan nanoparticles is dependent on the swelling behaviour of chitosan and drug-carrier interactions, which are influenced by pH of the medium [32]. One of the characteristics of the tumour region is its acidic medium (pH around 6.5), due to a high anaerobic glucose metabolism in tumour cells. Also inside cells, in intracellular organelles, as liposomes or endosomes, pH is even lower, between 3.0-5.5, regions where drug release will continue to happen. Doxorubicin release behaviour has shown to be better on acidic pH due to its higher solubility and to chitosan degradation in this type of medium [31]. Chitosan structure suffers changes with variation of pH because of the reversible bonds of ionically crosslinked chitosan, which makes it able to be modified by external conditions after administration. Swelling behaviour of chitosan is influenced by its crosslinking density, which is defined at its formation. Thus, increasing the crosslinking density also increases the charge density of the crosslinker, leading to a decrease in swelling and pH-sensitivity, improving the stability of the structure of chitosan [29].

Other parameters that influence chitosan swelling behaviour are its ion-sensitivity and its molecular weight. In presence of ions, the ionic interactions of chitosan network get weaker through a shielding effect that increases the swelling of chitosan. The molecular weight of chitosan is also a factor because when it decreases, the swelling also decreases [29].

## 2.5 Drug release from chitosan nanoparticles

There are three different mechanisms of drug release from nanoparticles: release from the surface of nanoparticles, diffusion from the swollen nanoparticle and release due to polymer erosion. Most of the times, drug release involves more than one of these mechanisms, and they usually occur sequentially [26, 27].

Releasing the drug from the surface of the particles happens when the drug immediately dissolves when in contact with the release medium. This kind of mechanism leads to burst effect in the early stages of dissolution.

Drug diffusion from the swollen nanoparticle is divided in three steps. The first step is the swelling of the polymer matrix due to water penetration into the system. Secondly chitosan changes from a glassy polymer into a rubbery matrix. And finally the drug diffuses from the swollen rubbery matrix of chitosan. Through this mechanism the release is slow at the beginning and later increases its velocity. Usually happens more in chitosan hydrogels [27]. Consequently there are two moving boundaries in swelling controlled release systems; one is the swollen rubbery portion, which is more mobile, and the second one is the glassy one that happens to be less mobile. The moving region where this process occurs and that separate these last two portions of the polymer is called *swelling front*. The polymer structure can have dissolved and non-dissolved drug at the same time. The separation of the region of the swollen matrix that has only dissolved drug and the region with the two of them is called *diffusion front*; this front is also moving during the process [27, 33].

### 2.5.1 DOX release profile from chitosan nanoparticles – *state of the art*

Studies of doxorubicin release profile from chitosan nanoparticles and some of its derivatives have already been made. In all of them release profile is studied by putting the drug delivery system in a dialysis bag and measuring the drug release into a medium that represents a biological environment, and varying its pH. In this sub chapter some of the most recent studies involving DOX release from a nanocarrier composed of chitosan are presented.

Kevin Janes *et al.* [4] have studied the release profile of doxorubicin from chitosan-TPP nanoparticles in acetate buffer, with pH 4. Their results showed a burst release of 4.5% after 2h, which was maintained more or less stable through the next 5 days. This result was explained by the interactions between DOX and chitosan that bind the drug to the polymer, in a very stable way. DOX and chitosan show overwhelming charge repulsion between them, but even then small quantities of DOX are able to complex with chitosan. This fact may be explained by the amphoteric property of this drug and also due to the hydrophobic/hydrophilic interactions and resonance effects. In this way, they concluded that any amount of drug release is caused by the

degradation of chitosan or by the release of DOX bonded to chitosan surface. *In vitro* studies have showed that chitosan nanoparticles enter the cells through endocytosis and are degraded intracellularly, causing DOX release.

Yuan *et al.* [32] have studied chitosan clay and chitosan-aluminosilicate clay nanocomposite as drug carriers. DOX release was studied at 37 ºC for pH 1.2, 5.3 and 7.4. In this study, pH 1.2 represents the gastric fluid; although the nanocarrier do not need to stay long time in this really acidic pH in an *in vivo* system, as DOX has a low transition time. Control experiments were made by submitting free DOX (drug solution only) to the same temperature and pH conditions. Testing free DOX release in acidic medium is important because in this pH this drug can behave similarly to chitosan. In these controls DOX was completely released in 1h, 5h or 12h from pH 1.2, 5.3 and 7.4, respectively. When loaded to the nanocarrier, DOX release was slower, never releasing 100% of its quantity. These results confirm that DOX release is more controlled when it is associated to a nanocarrier.

There are also some studies of DOX release profile from chitosan coated superparamagnetic iron oxide nanoparticles (Cs SPION's) that present similar behaviours compared to release from chitosan nanoparticles. In this way, Javid *et al.* [24] studied DOX release profiles from Cs SPION's for a period of 48h. Different mediums with pH between 1.5 and 7.0 were tested and it was observed that highest pH lead to a lower quantity of drug released. This was a desired situation, as there is no interest on releasing the drug before the nanocarrier arrives to the tumour area. Maximization of DOX release was verified for pH between 4.5 and 6.5, corresponding to internalization and endocytosis of drug loaded SPIONs in tumour cells. In a more recent research, Unsoy *et al.* [31] studied DOX release from Cs SPION's with different sizes. Release profiles were studied in buffers with different pH (4.2 and 5.0) at 37 ºC for a maximum period of 30h, to simulate endosomal environment. A burst release in the first 30 min was observed followed by a slower release rate after 7h of the beginning of the experiment. The difference in release profiles from different sizes of the nanoparticles was only 10%, where the smaller ones released more quantity of drug. Higher DOX release was observed in the most acidic medium (4.2). On chitosan coated SPION's (CS SPION's) loaded with DOX there are more crosslinking sites on chitosan structure than on CS SPION's without DOX, which leads to a lower swelling on the first ones [31].

When analysing DOX release profiles it is also important to study its encapsulation efficiency in the nanoparticles, in order to truly understand the meaning of the quantity of drug released measured. Usually, encapsulation efficiency is indirectly determined through the measurement of drug concentration in the supernatant after centrifugation of DOX loaded Cs nanoparticles [4, 5, 34]. For Cs-TPP nanoparticles, Kevin Janes *et al.* [4] obtained a DOX encapsulation efficiency around 9%. Higher entrapment efficiency, around 60%, was obtained by Mitra *et al.* [34] as they conjugated dextran with doxorubicin when producing DOX loaded Cs nanoparti-

cles. For chitosan coated magnetic nanoparticles Unsoy *et al.* [31] achieved 99% of DOX loading efficiency to 150 μg/ml and 81% to 600 μg/ml, difference justified by DOX saturation.

### 2.6 Chitosan derivative: *o*-HTCC

As chitosan is insoluble in biological pH (greater than 6.5), some researchers have synthesized chitosan derivatives that are soluble in a larger pH range [35]. Without the solubility problem, chitosan may have an increased efficiency as an absorption enhancer and become more suitable for a targeted drug deliver to some regions as intestine and other organs. Some attempts were made to introduce hydrophilic portions by covalent linkage in C2 position in chitosan polymeric chain, such as carboxymethylation, akylation or quaternarization of chitosan. *O*-(2-hydroxyl) propyl-3-trimethyl ammonium chitosan chloride (*o*-HTCC), with its structure represented in Figure 2.3, results from coupling of glycidyl trimethylammonium chloride (GTMAC) to chitosan [36]. Due to the additional quaternary ammonium group this derivative presents greater water solubility than chitosan, being soluble in a major pH range [37].

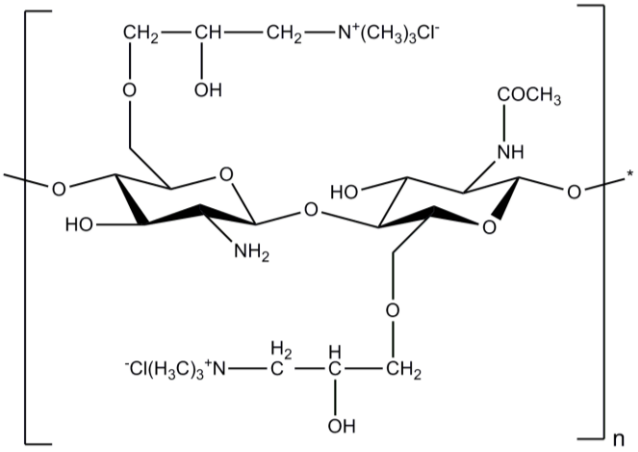


**Figure 2.3 - Chemical structure of o-HTCC, a chitosan derivative.**

Wan *et. al* [36] prepared *o*-HTCC and chitosan nanoparticles through ionic gelation, using TPP as a crosslinking. Comparing both of them they concluded that *o*-HTCC presents high water solubility in a wide pH range. They also verified that *o*-HTCC nanoparticles size was around 537 nm and chitosan nanoparticles was 372 nm. Cs NP's size was higher when loaded with BSA than Cs by itself but BSA loaded *o*-HTCC nanoparticles presented a smaller size than only *o*-HTCC nanoparticles. This is due to the compact structure of BSA loaded *o*-HTCC nanoparticles produced by ionic gelation, as a result of its strong ionic interactions.

# 3 Superparamagnetic iron oxide nanoparticles (SPION's)

## 3.1 Structure and properties of SPION's

Magnetic nanoparticles are being used as drug delivery carriers in targeted tumour treatments, especially superparamagnetic iron oxide nanoparticles (SPION's), due to its nano-size and superparamagnetic properties. Usually made of magnetite ($Fe_3O_4$) or maghemite ($\gamma$-$Fe_2O_3$), SPION's have proven to be biocompatible and biodegradable [38]. Magnetite has iron cations in two valence states, $Fe^{2+}$ and $Fe^{3+}$, and its magnetization happens due to the electronic movements of these two ions. Magnetite nanoparticles with less than 20 nm of size are superparamagnetic which means that they behave as a single magnetic dipole, having a high magnetic momentum [39]. This high magnetization allows the control of their movement in the bloodstream with an external magnetic field and then confining them to the targeted tissue. Due to their superparamagnetic phenomena and quantum tunnelling of magnetization [40], they only become intensely magnetized when in presence of a magnetic field; on its absence they do not possess any magnetization [25]. So each particle can be considered as a single magnetic domain [40]. Apart from the superparamagnetic property, other advantages of iron oxide nanoparticles are its biodegradability, low toxicity and allowance to surface modifications. That is why these nanoparticles are promising for magnetic resonance imaging or cancer therapy using external magnetic fields [40]. SPION's show an elevated surface area to volume ratio that allows a high drug loading and the attachment of some other surface compounds [6].

High magnetic susceptibility, superparamagnetic behaviour, tailored surface chemistry and the size of the nanoparticles are all factors that influence the effectiveness of these kinds of particles [40].

## 3.2 Production of SPION's

SPION's synthesis is very challenging in order to optimize size and shape, so that the above-mentioned properties can be achieved. For that there are the physical and chemical methods. The first ones, such as electron beam lithography, are very elaborate procedures and do not allow nanoparticles size control. Chemical procedures are more tractable, simple and easier to control size, shape and composition of the nanoparticles [40].

SPION's can be produced by different chemical methods, such as co-precipitation [40], thermal decomposition [39, 41, 42], water-in-oil microemulsions [43] and hydrothermal synthesis [44].

- Co-Precipitation [40]

Co-precipitation of $Fe^{2+}$ and $Fe^{3+}$ aqueous salt solutions by adding a base is a chemical procedure to produce magnetite and some others iron oxides. Through this method nanoparticles characteristics are controlled by the pH, ionic strength of the media, $Fe^{2+}$ and $Fe^{3+}$ ratio and the type of salt used.

Usually the base is added to an aqueous mixture of $Fe^{2+}$ and $Fe^{3+}$ salts with 1:2 molar ratio under a non-oxidizing oxygen free environment and it is expected that a complete precipitation of $Fe_3O_4$ occur at pH between 9 and 14. To maintain this ideal environment the production of magnetite nanoparticles must be performed by passing $N_2$ gas through the reaction area, which allows controlling reaction kinetics and particle size as it also prevents critical oxidation of magnetite.

- Thermal decomposition [39, 41, 42]

This method is based on the decomposition of ionic precursors, such as $Fe(acac)_3$ or $Fe(Co)_5$, in a solvent, e.g. triethylene glycol (TREG), at high temperatures. These ionic precursors are used in high quantities but as they are very toxic, the generated nanoparticles through the process need purification. Changing the procedure parameters, such as concentration of iron salts, duration of the reaction or the surfactant, allows controlling size and shape of SPION's produced. Using TREG as a solvent has three important roles: is a reducing agent, it works as a high-boiling solvent and is also a stabilizer to the nanoparticles produced, working itself as a surfactant. This method results in stable and uniform magnetite nanoparticles.

### 3.3 SPION's coating and surfactants

Due to hydrophobic interactions between the magnetic nanoparticles they tend to aggregate and form large clusters, increasing the size of the particle. These clusters have strong magnetic dipole-dipole attractions between them, which lead to further magnetization of each cluster, because they start to belong to their neighbours' magnetic field due to their size. This result in increased aggregation of the NPs [40]. To solve or improve this aggregation problem, coating the superparamagnetic nanoparticles with surfactant has proven to be a good solution, as it increases their stability [25, 40]. Several surfactants can be used and, its origin leads to changes in SPION's functionality, such as increasing the cell uptake, decrease the risk of immunogenicity or changing the surface charge [25]. However, some studies showed that these surfactants do not lead to severe changes in SPION's magnetic and physiochemical properties, except for the case of oleic acid [45].

SPION's surfactants can be carboxylate, like sodium citrate and oleic acid, natural polymers, such as gelatin, dextran and chitosan, synthetic polymers, as PVA (polyvinyl alcohol) or Triton X-100, and even inorganic materials such as gold or silica [40, 45].

# 4 Mathematical modelling for drug delivery systems

To understand drug release from nanoparticles, there are some mathematical models that try to explain and predict the system performance. The use of a mathematical model allows improving the delivery system in terms of efficiency and easiness of application. It also has the advantages of reducing time and costs, because it allows reducing the number of experiments made and optimizing the procedures. Since Takeru Higuchi, in 1961, [46] that was the beginner of mathematical modelling for drug release systems, there have been numerous models, for different kinds of systems. These models can be split into empirical/semi-empirical or mechanistic realistic. On empirical/semi-empirical models the predictable power is usually low due to the fact that the mathematical treatment is only descriptive and does not take into account the real biological phenomena. Thus it is important to be careful using these kinds of mathematical models when making quantitative predictions or mechanistic conclusions. They are useful when comparing different drug release profiles. On the other hand, the mechanistic mathematical models are different, as they take into account the real phenomena happening on the drug delivery system, such as diffusion, swelling, erosion or degradation. Hence, allows the prediction of different processes that are involved in the studied system. Therefore these models allow the understanding on how the system works and the theoretical prediction of the required and desired characteristics of production of the drug delivery system [33]. However, there is some divergence between theories and experimental data, especially because there are several driving forces in a single transport process [47].

It is important to take into account the swelling behaviour of chitosan when applying some mathematical model, because some of the models may not be appropriate for this kind of polymer. There have been made several efforts to modulate drug release from swelling materials but its viscoelastic properties make this a very hard task [48].

## 4.1 Mechanistic realistic theories

The mechanistic realistic theories explain the biological phenomena through equations, which often are partial differential equations. In these cases, the initial and boundary conditions should be known, such as the drug distribution before the system contacts with the release medium. The solutions of these equations may be analytical or numerical, according to the complexity of the set of mathematical equations that represents the system. Usually some approximations and simplifications are needed to achieve a relatively simple mathematical system [33].

Some of the mechanistic realistic models for drug delivery systems consider the polymer swelling, as it has already been verified that chitosan swelling behaviour is one of the most significant reasons for DOX release from the system. In this type of models it has to be consid-

ered the transition from the glassy to the rubbery state of the macromolecules. Through models already developed, drug release is quantified from polymer films showing swelling behaviour, using a complex set of partial differential equations [33]. In this way, they are not of easy application to experimental data and they are not going to be used in this work.

### 4.2 Empirical/semi-empirical theories

These are very useful models for experimental studies of drug release profiles, by giving indication of the underlying release mechanism and allowing the comparison between different drug release profiles [33].

The most used empirical/semi-empirical models are all represented in Table 4.1.

Zero-order kinetics model implies that drug release from the nanocarrier is slow, that no equilibrium conditions are reached and there's no dosage form disaggregation. It describes release from low soluble drugs incorporated in matrix tablets. First-order kinetics modulates dissolutions profiles where the quantity of drug released is proportional to the amount that is still in the dosage form and it decreases by unit of time [49, 50]. It is usually used for porous dosage forms containing water-soluble drugs [51]. On the other hand, Higuchi model describes the release as Fickian diffusion, dependent of the square root of time. It's usually used for matrix tablets with soluble drugs or transdermal systems [49, 50]. Higuchi model is more precise in systems of unidimensional matrixes with low solubility, in which drug diffuses in only one direction and without swelling behaviour [52]. Another model is Hixson-Crowell that describes systems where there's a changing in diameter and surface area of tablets or particles while drug releasing, which means that the geometry of the systems is maintained constant [51, 53]. Some other model was developed by Hopfenberg to describe drug release from surface eroding polymers, where polymer surface area stays constant [50]. Another model was described by Peppas and Sahlin with an equation with two parcels; the first one represents Fickian diffusional contribution and the second one is related to dissolution and relaxation of polymeric chains contribution to release. This model equation ha also an exponent, *m*, that is truly related with *n* exponent of Korsmeyer-Peppas model, as its values should be the same [54].

Finally, there is the simplest model to describe drug release from polymers that is called Korsmeyer-Peppas model and is based on a power law equation [55]. This mathematical model is also applicable to swelling polymeric systems and its constants assume different values depending on the release mechanism, with different boundary values according to the geometry of the device. As we are working with chitosan nanoparticles, there is only interest in the release from spheres [56]. This model is applicable to experimental data by doing the approximation to the first 60% of release, which means that $\frac{M_t}{M_\infty} < 0.6$, where $M_t$ is the amount of drug released at time *t* and $M_\infty$ is the cumulative quantity of drug released when time approaches infinite

(equilibrium state of release) [13, 49, 56, 57]. Depending on the value of the diffusional exponent *n* different types of release profile can be identified, as it is mentioned in Table 4.1 when referring this model. If $n \leq 0.43$ means that we are in the presence of Case I or Fickian diffusion where diffusion rate is less than relaxation rate. When $n = 0.85$, it is Case II transport or also called relaxation-controlled transport where relaxation rate is slower than diffusion rate. When *n* is in between these values it is called anomalous or non-Fickian diffusion, where there is a similarity between diffusion and relaxation rate [57]. There is a last category of release profile, when $n > 0.85$, called Super Case II transport [49, 58]. The other constant present in the equation of this model is *k*, which is related to the shape and structure of the polymer [33]. These two constants allow the comparison of experimental data of systems with different characteristics and the understanding of release mechanism.

There is also a mathematical function that usually fits most of the drug release profiles, named Weibull equation, used to describe the initial 60% of release, which is shown in Table 4.1. While not properly a model, as it was not designed to describe specifically a drug release system, it does seem to fit most of release profiles, even though there is no kinetic basis to its use and its parameters are not well physically described [59]. This equation has two constants *a* and *b*. The first one, constant *a*, is a time scale factor and *b* is a shape factor: $b = 1$ means it is exponential, $b > 1$ it is sigmoid and $b < 1$ means it is parabolic, with a higher slope in the beginning, when compared to exponential one [60]. In 2006, Vasiliki Papadopoulou *et al*. [59] have presented a correlation between this *b* parameter of Weibull model with *n* exponent of Korsmeyer-Peppas model. In this way, *b* can be used as an indicator for the mechanism of drug release. This study indicates that for $b \leq 0.75$ it is a Fickian diffusion, for $0.75 < b < 1$ is a mixed mechanism, between Fickian diffusion and Case II transport, and finally for $b > 1$ drug is released through a complex release mechanism.

**Table 4.1 - Empirical/semi-empirical models for drug release profiles; $Q_0$ - initial quantitity of drug in solution; $Q_t$ - cumulative quantitity of drug released at time t.**

| Model | Equation | Application | Ref. |
|---|---|---|---|
| **Zero-order** | $Q_t = Q_0 + K_0 t$<br>$k_0$ - zero-order release constant | Systems where release rate is independent of the concentration of dissolved substance | [5, 61, 62] |
| **First order** | $\log Q_t = \log Q_0 + K_1 t$<br>$K_1$ - first-order release constant | Systems where release rate is dependent on the concentration | [5, 62, 63] |
| **Higuchi** | $Q_t = Q_0 + K_H t^{1/2}$<br>$K_H$ - Higuchi constant | Fickian diffusion | [5, 46] |
| **Hixson-Crowell** | $\sqrt[3]{Q_t} - \sqrt[3]{Q_0} = K_{HC} t$<br>$K_{HC}$ - Hixson-Crowell constant | Release by dissolution where the surface area and diameter particles change; related to erosion release mechanism | [5, 64] |
| **Hopfenberg** | $Q_t = 1 - \left(1 - \frac{k_0 t}{c_0 a}\right)^n$<br>$c_0$ - uniform initial drug concentration in the system<br>$a$ - radius of a sphere<br>$k_0$ - rate constant<br>$n$ - shape factor | Surface eroding polymer matrices | [5, 65] |
| **Korsmeyer-Peppas** | $Q_t = k t^n$<br>$n$ - empirical release exponent<br>k – related to polymer structure and geometry | Fickian: $n \leq 0.43$, Case II transport: $n = 0.85$, non-Fickian or anomalous: $0.43 < n < 0.85$, super Case II: $n > 0.85$ | [5, 56, 66] |
| **Weibull** | $Q_t = 100 \times \left[1 - e^{-\frac{t^\beta}{a}}\right]$ | Fickian diffusion: $b \leq 0.75$, combined mechanism of Fickian and Case II: $0.75 < b < 1$, complex mechanism: $b > 1$ | [59, 67] |
| **Peppas-Sahlin** | $Q_t = k_1 . t^m + k_2 . t^{2m}$ | $k_1$ – Fickian contribution; $k_2$ – relaxation contribution; $m$ - correspondent to $n$ exponent of Korsmeyer-Peppas model | [54, 68] |

# 5 Materials and Methods

As a way to study the influence of the molecular weight in the drug delivery system, chitosan and *o*-HTCC with four different molecular weights were used in some of the experiments of this work.

## 5.1 Chitosan depolymerisation

### 5.1.1 Materials

Chitosan (*Cognis*, DA 75.5%), sodium nitrite ($NaNO_2$) (*Sigma-aldrich*), acetic acid (*Panreac*), NaOH (*Eka*)

### 5.1.2 Procedure

As it has been referred before, this thesis is a continuation of other thesis still in development. In this way, chitosan depolymerisation was performed in that work and here was used the resultant chitosan with different molecular weights, so the procedure is going to be shortly presented.

Commercial chitosan with molecular weight Mw = 470 kDa was depolymerized to obtain three different molecular weights based on the method used by Huang *et al.* [69] in 2004 and by Loh *et al.* [70] in 2010. Chitosan (1% w/v) was first diluted in acetic acid (1% v/v) overnight under magnetic stirring. Then sodium nitrite ($NaNO_2$) was added using three different $NaNO_2$:Cs ratios: 1:25, 1:100 and 1:200, in order to obtain the three different molecular weights. This solution stayed under mechanical stirring at 300 rpm for 1h. Each one of these three samples of depolymerized chitosan was precipitated with NaOH 4M, until the pH reached approximately 9. After this, the solution was centrifuged (Heraeus Multifuge X1R centrifuge – *Thermo Scientific*) at 10000 rpm for 10 min at 20ºC. The resultant pellet was washed several times with ultrapure water until neutral pH and the final product was freeze-dried ($VaCO_2$ ZIRBUS technology; -45 ºC and 0.07 mbar).

The molecular weight of depolymerized chitosan was measured by dilute solution viscometry (Schott Geräte Typ 53201/0a; solvent system: 0.2 M acetic acid/0.1 M sodium acetate, 30ºC) using the Mark-Houwink equation (K= 2.26x10-5 dl/g, α=0.95) [71]

## 5.2 Synthesis of *o*-HTCC

### 5.2.1 Materials

Acetic acid (*Panreac*), Methanol (*Sigma-Aldrich*), Benzaldehyde (*Fluka*), Acetone (*Fisher chemical*), Isopropyl alcohol (*Panreac*), GTMAC (*Aldrich*), ethanolic HCl (*Fluka*).

### 5.2.2 Procedure

*o*-HTCC was also synthetized in a simultaneous work in the laboratory through an adapted method of Wang *et al.* [37] from the four molecular weights of chitosan.

First, 5 g of chitosan was dissolved in 250 ml of acetic acid (2% v/v) and 125 ml of methanol. Then 32 ml of benzaldehyde was added to the solution and the reaction occurred with mechanical agitation for 24h, until forming a white gel. To adjust the pH of the polymer, sodium hydroxide NaOH 1M was added until the pH reached 7.0. After this, the solution was filtered and washed in turns with methanol and acetone, and the product was freeze-dried. The obtained product was mixed with 50 ml of isopropyl alcohol and 5 g of glycidyl-trimethylammonium chloride (GTMAC). This solution was placed under stirring for 16 hours at 70ºC and the resultant precipitate was washed with methanol and acetone alternately. After freeze-dried, this product was added to 100 ml of ethanolic HCl 0.25M and was under reaction for 24 hours at ambient temperature. Then, 25 ml of ultrapure water was added followed by excess of acetone was added in order to precipitate the final product. This product was filtered and washed with acetone and methanol for several times. To purify *o*-HTCC, this last product was dissolved in water and precipitated with excess acetone. After filtered and washed, the resultant *o*-HTCC was freeze-dried and stored in a dry place.

## 5.3 SPION's synthesis by thermal decomposition

### 5.3.1 Materials

Triethylene glycol (TREG) (*Alfa Aeser*, 99%), iron (III) acetylacetonate ($Fe(acac)_3$) (*Sigma Aldrich*, 97%), ethyl acetate (*Sigma Aldrich*, 99.5%), hydrochloride acid 37% (Panreac), 1,10-phenanthroline (*Applichem*), hydroxylamine (*Alfa Aeser*), ammonium acetate (*Sigma Aldrich*), distilled water.

### 5.3.2 Procedure

Superparamagnetic iron oxide nanoparticles were prepared by thermal decomposition of $Fe(acac)_3$ through an adapted method of Maitry *et al.* [42]. In a round flask, 0.7 g of $Fe(acac)_3$ were dissolved in 20 ml of TREG and magnetically stirred (200 rpm) in a ceramic plate, under a flow of nitrogen and with increase of the temperature. The experimental set-up is represented in Figure 5.1: (a) photograph and (b) scheme adapted from Lochte thesis [72]. When the temperature was 120 ºC the solution was dehydrated for 1h, then increased to 300 ºC and the reaction stayed at this temperature for 30 min. The resultant black solution was then cooled to room temperature. Then, 20 ml of ethyl acetate were added to the solution in order to precipitate the nanoparticles and then divided for four tubes and centrifuged for 15 min at 12000rpm. SPION's were not already precipitated so it was added another 10 ml of ethyl acetate to each tube and

they were centrifuged again under the same conditions. The supernatants were all removed and nanoparticles were dispersed in distilled water and stored all together in a flask.

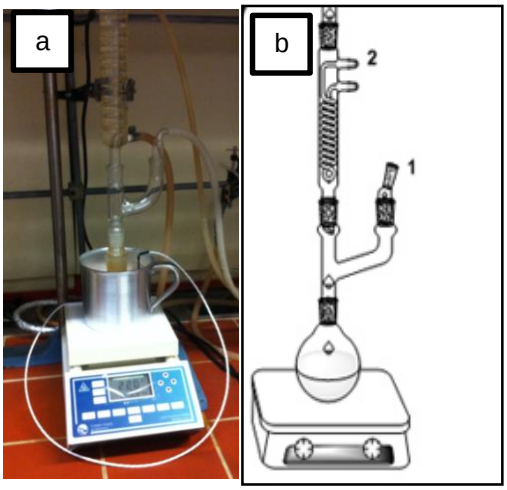


**Figure 5.1 - Experimental set-up for thermal decomposition procedure; (b) 1-gas inlet; 2-water inlet.**

After the production of SPION's it is necessary to know its iron concentration for further experiments. To do this it was followed a procedure of indirect measure through ultraviolet visible spectrophotometer (UV-Vis, T90+ PG Instruments) and 1,10-phenanthroline colorimetric method [73]. Using hydrochloric acid (HCl) (0.01 N), were prepared solutions of hydroxylamine hydrochloride at 100 mg/ml and phenanthroline 3 mg/ml. In an *eppendorf* were added 40 μl of diluted SPION's solution and 20 μl of HCl and waited for 1h. Then, it was added 100 μl of hydroxylamine hydrochloride (100 mg/ml) solution and 500 μl of phenanthroline solution (3 mg/ml). Finally 1140 μl of ammonium acetate (500mM) was added to the *eppendorf* and the absorbance of the solution was measured in UV-Vis spectrophotometer, at 510 nm. A calibration curve (Equation 1) to determine the concentration of iron in the solution was obtained using Mohr salt (Ammonium iron (II) sulphate, *Sigma*).

$$y = 4.5079x + 0.0753 \quad \textbf{Equation 1}$$

After the iron concentration was calculated, the SPION's solutions were freeze-dried in order to obtain the total NP's mass by weighting the final dry sample. From both experiments, the following relation was obtained:

[Fe] = 0.7 x [SPION's], that correlates the iron concentration with the total SPION's mass.

## 5.4 Preparation of chitosan, *o*-HTCC nanoparticles and coated SPION's

### 5.4.1 Materials

Chitosan (*Cognis*, DA 75.5%), sodium tripolyphosphate (*Sigma Aldrich*, 85%), acetic acid (*Panreac*).

### 5.4.2 Procedure

Chitosan nanoparticles were prepared based in the method developed by Calvo *et al.* [74] in 1997 where the nanoparticles were formed by the addition of sodium tripolyphosphate (TPP) to chitosan in acidic solution. Therefore, TPP (0.25% (w/v) in water) was slowly added to chitosan at 1.2% (w/v) in acetic acid 1% (v/v) in a disperser (IKA T10 basic ultra-turrax) for 5 min. To isolate the chitosan nanoparticles, the solution was centrifuged for 5 min at 10000 rpm and the pellet was resuspended in water.

To prepare *o*-HTCC nanoparticles the same method as for chitosan was used.

Chitosan or *o*-HTCC coated SPION's were prepared through this last procedure, with the difference of the addition of SPION's at 1 mg/ml in the proportion of 1:12 of SPION's to Cs or *o*-HTCC, before adding tripolyphosphate (TPP).

## 5.5 Characterization of chitosan and *o*-HTCC nanoparticles and coated SPION's

Different analyses were performed to characterize chitosan and *o*-HTCC nanoparticles and coated SPION's by its size, charge or spectrum.

### 5.5.1 TGA

Thermal gravimetric analysis (TGA) (Thermal Analyzer NETZSCH STA 449 F3 Jupiter®) was performed in either chitosan or *o*-HTCC nanoparticles to analyse the changes in their physicochemical characteristics as a function of temperature.

### 5.5.2 DLS and Zeta potential

Dynamic Light Scattering (DLS) (SZ-100 nanopartica series, Horiba, Lda) was made to analyse particle size distribution of chitosan and *o*-HTCC nanoparticles, for each molecular weight. Zeta potential was determined using in a way to evaluate the stability of chitosan and *o*-HTCC nanoparticles dispersion. Each trial was made in triplets.

### 5.5.3 FTIR

Fourier transform infrared spectroscopy (FTIR) of freeze-dried samples of both chitosan and *o*-HTCC, by itself and as nanoparticles, and of SPION's and coated SPION's was performed using a Nicolet 6700 – Thermo Electron Corporation Total Reflectance-Fourier Transform Infrared spectrometer (ATR-FTIR).

## 5.6 Evaluation of DOX encapsulation

### 5.6.1 Materials

Chitosan and *o*-HTCC with four different molecular weights, SPION's produced by thermal decomposition, doxorubicin hydrochloride (*European Pharmacopoeia reference standard*), acetic acid (*Panreac*), sodium tripolyphosphate (*Sigma Aldrich*, 85%), distilled water.

### 5.6.2 Procedure

In all experiments using DOX, its concentration in solutions was determined through calibrations curves with absorbance measured by ultraviolet visible spectrophotometer (UV-Vis, T90+ PG Instruments) in a range of concentrations between 5 and 50 µg/ml of DOX. The absorbance was measured in wavelength of 480 nm, DOX maximum absorbance peak [31, 38]. These DOX calibration curves were performed for all the solvents used in the experiments: water, phosphate buffer saline (PBS) with pH 7.4, PBS with pH 6.5 and Hac/NaAc (pH 4.5). These measures to obtain the calibration curves were made in quadruplicates.

Doxorubicin was incorporated during chitosan nanoparticles production (sub chapter 5.3). Before adding the crosslinker (TPP), DOX with different concentrations was added to chitosan acidic solution (1.2% w/v in acetic acid at 1% v/v) and was in magnetic stirring for 10 min. After adding TPP (0.25% (w/v)) to 0.5 ml of DOX+Cs solution, the solution was centrifuged (Sigma 1-13 centrifuge) for 5 min at 10000 rpm. Supernatant was removed and 1 ml of distilled water was added to the pellet and was centrifuged again under the same conditions. This resultant supernatant was also removed. The absorbance of the two supernatant DOX concentrations was measured by UV-VIS spectroscopy at wavelength of 480 nm and encapsulation efficiency (EE) was calculated (Equation 2).

$$\boldsymbol{EE}\ (\%) = \frac{(\boldsymbol{initial\ mass\ of\ DOX}) - (\boldsymbol{mass\ of\ DOX\ in\ supernatants})}{\boldsymbol{initial\ mass\ of\ DOX}} \times \mathbf{100} \quad \textbf{Equation 2}$$

In a way to study its influence and to reduce the quantity of reagents used, to a solution with 1:3 (w/w) DOX to Cs, with a concentration of 1.33 mg/ml of DOX, the encapsulation efficiency was tested for different ratios of crosslinking agent (TPP) to chitosan: 1:4.8 (w/w), 1: 2.4 (w/w) and 1:1.6 (w/w). Encapsulation efficiency to a ratio of 1:0.533 of TPP:Cs was investigated as well, in this case using a concentration of 1 mg/ml of DOX, as it were the conditions used in the study of DOX release profile.

Also in order to try to minimize the quantity of DOX used, four different experiments were made by fixing TPP:Cs ratio to 1:1.6 (w/w) (1500 µl of TPP) and varying the proportion of DOX in relation to chitosan: 1:3 (w/w) (1.33 mg/ml of DOX), 1:6 (w/w) (1 mg/ml of DOX), 1:12 (w/w) (0.67 mg/ml of DOX) and 1:24 (w/w) (0.4 mg/ml DOX). These experiments described above were performed for all four molecular weights of chitosan in study.

Encapsulation efficiency was also determined for DOX loaded *o*-HTCC nanoparticles and for DOX loaded chitosan coated SPION's and *o*-HTCC coated SPION's, through the same method as for Cs nanoparticles. In the case of *o*-HTCC nanoparticles, was studied the influence of the proportion of TPP:*o*-HTCC in the encapsulation efficiency, by testing it to different TPP:*o*-HTCC ratios: 1:4.8 (w/w), 1:2.4 (w/w), 1:1.6 (w/w) and 1:0.533 (w/w), for the four *o*-HTCC molecular weights in study and using 1 mg/ml concentration of DOX.

As for Cs or o-HTCC coated SPION's, it was only determined the encapsulation efficiency on the conditions used later in the study of DOX release profiles, which were 1:0.533 TPP:Cs or TPP:*o*-HTCC ratio, depending on the case, and 1:6 DOX:Cs or DOX:*o*-HTCC, respectively, which means an initial concentration of DOX of 1 mg/ml. In these coated SPION's were only used polymers (chitosan or *o*-HTCC) with the highest and the lowest molecular weight.

All experiments using DOX were performed in the absence of light in order to avoid its photodegradation. Each type of experiment was performed in triplets.

## 5.7 DOX release studies

### 5.7.1 Materials

Chitosan and *o*-HTCC with four different molecular weights, SPION's produced by thermal decomposition, doxorubicin hydrochloride (*European Pharmacopoeia reference standard*), acetic acid (*Panreac*), sodium tripolyphosphate (*Sigma Aldrich*, 85%), distilled water.

### 5.7.2 Procedure

Doxorubicin release profiles were determined in buffers with pH 7.4, 6.5 and 4.5, which represent some physiological conditions found in the body and in tumour cells. All release studies started with 1 mg of DOX. It was used DOX + Cs solution in a proportion of 1:6 (m/m), with TPP in 1:0.533 (m/m) TPP to Cs.

First, 1ml of Cs+DOX was added to 4.5 ml of TPP (0.25% w/v), stirred in ULTRA-TURRAX for 5 min. This solution was then centrifuged (Heraeus Multifuge X1R centrifuge – *Thermo Scientific*) for 10 min at 12000 rpm. The resultant supernatant was stored and 3 ml of water were added to the pellet; the solution was centrifuged again in the same conditions and this resultant supernatant was also stored. The resultant pellet was resuspended in 1 ml of PBS with pH 7.4, in a way that nanoparticles were well dispersed in the solution. Then this 1 ml of solution was dialyzed (Spectrum Laboratories, cut off Mw = 10-12 kDa), as it is shown in Figure 5.2, in 10 ml of release buffer at 37ºC for 72h. Periodically, 3ml of release medium was removed and the same volume of new buffer was added. The absorbance of all the samples was measured at 480nm, including the two supernatants resultant from the two initials centrifugations. With these values of absorbance and with the help of DOX calibration curves, mentioned

in subchapter 5.6, DOX concentration values were determined, allowing the calculation of the percentage of drug released at each period of time.

Controls were also made in the same way by dialyzing 1 ml of free DOX and varying the pH of the release medium (4.5, 6.5 and 7.4).

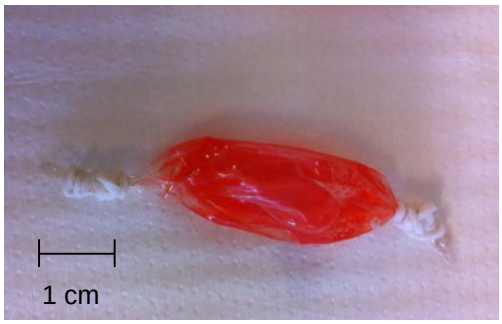


**Figure 5.2 - Dialysis membrane containing DOX loaded chitosan nanoparticles solution before starting release experiments.**

Freeze-dry is a way to prevent polymer degradation and drug leakage and desorption and nanoparticles appear to be easily redispersible when dried [28]. After doing some experiments through this procedure, it was decided to try to work with freeze-dried nanoparticles, as this is one of the most used ways to preserve and store polymeric nanoparticles. In this way, the last procedure was slightly changed in the initials steps, cutting of the centrifugations. So 1ml of Cs+DOX was added to 4.5 ml of TPP (0.25% w/v), stirred in ULTRA-TURRAX for 5 min, and then freeze-dried for 24h ($VaCO_2$ ZIRBUS technology; -45 ºC and 0.07 mbar). The resultant powder of DOX loaded Cs nanoparticles was then resuspended in 1 ml of PBS with pH 7.4 and dialyzed. The rest of the steps were exactly the same. Using freeze-dried nanoparticles it was possible to make sure that the initial mass of DOX was always the same (1 mg) in each experiment, what did not happened in the first trials, due to the two centrifugations. It also allowed the same swollen state of chitosan in each trial, as it was all dried in the beginning. Thus, this was the chosen method for all the drug release studies done.

DOX release profile from chitosan nanoparticles was performed for each one of the four molecular weights in study.

Besides chitosan nanoparticles, it was also studied DOX release profile from *o*-HTCC nanoparticles for its four molecular weights, from Cs coated SPION's and from *o*-HTCC coated SPION's, always through this last referred procedure. In this last case, SPION's coating was made with only the highest and the lowest molecular weight of chitosan or *o*-HTCC, respectively.

All these drug release experiments using freeze-dried nanoparticles were made in triplets; the first ones without freeze-drying were only performed in triplets for pH 7.4, in the others pH were a one time trial. A summary of all DOX release trials made is presented in Table 5.1

**Table 5.1 - Summary of all DOX release profiles experiments.**

| Nanoparticle type | Freeze-dried | Polymer Mw (kDa) | pH | Samples |
|---|---|---|---|---|
| **Cs NP's** | No | 39<br>167<br>264<br>470 | 7.4<br>6.5<br>4.5 | x 3<br>x 1<br>x 1 |
| | Yes | 39<br>167<br>264<br>470 | 7.4<br>6.5<br>4.5 | x 3 |
| ***o*-HTCC NP's** | Yes | 48<br>166<br>292<br>470 | 7.4<br>6.5<br>4.5 | x 3 |
| **Cs coated SPION's** | Yes | 39<br>470 | 7.4<br>6.5<br>4.5 | x 3 |
| ***o*-HTCC coated SPION's** | Yes | 48<br>470 | 7.4<br>6.5<br>4.5 | x 3 |

## 5.8 Mathematical modelling of release profiles

To apply the mathematical models to the experimental data of each type of DOX release profile studied was used a freely available Excel Add-In called DDSolver. This program was developed by Yong Zhang *et al.* [75] in 2010 in order to simplify the tasks of applying mathematical models to dissolution profiles of this type, as there was no existence of an easy and reliable software to do this. To each type of experiment of DOX release was applied all the models presented in Table 4.1: zero-order, first-order, Higuchi, Hixson-Crowell, Hopfenberg, Korsmeyer-Peppas, Weibull and Peppas-Sahlin.

## 5.9 Cytotoxicity and cell viability assays

Chitosan and *o*-HTCC nanoparticles, SPION's and coated SPION's cytotoxicity was measured by a simple method using resazurin dye. When there's cellular activity it happens the transference of electrons to resazurin, being reduced to resofurin. In this way, measuring the absorbance by spectrophotometry allows the quantification of the level of resazurin reduction, as the absorption peaks of resazurin and resofurin shifts: 600 nm and 570 nm respectively [76]. This enables measuring the quantity of cells that present activity and the ones that are dead, allowing the quantification of the viability of the material in study.

Cytotoxicity assays were performed with VERO (kidney mammalian cells) and SaOs (osteoblasts lineage) cells. In all experiments were only used two molecular weights of chitosan, with the lowest and the highest molecular weight, because if these two don't appear to be cytotoxic, the ones with intermediate molecular weights aren't also. Different concentrations of either chitosan or *o*-HTCC nanoparticles were tested to find the limit of cytotoxicity. The highest concentration was 5 mg/ml and this solution was successively diluted, until reached 0.039 mg/ml. In the case of magnetic nanoparticles, cytotoxicity was tested to SPION's without any coating, to chitosan coated SPION's and to *o*-HTCC coated SPION's. For uncoated SPION's the range of concentrations was 0.06 - 2 mg/ml; for the coated SPION's polymer concentration was maintained (0.039 – 5 mg/ml) and magnetic nanoparticles concentrations were 0.005 – 0.145 mg/ml, in correspondence.

For SaOS cells was used McCoy 5A medium (*Sigma Aldrich*), supplemented with 10% of fetal bovine serum (*Life Technologies*) and 1% of Penicillin-Streptomycin (10,000 U/mL) (*Life Technologies*). The medium used for VERO cells is composed of DMEM (*Sigma Aldrich*), also supplemented with 10% of fetal bovine serum (*Life Technologies*) and 1% of Penicillin-Streptomycin (10,000 U/mL) (*Life Technologies*) and with Sodium Pyruvate (100 mM) (*Life Technologies*) and GlutaMAX™ Supplement (*Life Technologies*).

In a cell culture assay the first step is to defrost the cells. In this way, cells were defrosted by removing them from -80ºC directly to a water bath at 37ºC until they were almost defrost. Then 1 ml of cells solution was added to 5 ml of medium in a T25 cell culture flask and was placed in the incubator at 37ºC and 5% $CO_2$. In the next days the medium was changed to allow cells proliferation and growing.

The second step was seeding the cells in a 96-well plate with a density of approximately 5000 cell/well. The medium in the T25 was removed and the cells were washed with 5 ml of PBS -- (without $Ca^+$ and $Mg^+$). Then 500 µl of trypsin was added and the cell culture was placed in the incubator for 5 min. After this time, cells were transferred to a tube and were counted in 16 µl in the optical microscope and some calculations were made to estimate how many cells there were in the tube. Then 100 µl of this cells solution was placed in each well of the 96-well plate. There were three controls in this assay where there weren't placed any nanoparticles. The positive control had medium with 10% of DMSO, so that the cells would die. The negative control had only cells so that all the cells should live. Finally the medium control had only medium, in a way to verify that it did not present any contamination.

After 24h, the medium of each well was washed and 100 µl of chitosan or *o*-HTCC nanoparticles or SPION's were added to each well, with the different concentrations referred before.

On the next day the resazurin test was made. In this way, all plates were washed with PBS ++ at least 3 times to remove all the residues of nanoparticles and 100 µl of resazurin diluted in medium in a ratio of 1/10 was added in all plates. The 96-well plates were placed in the

incubator for 2h. Then the absorbance was measured at 570 nm and 600 nm and finally cellular viability was measured.

# 6 Results and discussion

One of the goals of this work was the study of the influence of the molecular weight of chitosan or its derivative *o*-HTCC in a drug delivery system. Chitosan with the highest molecular weight in study is 470 kDa and in Table 6.1 are presented the other molecular weights used, resultant from depolymerisations made with different ratios of $NaNO_2$:Cs. Thus the different chitosan molecular weights used in this work will be referred as Cs 39 kDa, Cs 167 kDa, Cs 264 kDa and Cs 470 kDa.

**Table 6.1 - Chitosan molecular weights after depolymerisation.**

| $NaNo_2$:Cs ratio | Chitosan Molecular Weight (kDa) |
|---|---|
| 1:25 | 39 ± 2 |
| 1:100 | 167 ± 19 |
| 1:200 | 264 ± 21 |

Chitosan derivative *o*-HTCC was also used with four different molecular weights. The starter one has also 470 kDa, which is *o*-HTCC with the highest molecular weight, and the others are presented in Table 6.2. These different *o*-HTCC molecular weights will be referred from now on as *o*-HTCC 48 kDa, *o*-HTCC 166 kDa, *o*-HTCC 292 kDa and *o*-HTCC 470 kDa.

**Table 6.2 - o-HTCC molecular weights.**

| $NaNo_2$:*o*-HTCC ratio | *o*-HTCC Molecular Weight (kDa) |
|---|---|
| 1:33 | 48 ± 6 |
| 1:100 | 166 ± 6 |
| 1:200 | 292 ± 14 |

From the synthesis of magnetic nanoparticles through thermal decomposition was obtained a well-dispersed and stable solution, brown coloured. The concentration of SPION's in the solution was 5.51 mg/ml. This was the SPION's solution used in all experiments, usually with some dilution, to get the desired concentration.

## 6.1 Characterization of Cs and *o*-HTCC nanoparticles and coated SPION's

### 6.1.1 Size and Zeta potential

Size and zeta potential of Cs and *o*-HTCC nanoparticles measured through dynamic light scattering (DLS) are presented in Table 6.3 and Table 6.4, respectively. Nanoparticles hydrodynamic size is an important characteristic as it can change their behavior when used for

targeted drug delivery. It could be predictable that the hydrodynamic size would get higher as the molecular weight was increasing, as it happened in the research made by Wu *et al.* [20]. In the case of chitosan nanoparticles (Cs NP's), zeta-average size varies with the different molecular weights and it is higher for the highest molecular weight (303 ± 77 nm) when comparing to the lowest molecular weight (112 ± 12 nm). Polydispersity index (PI) gives information about homogeneity of the solution; a higher PI indicates a higher variety of particle size, proving less homogeneity of the solution. The results for Cs NP's show a higher PI for the highest molecular weight, indicating lower homogeneity in this case. As for the zeta potential all the samples presented a positive and similar charge, as expected.

**Table 6.3 - Zeta-average size, polydispersity index and zeta potential of chitosan nanoparticles for different molecular weights.**

| Cs NP's | Zeta-average size (nm) | Polydispersity index (PI) | Zeta potential (mV) |
|---|---|---|---|
| Cs 39 kDa | 112 ± 12 | 0.4 ± 0.1 | + 41 ± 1 |
| Cs 470 kDa | 303 ± 77 | 0.6 ± 0.2 | + 38 ± 6 |

For *o*-HTCC nanoparticles (Table 6.4), there is a similar situation as it was for chitosan: the highest molecular weight has the highest zeta-average size. In this case there is a huge difference between zeta-average sizes of both Mw and for o-HTCC 470 kDa the size is no longer at the order of nanometer but is around 6 μm. The polydispersity index also confirms this absence of a homogeneous dispersion in the higher molecular weight. Increasing *o*-HTCC molecular weight leads to a non-homogeneous nanoparticle size and polydispersity index increases. Zeta potential values for *o*-HTCC nanoparticles increase when increasing its molecular weight. Comparing with Cs NP's zeta potential values, they are slightly lower for *o*-HTCC NP's, as it was reported in Sun *et al*. research [35].

**Table 6.4 - Zeta-average size, polydispersity index and zeta potential of o-HTCC nanoparticles for different molecular weights.**

| *o*-HTCC NP's | Zeta-average size (nm) | Polydispersity index (PI) | Zeta potential (mV) |
|---|---|---|---|
| *o*-HTCC 48 kDa | 115 ± 18 | 0.07 ± 0.04 | + 22 ± 4 |
| *o*-HTCC 470 kDa | 6086 ± 656 | 2.5 ± 0.2 | + 36 ± 4 |

### 6.1.2 FTIR analysis

In order to analyse chitosan nanoparticles composition, FTIR analysis was performed to Cs NP's with 39 kDa (Figure 6.1 (a)) as well as Cs 39 kDa and TPP, the crosslinking agent used in the nanoparticles production. Observing Cs 39 kDa FTIR spectrum (black curve Figure 6.1(a)) there are three main bands at 3220 $cm^{-1}$ due to the O-H stretching vibration band, 1656 $cm^{-1}$ for the presence of $NH_2$ group and 1375 $cm^{-1}$ of C-O-C stretching vibration band [20]. Compared with Cs NP's spectrum, there are some visible differences. The band around 3220 $cm^{-1}$ is more intense and larger, meaning that there is a stronger hydrogen bonding. Also the band correspondent to the anti-symmetric N-H vibrations of $NH_3^+$ ion was shifted to 1637 $cm^{-1}$ and C-O-C stretching vibration band was at 1382 $cm^{-1}$ [20, 77]. In Cs NP's it is also present the band related to $PO_2^-$ groups anti-symmetric stretching vibrations, at 1211 $cm^{-1}$, confirming the ionic crosslinking between chitosan and TPP [77].

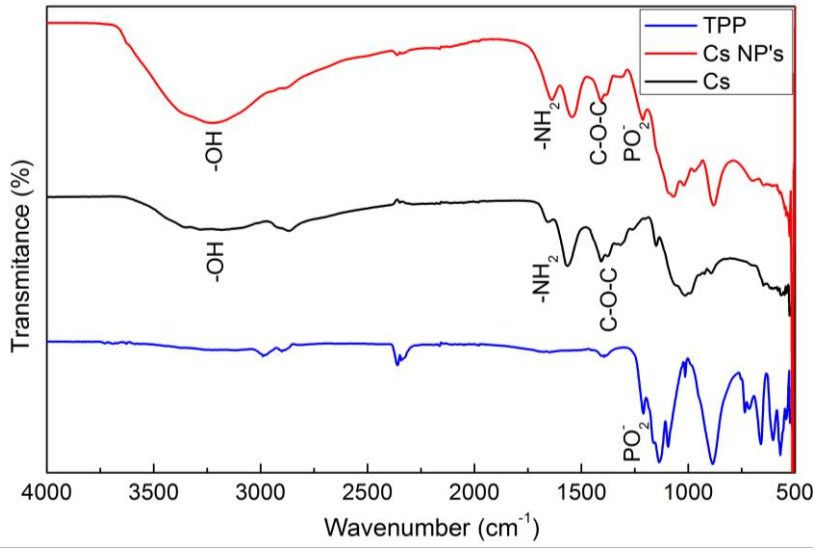


**Figure 6.1 - FTIR spectrum of TPP, Cs 39 kDa and Cs NP's with 39 kDa.**

Comparing FTIR spectrum for chitosan nanoparticles with highest and lowest molecular weight, as it is shown in Figure 6.2, there is a huge similarity in the spectrums, confirming that despite the molecular weight, the structure of chitosan nanoparticles is maintained.

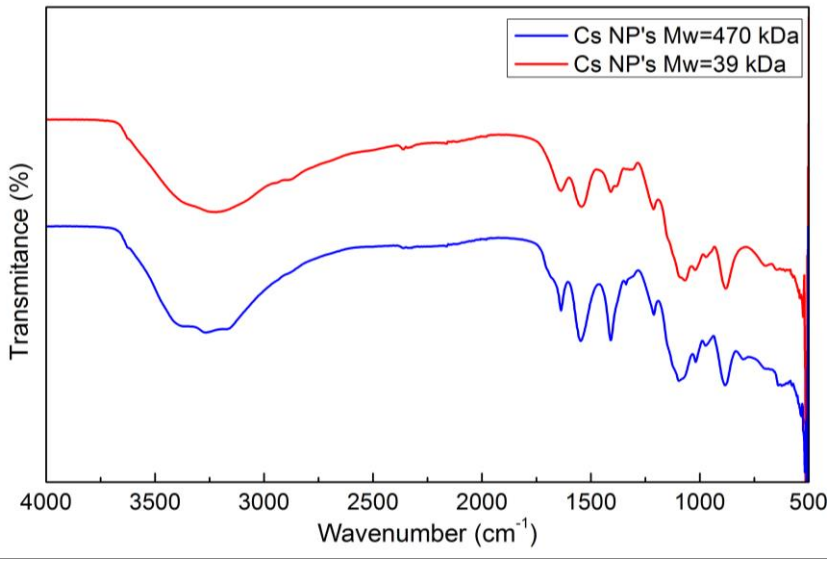


**Figure 6.2 - FTIR spectrums comparing Cs NP's with 39 kDa and with 470 kDa.**

Observing FTIR spectrum of *o*-HTCC and its nanoparticles, in Figure 6.3, it is visible sharp bands at 1627 $cm^{-1}$ and 1637 $cm^{-1}$, associated to $NH_2$ group. It suffered a slight shift in comparison with the same band in chitosan spectrum (1656 $cm^{-1}$), which can suggest that chitosan did not suffer N-alkylation. Another absorption band is visible for both *o*-HTCC by itself and in nanoparticles at 1064 $cm^{-1}$, due to $CH_2$-O-$CH_2$ [35]. There is also present a band around 3200 $cm^{-1}$ due to O-H stretching band, as it was for chitosan. Also has a band at 1480 $cm^{-1}$, related to trimethylammonium group of *o*-HTCC.

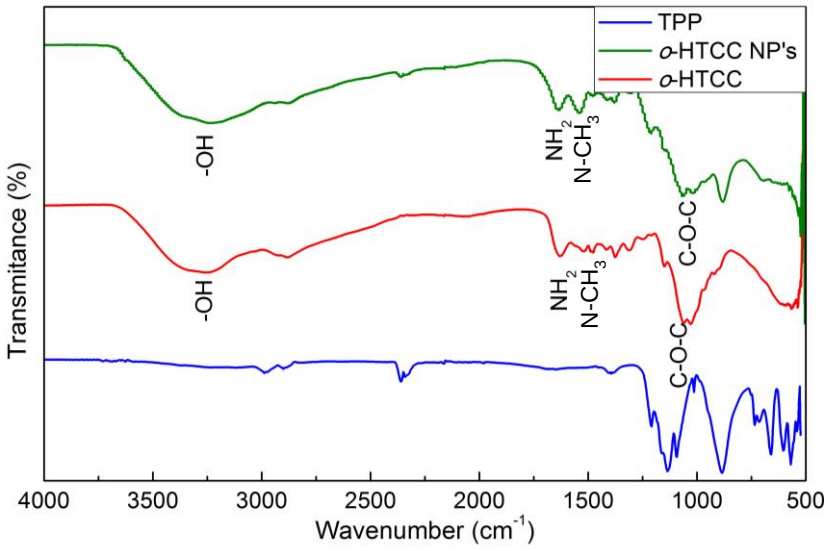


**Figure 6.3 - FTIR spectrums of TPP, *o*-HTCC 470 kDa and *o*-HTCC NP's with 470 kDa.**

For the case of coated SPION's, in Figure 6.4 are presented FTIR spectrums for SPION's, chitosan nanoparticles and Cs coated SPION's, always with Cs 39 kDa. In the case of SPION's spectrum there are three main bands: 561 $cm^{-1}$ related to Fe-O stretching vibration mode, 1614 $cm^{-1}$ due to O-H stretching vibration and a band around 3000 and 3500 $cm^{-1}$ is related to O-H stretching vibration mode due to water vapour [45]. Observing the spectrums of both chitosan nanoparticles and chitosan coated SPION's, are visible the peaks already described which characterize the presence of chitosan, meaning that chitosan is present and coating SPION's. Cs SPION's also has a band around 553 $cm^{-1}$ showing the presence of $Fe_3O_4$ [30].

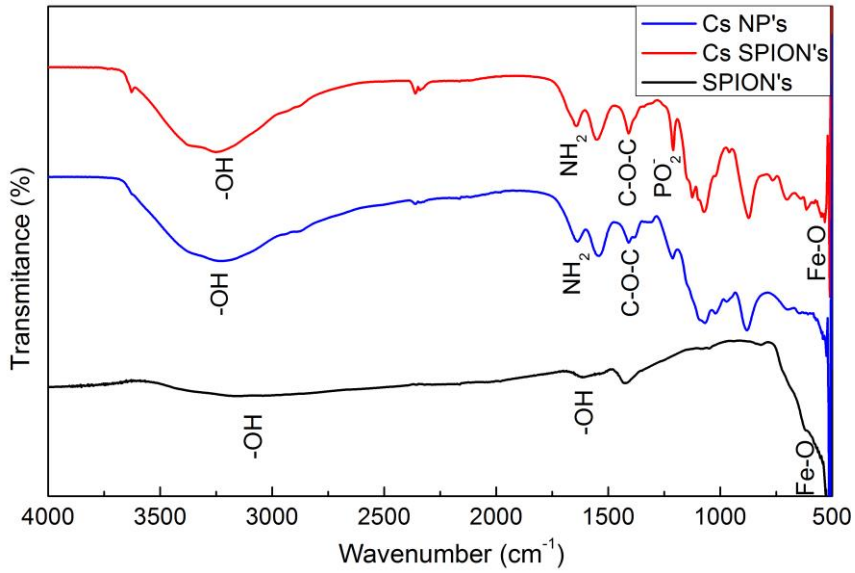


**Figure 6.4 – FTIR spectrums of SPION's, chitosan nanoparticles and Cs coated SPION's.**

### 6.1.3 TGA analysis

Another technique was used in order to characterize the different nanocarriers in study, which was thermal gravimetric analysis (TGA), which allows understanding the material behaviour to high temperatures and its influence in mass weight.

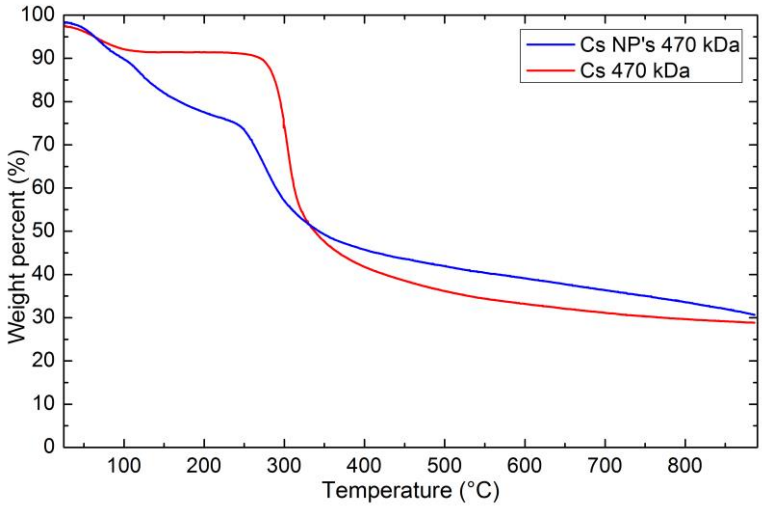


**Figure 6.5 - TGA of chitosan and chitosan nanoparticles with Mw=470 kDa.**

In Figure 6.5 the results of TGA for chitosan and chitosan nanoparticles with the highest molecular weight are presented. The graphic of the derivative of weight loss is not presented, but it helped on finding the exact temperature values where the weight loss occurred. It is noticeable that both of them suffer a weight loss below 150 ºC, which is related to a loss of residual water in the sample. Then, between 250 and 300 ºC, a huge weight loss is visible, due to chitosan disintegration [30]. For chitosan only, it is an intense decrease in weight (about 60 %) after 300 ºC. In the case of Cs nanoparticles it has this decrease due to chitosan disintegration but is softer, and starts earlier, around 120 ºC, possibly due to the presence of crosslinking agent, TPP, and their linkage disintegration. In totality, both chitosan and chitosan nanoparticles suffered a 70% weight loss.

For the case of chitosan derivative, *o*-HTCC, TGA results for both polymer and nanoparticles are shown in Figure 6.6. The first visible weight loss occurred bellow 100 ºC for both of them, due to loss of residue water in the samples. Then, in the case of *o*-HTCC polymer, there is a huge weight loss at 200ºC, possibly due to its structure degradation as it occurred for chitosan, leading to a total of 75% of weight loss. As for *o*-HTCC nanoparticles, polymer degradation only occurred at 250 ºC and its degradation was not that high in comparison to the polymer by itself, leading to a total loss of only 55%.

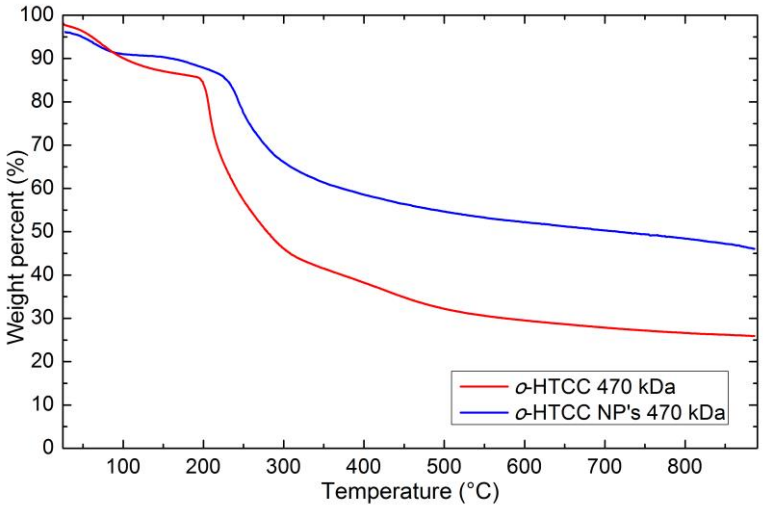


**Figure 6.6 - TGA for o-HTCC and o-HTCC nanoparticles with Mw=470 kDa.**

Adding doxorubicin to Cs Np's lead to slight changes in TGA analysis in comparison to only Cs NP's results, as it can be observed in Figure 6.7. First weight loss occurs at 61 ºC, which is similar to only Cs NP's that is around 65 ºC and do not possess the loss around 100ºC, related to residual water in the sample. Then DOX loaded Cs NP's only suffers another weight loss at 255 ºC, due to chitosan degradation. At the final, the weight loss of DOX loaded Cs NP's is around 15% higher than only Cs NP's, leading to a total weight loss of around 55%. This can lead to the conclusion that DOX somehow stabilizes chitosan nanoparticles and lead to a less sensibility to temperature, as chitosan degradation appear to be lower in this case.

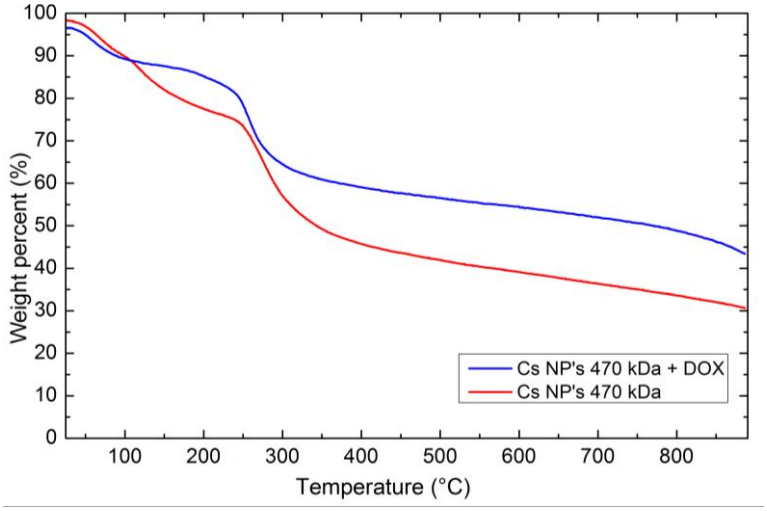


**Figure 6.7 - Comparison of TGA analysis of Cs NP's with and without DOX.**

For the case of DOX loaded in *o*-HTCC nanoparticles, the comparison of TGA with only *o*-HTCC NP's is represented in Figure 6.8. It is visible that the curves are similar, with weight losses happening in almost the same temperatures. In this case there are two relevant weight

losses: below 100 ºC, due to residual water present in the samples, and around 250 ºC, caused by *o*-HTCC degradation. In the presence of DOX, this type of nanoparticles lost around 45% of weight, instead of 55%.

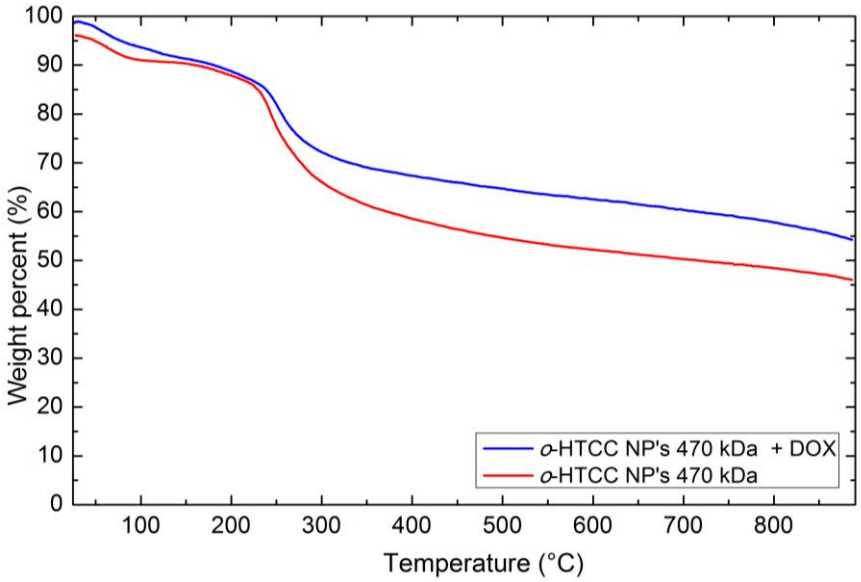


**Figure 6.8 - Comparison of TGA analysis of o-HTCC NP's with and without DOX.**

## 6.2 DOX encapsulation efficiency

Simultaneously to drug release experiments, DOX encapsulation efficiency in chitosan nanoparticles was studied and three parameters were tested. On one hand, the proportion between the crosslinking agent (TPP) and chitosan was varied, maintaining initial drug amount. As it can be seen in Figure 6.9, the higher the TPP:Cs ratio, the higher will be DOX encapsulation efficiency, achieving a value around 70%. Also no significant difference of EE for 1:1.6 and 1:0.533 of TPP:Cs ratio is verified, even though the initial concentration of DOX is slightly different: 1.33 mg/ml and 1 mg/ml, respectively. This occurred possibly due to a saturation of chitosan, ceasing to exist regions in the polymer to bond with the drug. It is also observed that for a low quantity of TPP in respect to chitosan, which means a low ratio between them (1:4.8), there is no encapsulation of DOX in the nanoparticles. Therefore, choosing the right proportion between chitosan and crosslinking agent is really important when designing a system for drug delivery, as it influences the percentage of drug encapsulated in the nanoparticles.

Simultaneously, the influence of the molecular weight of chitosan in DOX encapsulation efficiency was tested when varying TPP:Cs ratios. No significant differences in DOX encapsulation efficiency for the four molecular weights are verified, indicating that this parameter does not influence the encapsulation efficiency of this drug.

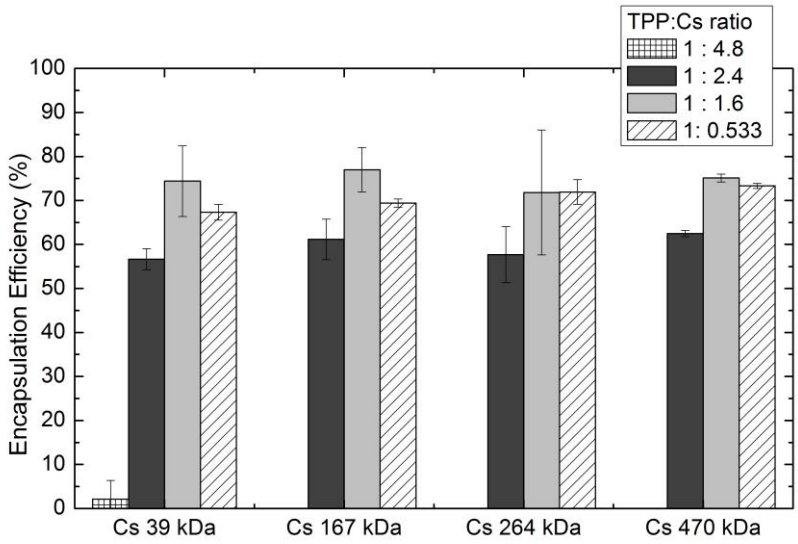


**Figure 6.9 - DOX encapsulation efficiency for chitosan nanoparticles for different TPP:Cs ratios.**

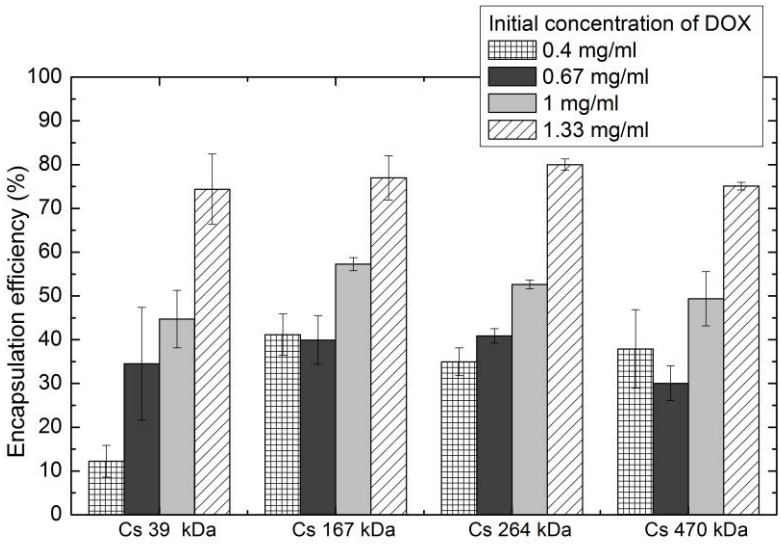


**Figure 6.10 - DOX encapsulation efficiency in Cs NP's for different initial concentrations of drug.**

On the other hand, DOX amount during formation of nanoparticles was changed, in order to evaluate how this parameter could affect the encapsulation efficiency. As it is evident in Figure 6.10, increasing the initial quantity of DOX in the formation of chitosan nanoparticles also increases its encapsulation efficiency, for most of chitosan molecular weights. No saturation of chitosan was verified in this case and an encapsulation of around 80% was achieved for the highest drug concentration tested. Apparently, there is also no significant variation between the different Cs molecular weights in this case of study, except for the lowest molecular weight (Cs

39 kDa) in the lowest concentration of drug used (0.4 mg/ml), as it has around 12% of efficiency versus an EE around 35% for the remain molecular weights.

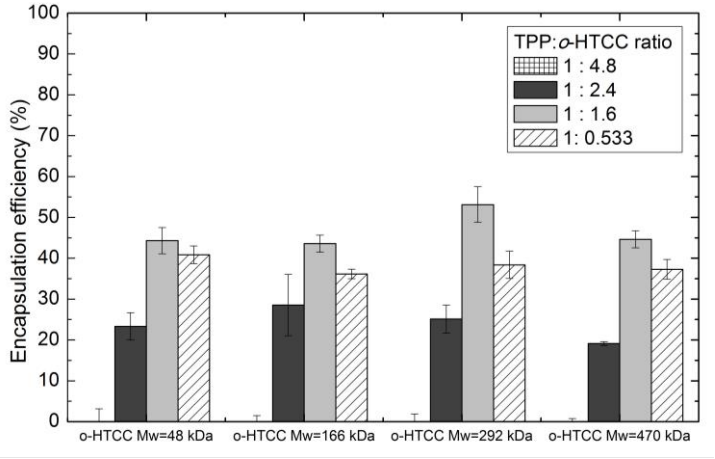


**Figure 6.11 - DOX encapsulation efficiency in o-HTCC nanoparticles for different TPP:o-HTCC ratios.**

DOX encapsulation efficiency into *o*-HTCC nanoparticles was also evaluated, where the influence of TPP proportion to *o*-HTCC was studied, with a DOX initial concentration of 1 mg/ml. These results are graphically presented in Figure 6.11. As it occurred to chitosan nanoparticles, for 1:4.8 TPP:*o*-HTCC ratio there is no DOX encapsulation, which probably means that there is no formation of *o*-HTCC nanoparticles in this case, so DOX stays free in solution and is all removed from the supernatants resultant from centrifugations. In this type of nanoparticles, the highest EE percentage was for a proportion between TPP and *o*-HTCC of 1:1.6 and was around 45%. Comparing this value with the same case in chitosan nanoparticles, encapsulation efficiency was substantially lower than in Cs NP's, which can be justified by higher electronic repulsion in *o*-HTCC, as it has more positive charges in its surface. These different TPP:*o*-HTCC ratios were also tested for the different *o*-HTCC molecular weights and there is conformity of results between them, existing only slightly differences of percentage of encapsulation between each of them. It is possible then to conclude that *o*-HTCC molecular weight does not influence the encapsulation efficiency of doxorubicin in this type of nanoparticles.

At last, DOX encapsulation efficiency for coated superparamagnetic iron oxide nanoparticles (SPION's) was determined in the conditions used in further work, when studying DOX release profile from this type of nanoparticles. Thus, to a ratio between the crosslinking agent (TPP) and the polymer, chitosan or *o*-HTCC, of 1:0.533 and to an initial concentration of DOX of 1 mg/ml, the encapsulation efficiency obtained is summarized in Table 6.5. Comparatively to what happened in the case of chitosan nanoparticles in these conditions, where the percentage of DOX encapsulation was 67% and 73% for Cs 39 kDa and 470 kDa, respectively, the values are lower in the case of Cs coated SPION's. This is possibly due to SPION's affinity to the posi-

tive charges of chitosan, occupying the spaces where doxorubicin could bind to chitosan. In the case of *o*-HTCC NP's, in these conditions the encapsulation efficiency was around 41% and 37% for *o*-HTCC 48 kDa and 470 kDa, respectively, and comparing with the values of SPION's coated with this polymer (Table 6.5), it is noted that there was an increase in the percentage of DOX encapsulation. This probably occurred due to the presence of more positive charges in *o*-HTCC, as it has been referred before, leading to more spaces to SPION's and DOX bind, leading to a higher % EE.

**Table 6.5 - DOX encapsulation efficiency in coated superparamagnetic iron oxide nanoparticles.**

| | **Cs SPION's** | | ***o*-HTCC SPION's** | |
|---|---|---|---|---|
| | **Cs 39 kDa** | **Cs 470 kDa** | ***o*-HTCC 48 kDa** | ***o*-HTCC 470 kDa** |
| **Encapsulation Efficiency (%)** | 54 ± 4 | 60 ± 1 | 52 ± 3 | 54 ± 9 |

## 6.3 DOX release studies

Doxorubicin release studies in mediums with different pH were performed for free DOX, as a control and a way to understand this drug behaviour to the variation of pH, and for the different nanocarriers under investigation. In Figure 6.12 are presented the results of free DOX release for the pH 7.4, 6.5 and 4.5. It is visible that this drug behaves differentially for each pH, presenting a faster release in the most acidic medium. In this pH (4.5) DOX is completely released in the first 8h achieving then a plateau. In the intermediate pH (6.5) DOX is almost totally released, achieving 90% release threshold, possibly because of its great stability in pH between 3 and 5 [4]. As in the case the neutral pH (7.4) this drug is not entirely released; only 60% of it gets out of the dialysis membrane.

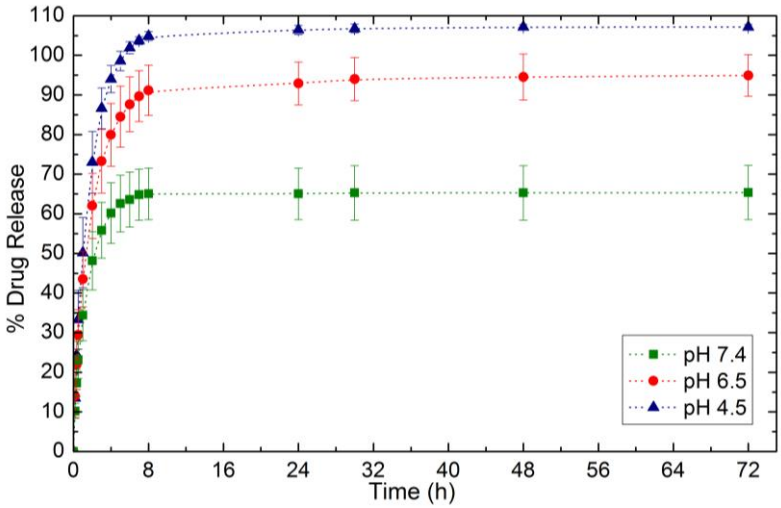


**Figure 6.12 - Release of free DOX for different pH of the medium (controls).**

After observing this behaviour, the main purpose of designing a drug carrier for doxorubicin is to achieve a controlled release, maintaining pH sensitivity.

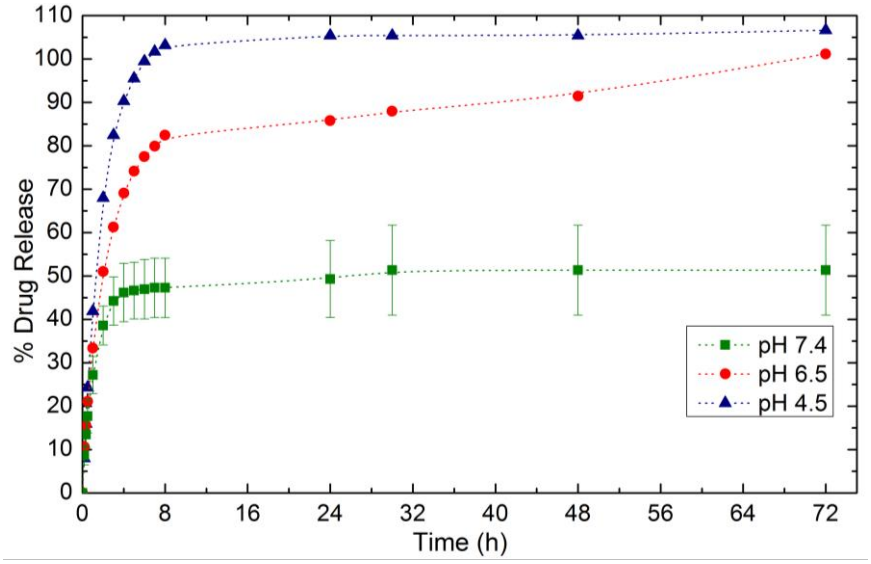


**Figure 6.13 - DOX release from non-freeze-dried chitosan nanoparticles with Cs 39 kDa for different pH.**

In a first approach, doxorubicin release profiles were performed in chitosan nanoparticles in solution, which means that chitosan was already in a certain swollen state. In Figure 6.13 the results of DOX release in the case of non-freeze-dried chitosan nanoparticles with 39 kDa are represented. Several things can be observed in this graphic. First, it is visible the different percentage of drug release in the three pH, maintaining a similar profile to free DOX release. Comparing with those controls it is possible to conclude that these non-freeze-dried nanoparticles did not allow such a controlled release as it was thought, as there was only a slightly decrease in the percentage of drug release achieved in each pH; except for 4.5 where all drug was released. As this drug presents a higher release in more acidic mediums, it can indicate that DOX is favourably released in the endosomal/lysosomal compartment of the cell, where it is more protected from drug efflux [6]. Something not expected occurred for pH 6.5 as the plateau was not achieved after the 72h of the experiment, probably due to experimental error. A burst release is observed in the first 8h in the case the more acidic mediums and in the first 4h for pH 7.4 and it was slower for the rest of the time of experiment. This burst effect is unlikely to be due to DOX that did not encapsulate in the nanoparticles, as centrifugations were performed to remove this percentage of drug.

After some trials using these non-freeze-dried nanoparticles, freeze-drying the samples before starting the release in the buffer solution was tested. And this was the chosen procedure for all the other experiments of DOX release performed.

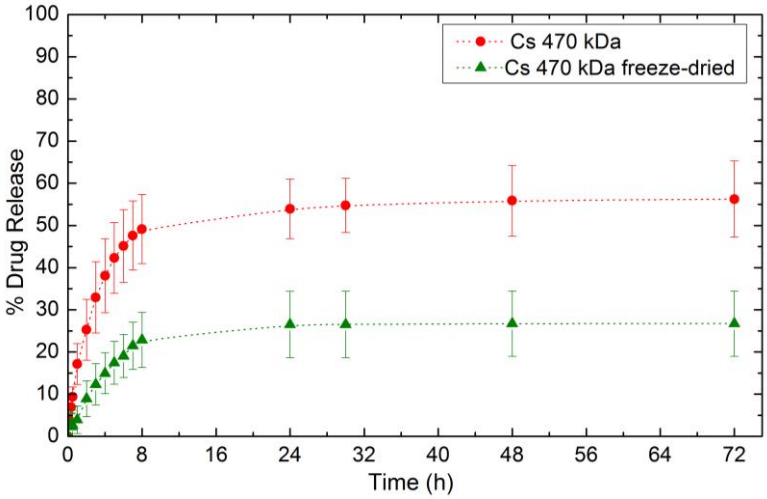


**Figure 6.14 - Comparison of DOX release between freeze-dried and non-freeze-dried Cs NP's with Cs 470 kDa for pH 7.4.**

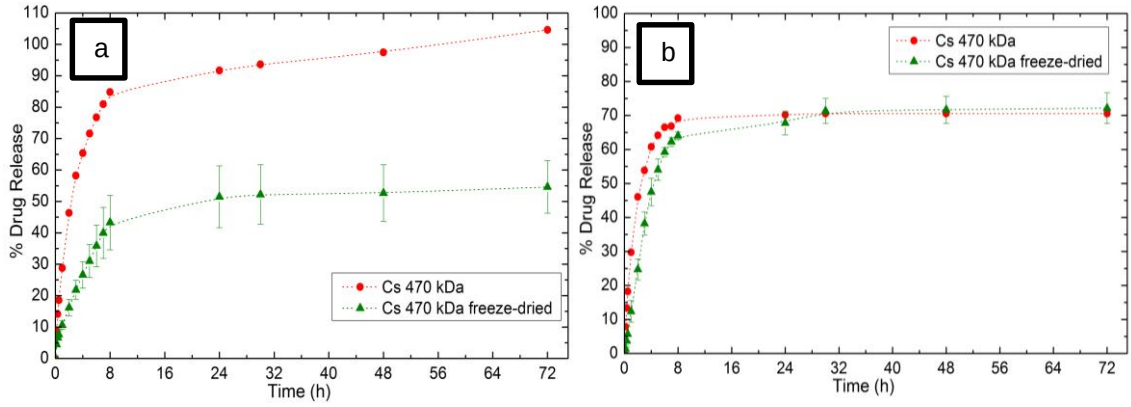


**Figure 6.15 - Comparison of DOX release between freeze-dried and non-freeze-dried Cs NP's with Cs 470 kDa for (a) pH 6.5 and (b) pH 4.5.**

In this way, for chitosan nanoparticles exists results from both methods, allowing a comparison of the percentage of DOX release between freeze-dried and not freeze-dried samples. In Figure 6.14 and Figure 6.15 are represented the results for this two methods using chitosan nanoparticles with Cs 470 kDa, the highest molecular weight, for each pH. It is visible a huge difference between them for pH 7.4 (Figure 6.14) and 6.5 (Figure 6.15 (a)), as it achieves a lower percentage in the case of freeze-dried nanoparticles; at pH 7.4 it reaches only 26% instead of the 56% of release from the non-freeze-dried and for 6.5 the freeze-dried releases 55% instead of 100%. Also in this intermediate pH it reaches a more stable plateau, in contrary of what happened to the non-freeze-dried, where no stability was achieved. In these pH it is clear that freeze-drying the nanoparticles is a good procedure as it leads to a more controlled release, as chitosan is not in a swollen state and starts to release DOX slowly and with more control. As for pH 4.5, represented in Figure 6.15 (b) the release curves are similar and achieve the same percentage of 70%. This possibly occurred because an acidic environment is favourable for both doxorubicin and chitosan and being dry does not change this characteristic.

Considering only the release experiments with freeze-dried chitosan nanoparticles, a controlled release in the three different mediums investigated was verified. In this case the influence of chitosan molecular weight in DOX release profile was also evaluated. In Figure 6.16 are the results of DOX release from chitosan nanoparticles synthetized with different chitosan molecular weights, in comparison with the control of releasing free DOX, for pH 7.4. It is visible that the curves are similar but the percentage of release is in a wide range, between 20% and 40% for the four Mw, which is low as expected, as there is no interest in releasing a great amount of drug in the pH that represents the bloodstream. A standard could be expected for the release percentage with the molecular weight, for example an increased release for higher molecular weights, or the contrary. However it is visible that for pH 7.4 the release increases by a random order of molecular weight: Cs 39 kDa, Cs 470 kDa, Cs 167 kDa and Cs 264 kDa. Therefore, the molecular weight does not seem to influence DOX release from Cs NPs.

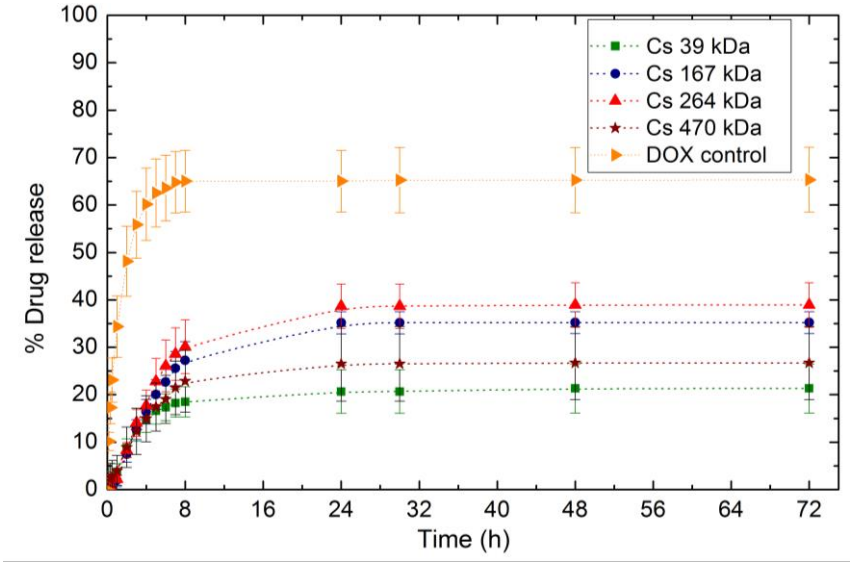


**Figure 6.16 - DOX release profile from Cs NP's for different chitosan molecular weights at pH 7.4.**

In the most acidic medium (pH 4.5) there are also no significant differences between DOX release for each molecular weight, as it is seen in Figure 6.16, achieving all around 70% of release.

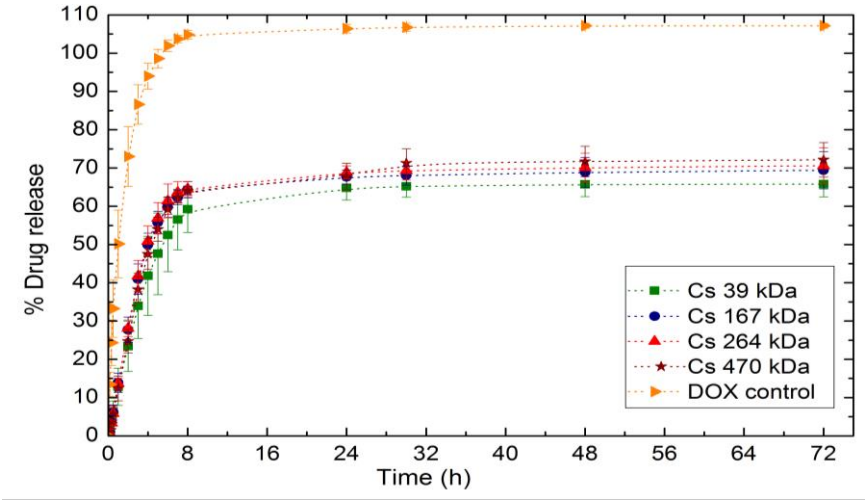


**Figure 6.17 - DOX release profiles from chitosan nanoparticles for different Cs molecular weights for pH 4.5.**

This fact is possibly due to the acidity of the medium and the swelling of chitosan in these conditions, thus chitosan network achieves the same swollen state independently of its molecular weight, releasing the same quantity of DOX. The same situation occurred for pH 6.5, even though the results are not graphically presented (Appendix A - Figure 0.1); the total release was about 60% in this medium. Since the molecular weight does not seem to influence DOX release, a comparison was performed using the lowest Mw and changing the pH of release medium (Figure 6.18). It can be observed that there are no meaningful differences between pH 6.5 and 4.5, which may not be a significant difference to change the swelling state of chitosan, and therefore, DOX release behaviour.

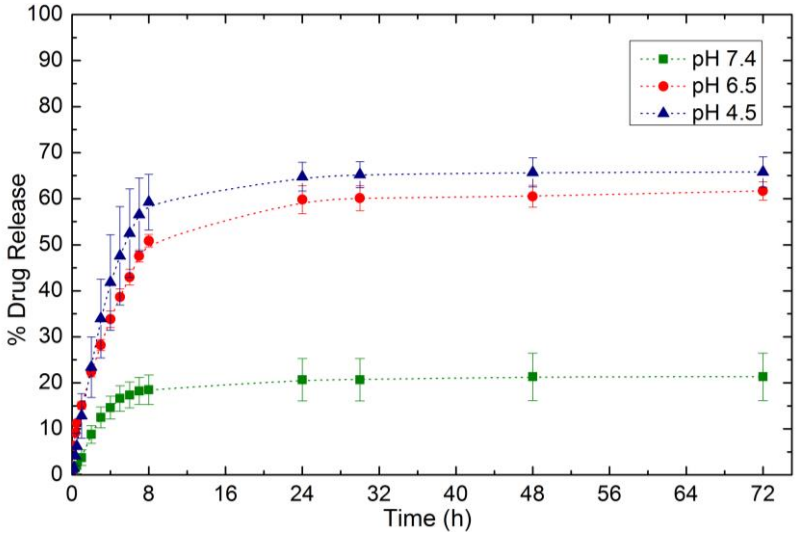


**Figure 6.18 - DOX release profile from chitosan nanoparticles with Cs 39 kDa for different pH.**

Doxorubicin release was also studied for nanoparticles synthetized with *o*-HTCC. This nanocarrier also presents pH-sensitivity, behaving like chitosan with the variation of the medium and releasing more quantity of drug in the most acidic one. In a first look to the graphics for the *o*-HTCC nanoparticles with lowest molecular weight (Figure 6.19 (a)), the initial release seems to be longer, as the curve slope is smaller, taking more time to achieve the plateau. This is more visible in the case of pH 6.5 for these nanoparticles, as it only stabilizes after 48h of *in vitro* releasing.

The influence of the molecular weight in DOX release was also studied for *o*-HTCC NP's. At pH 7.4 the curves of the four molecular weights almost match each other, achieving around 20% however at pH 6.5 and 4.5 the values of release are in the range of 50%-70% and 60%-85%, respectively. Thereby, it can be concluded that the molecular weight of *o*-HTCC influences DOX release, especially in the case of pH 6.5 where the release curves are quite different between them.

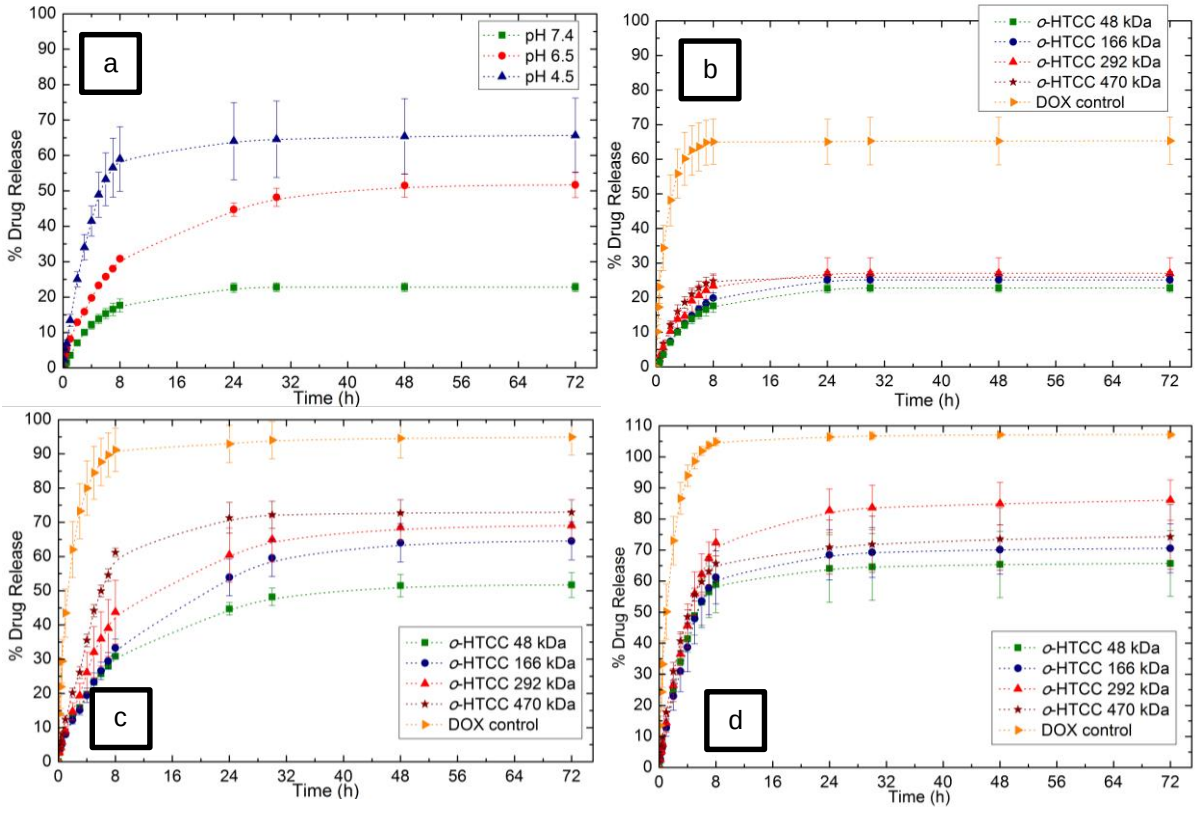


**Figure 6.19 - DOX release profile from o-HTCC nanoparticles (a) with o-HTCC 48 kDa for different pH and for different molecular weights for (b) pH 7.4, (c) pH 6.5 and (d) pH 4.5.**

This chitosan derivative has increased water solubility in a wide pH range when compared to chitosan itself [36]. In this way it could be predictable that *o*-HTCC nanoparticles would release doxorubicin differently than chitosan nanoparticles, especially at pH 7.4, where the sol-

ubility of the polymers is really diverse. Figure 6.20 presents the release results for either chitosan or *o*-HTCC nanoparticles with the highest molecular weight, Cs 470 kDa and *o*-HTCC 470 kDa, respectively. It is presented only this one but the same phenomena have happened for the other molecular weights. As it is observed in figure 6.12 (a) and (c), for the pH 7.4 and 4.5 the curves totally match, allowing to conclude that for these mediums DOX release happens in the same way for both Cs and o-HTCC nanoparticles. Although this is not the case of pH 6.5, where *o*-HTCC nanoparticles released a higher percentage (around 70%) than chitosan nanoparticles (around 50%).

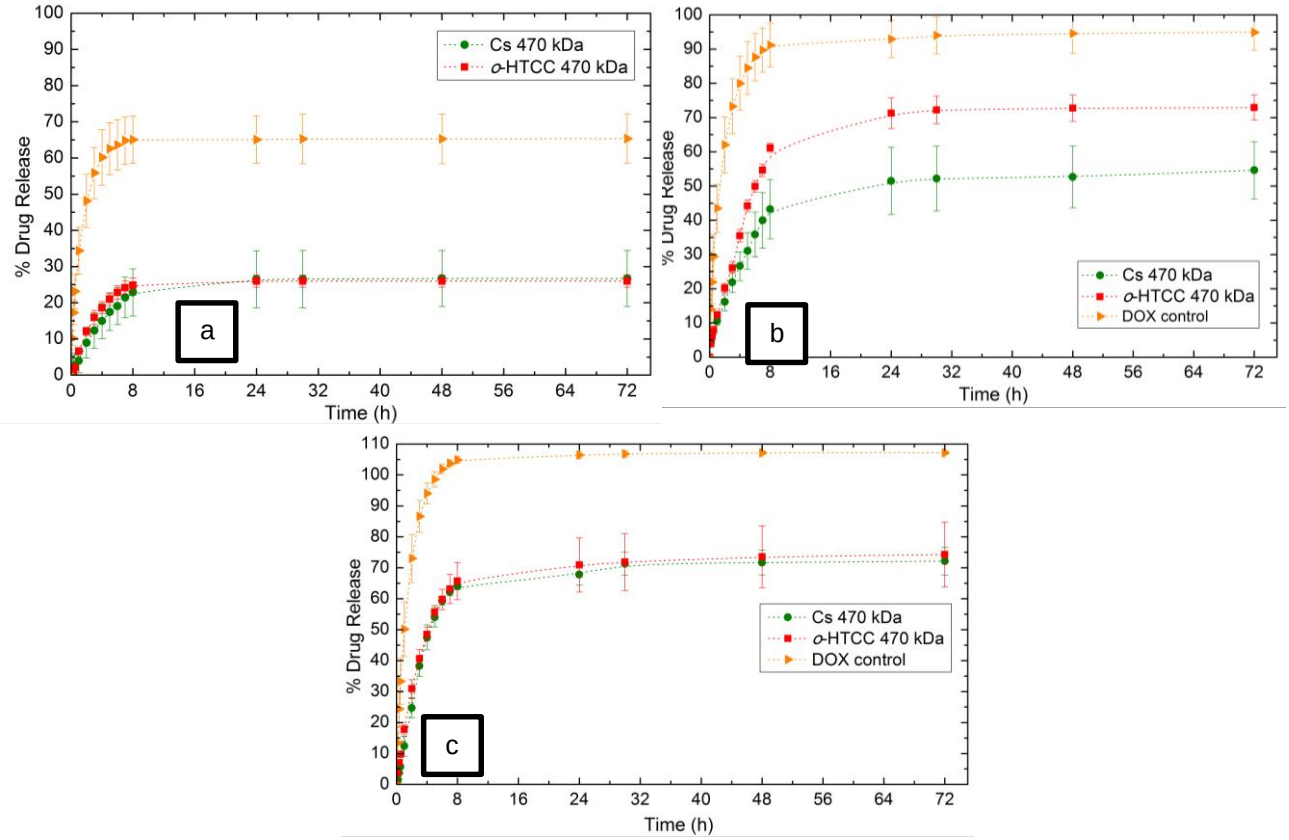


**Figure 6.20 - Comparison of DOX release from Cs NP's and o-HTCC NP's for Mw 470 kDa at (a) pH 7.4, (b) pH 6.5 and (c) pH 4.5.**

Finally, doxorubicin release studies from coated, with either chitosan or *o*-HTCC, superparamagnetic iron oxide nanoparticles were performed. These experiments were made using only the polymers with the highest and the lowest molecular weights. Analysing first the ones, with chitosan coating, the results are presented in Figure 6.21.

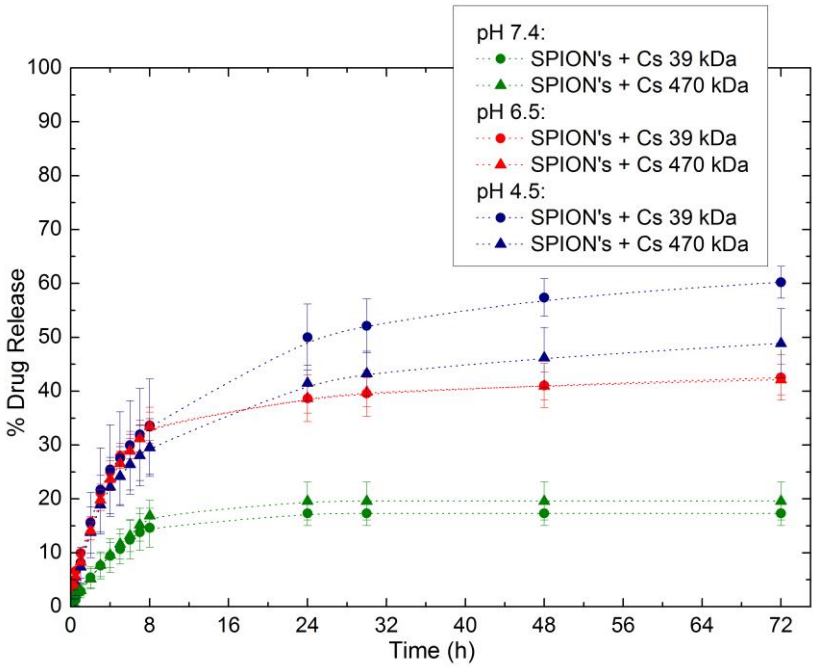


**Figure 6.21 - DOX release profiles from Cs SPION's with two molecular weights and for different pH.**

The curves present similarity to the ones without magnetic nanoparticles and the different release between the three pH is still observed. Still, it's observable that it takes more time in this case to achieve the stability, especially for the most acidic medium. Observing these graphics it is also visible that on the first 8h of trial, the curve of release is quite similar for pH of 6.5 and 4.5, possibly releasing DOX molecules that are more in the surface of the nanoparticles, and not truly encapsulated. When comparing the two chitosan molecular weights it seems that they don't cause differences in the release, except for the most acidic medium (pH 4.5), where the release is higher for the lowest molecular weight, even though the difference is not that meaningful as it releases 60% instead of the 50% from the highest molecular weight.

In comparison to chitosan nanoparticles, the release curves are almost the same for pH 7.4, achieving 20%, reason why the graphics are not shown (Appendix A- Figure 0.2). As for the other pH, the graphics are presented in Figure 6.22, and the release is substantially different, being lower in the case of Cs SPION's. For the intermediate pH, Figure 6.22 (a), the percentage of release only reaches 40%, instead of the 60% of chitosan nanoparticles. This low value is possibly due to some DOX molecules that are bonded to the iron oxide core through hydrophobic interactions, leading to a limited DOX release [6]. As for the most acidic medium, DOX release achieves almost the same percentage value (around 60%), although it has a slower release, as it only achieves the plateau after 48h of trial.

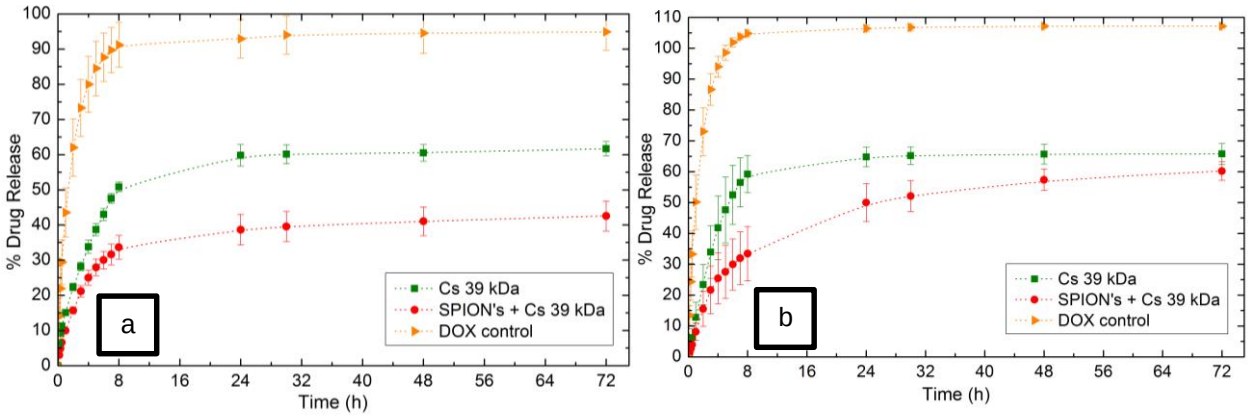


**Figure 6.22 - Comparison of DOX release profiles between Cs NP's and CS SPION's with Cs 39 kDa for (a) pH 6.5 and (b) pH 4.5.**

Observing now the results of DOX release from *o*-HTCC SPION's presented in Figure 6.23, it is visible that the differences between the release for pH 6.5 and 4.5 are minimal, in particular in the first 8h of trial. The difference in the pH between 6.5 and 4.5 is probably not relevant for the composition of *o*-HTCC, behaving almost the same way for each of them. Comparing the two molecular weights of o-HTCC used to coat the SPION's, it is also observable that this parameter does not influence much DOX release from this type of nanoparticles.

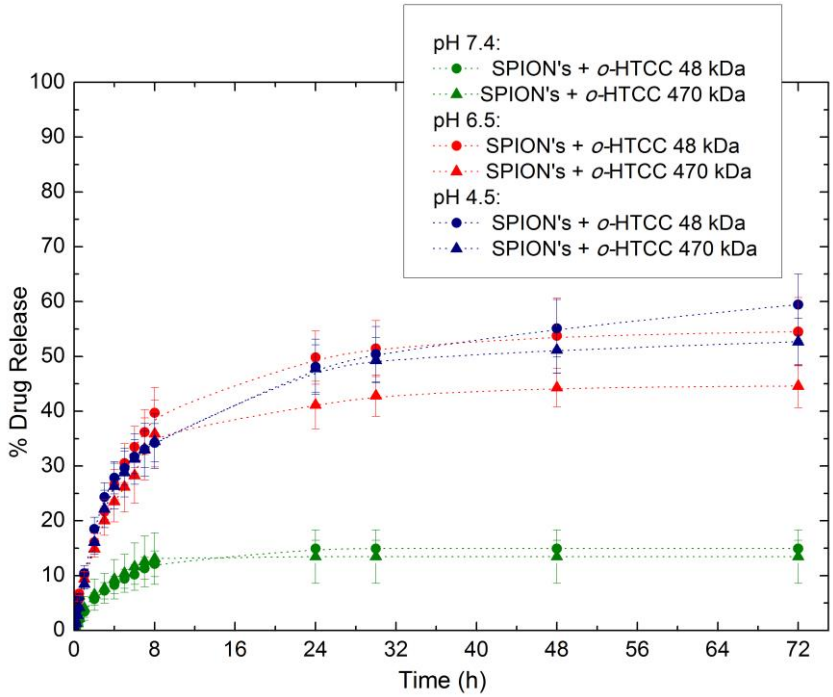


**Figure 6.23 - DOX release profiles from o-HTCC SPION's with two molecular weights and for different pH.**

## 6.4 Mathematical modelling of DOX release profiles

For the application of the mathematical models that are used to describe drug release profiles was used DDSolver, an add-in for Excel. This software application is easy to use, as the user only needs to select the release data of some experiment, a column of the time intervals, set the time unit where data was collected, e.g. minutes or hours, and choose the model to apply. After these steps, press "Run" and after some seconds a new excel sheet is created with all the results for this specific modulation. In this sheet, are all the data inserted by the user, predicted data calculated by the application, model constants and statistical values evaluating the correlation between data and modelling results. In this way, this procedure was made for all DOX release experimental data and the best fit was evaluated through the correlation coefficient ($R^2$). The model with the highest correlation coefficient is the model that best describes that drug release [5, 75]. Some examples of DDSolver add-in menus are shown in appendix B. As an example, a graphic from this simulator for the application of Korsmeyer-Peppas to DOX release from freeze-dried Cs 470 kDa NP's at pH 4.5 is shown in Figure 6.24.

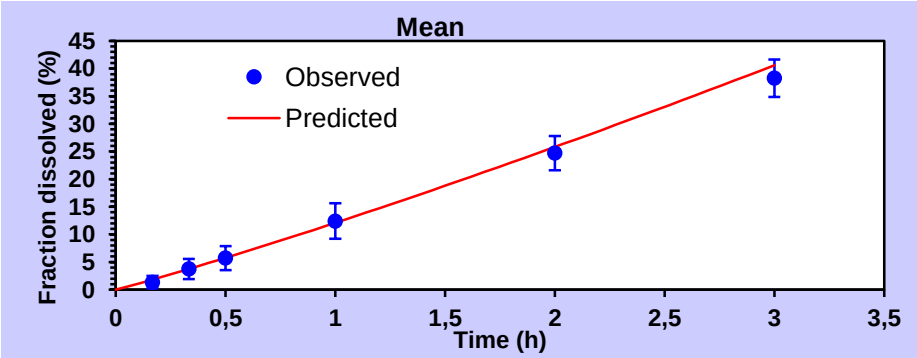


**Figure 6.24 - Example of Korsmeyer-Peppas model fitting DOX release data from freeze-dried Cs 470 NP's at pH 4.5.**

The applied models were: zero-order, first order, Higuchi, Hixson-Crowell, Hopfenberg, Korsmeyer-Peppas, Weibull and Peppas-Sahlin. After applying all of these to DOX release data from each type of nanoparticles studied, was verified that the correlation coefficients resultant from the simulations were really small or even negative for some models, which has no sense in mathematical terms. The models in question are zero-order, first order, Higuchi, Hixson-Crowell and Hopfenberg. This happened due to a non-fit of these models to the data, signifying that these models do not represent the drug delivery system in study, as it could be expected, with the theoretical knowledge about them. Considering zero-order kinetics, as it is most used for low soluble drugs in matrix tablets, it was predictable that this was not the right model to describe DOX release from the nanocarriers in study, as they are nanoparticles. Also first-order kinetics was not expected to best fit our data as it describes drug absorption and is especially used in the case of water-soluble drugs in some porous material. In the case of Higuchi, it was also predictable that it wouldn't fit, as it consider some conditions contradictory to chitosan na-

noparticles and the other nanocarriers studied in this work, such as non-swelling of matrix or drug diffusion in only one direction, and it is typically used for matrix tablets [51]. As for Hixson-Crowell model it is applicable for systems where the surface area and diameter of tablet or particle is maintained constant, being more used for tablets. As chitosan presents swelling behaviour, especially when varying its medium, there was no chance that its surface area did not suffer changes, so this model was expected not to fit. Finally, Hopfenberg model describes drug release from eroding polymers and its area is also maintained constant, which again has no concordance to what is known about chitosan. In this way, the results of fitting these models to experimental data are not shown, as they do not fit and make sense to the type of drug delivery system that is being studied. In this way, only the results from Korsmeyer-Peppas, Weibull and Peppas-Sahlin models are going to be examined in detail to each experiment of *in-vitro* release performed.

In order to better analyse the results it is important to remember each of these three models. Starting with Korsmeyer-Peppas model it has two constants, $n$ and $k$, that give information about release profile. The first one, $n$ exponent, informs about release mechanism in action. If $n \leq 0.43$ it is a Fickian diffusion type of release; for $n = 0.85$ it is a case II transport, mostly related to polymer matrix relaxation and swelling; in the case of $0.43 < n < 0.85$ it tells us that it is an anomalous transport, resultant from a combination of Fickian diffusion and case II transport; and if $n > 0.85$ it is a super case II transport [49]. In this model, $k$ constant is related to polymer structure and shape [33]. Weibull model it also has two constants: $a$, a time factor, and $b$, related to the shape of release curve. As it was already mentioned in chapter 4, this $b$ constant can be correlated to $n$ exponent of Korsmeyer-Peppas and also allow some definition of the release mechanism: $b \leq 0.75$ it is a Fickian diffusion; for $0.75 < b < 1$ is a combined mechanism, between Fickian diffusion and Case II transport, and finally for $b > 1$ drug is released through a complex release mechanism [59].

Starting with chitosan nanoparticles, its modelling results are presented in Table 6.6. According to correlation values, release data is well fitted to Weibull model in the case of pH 4.5 and 7.4 and to Korsmeyer-Peppas for pH 6.5. It should be noticed that these two models are only applicable for the first 60% release, coinciding with the first 3 to 5 hours of release, where it has a straight profile. Although these models had the greatest correlation coefficients, it is noticeable that the differences between those values for the three models are almost insignificant, especially in the case of Weibull and Korsmeyer-Peppas. Observing the results for Peppas-Sahlin model for all samples of chitosan nanoparticles, constant *k1* is always much higher than *k2*, which even has negative values, leading to the conclusion that the release happened more through Fickian diffusion and with less contribution of chitosan relaxation, according to this model parameters. However, the m exponent should be similar to the $n$ exponent of Korsmeyer-Peppas model, but in these simulations it was always obtained $m = 0.45$, which is much lower than $n$ values for these samples, but stays in the interval correspondent to an anomalous re-

lease. This fact may lead to the conclusion that probably this Peppas-Sahlin model was not well simulated and predicted by DDSolver. It is also noticeable that correlation coefficient for this model is greater for pH 4.5 and for the other two mediums $R^2$ is not quite good to say that it fits the data.

Observing results of DOX release from freeze-dried Cs NP's in pH 4.5, Weibull model is the best fit and it is visible that for freeze-dried samples constant *b* is always higher that 1, meaning that this release mechanism is really complex, possibly due to a swelling behaviour of chitosan in this pH [59]. The other constant *a* has a value around 8 for the four molecular weights. Looking for Korsmeyer-Peppas results for these samples, *n* exponent is higher than 0.85 for all molecular weights, which indicates super case II transport, also meaning a complex release [49]. The constant *k* in this model gives information about shape and structure of the polymer and it is possible to see that there are no significant changes in chitosan nanoparticles structure for its different molecular weights at this acidic pH, as *k* values are in the same range.

In the case of DOX release from not freeze-dried Cs NP's at pH 4.5 also Weibull model is the best fit, as it was referred before. The *b* constant of this model is only higher than 1 for chitosan nanoparticles with the lowest molecular weight, meaning that with this nanocarrier DOX release happened through a complex procedure. For the other molecular weights it is visible that *b* value decreases while molecular weight increases and stays between 0.75 and 1, which means that release results from a combination between Fickian diffusion and case II transport. The other constant *a* increases with increasing chitosan molecular weight. As for the case of Korsmeyer-Peppas model, also *n* exponent decreases with increasing molecular weight, maintaining a correlation with *b* value. In this model, it is only super case II for Cs 39 kDa and Cs 167 kDa; for the two highest molecular weights it is described as an anomalous release, with similar relaxation and diffusion rates. Comparing with freeze-dried samples, apart from some difference in the release mechanism, there is also a difference in the constant *a*, related to shape and structure of chitosan nanoparticles. This value is substantially higher for the case of not freeze-dried samples (between 30 and 50) and it has a wide range in this case. This is possibly because chitosan nanoparticles are in solution and do not possess exactly the same structure between them and it is much different of freeze-dried, that are not in a swollen state. Taking into account the graphical information of these releases contained in subchapter 6.3, where release curves were coincident for both freeze-dried and not, these models, especially Weibull as it is the best fit for this pH, indicate that release mechanism is the same for almost all molecular weights, being a complex mechanism as a result from a combination between Fickian diffusion and relaxation of polymer chains.

**Table 6.6 – DOX release from chitosan nanoparticles modelling with Korsmeyer-Peppas, Weibull and Peppas-Sahlin models.**

| pH | Cs Mw (kDa) | Freeze-dried | Korsmeyer-Peppas | | | Weibull | | | Peppas-Sahlin | | | |
|---|---|---|---|---|---|---|---|---|---|---|---|---|
| | | | *n* | *K* | $R^2$ | *a* | *b* | $R^2$ | $K_1$ | $K_2$ | *m* | $R^2$ |
| 4.5 | 39 | Yes (Y) | 1.124 ± 0.219 | 11.578 ± 4.556 | 0.971 | 8.978 ± 4.874 | 1.136 ± 0.248 | **0.989** | 22.369 ± 0.804 | -1.971 ± 0.134 | 0.45 | 0.965 |
| | | No (N) | 0.930 | 43.672 | 0.992 | 1.802 | 1.052 | **0.998** | 40.363 | -4.006 | 0.45 | 0.918 |
| | 167 | Y | 0.985 ± 0.042 | 13.180 ± 2.790 | 0.952 | 8.076 ± 2.812 | 1.441 ± 0.497 | **0.969** | 19.154 ± 0.232 | -1.581 ± 0.142 | 0.45 | 0.957 |
| | | N | 0.895 | 50.992 | **0.926** | 1.565 | 0.995 | 0.921 | 37.265 | -3.544 | 0.45 | 0.928 |
| | 264 | Y | 1.158 ± 0.216 | 12.631 ± 1.612 | 0.963 | 8.616 ± 2.184 | 1.507 ± 0.582 | **0.972** | 19.522 ± 4.109 | -1.536 ± 0.650 | 0.45 | 0.945 |
| | | N | 0.775 | 36.373 | 0.977 | 2.001 | 0.924 | **0.989** | 47.378 | -4.518 | 0.45 | 0.938 |
| | 470 | Y | 1.122 ± 0.245 | 12.089 ± 3.178 | 0.979 | 8.267 ± 2.266 | 1.269 ± 0.230 | **0.992** | 17.962 ± 3.333 | -1.454 ± 0.296 | 0.45 | 0.953 |
| | | N | 0.742 | 30.145 | 0.999 | 2.824 | 0.814 | **1.000** | 39.501 | -3.720 | 0.45 | 0.946 |
| 6.5 | 39 | Y | 0.518 ± 0.025 | 15.918 ± 0.818 | **0.996** | 5.675 ± 0.314 | 0.569 ± 0.027 | 0.993 | 25.838 ± 4.918 | -2.402 ± 0.742 | 0.45 | 0.903 |
| | | N | 0.642 | 32.787 | **0.999** | 2.442 | 0.754 | 0.997 | 53.200 | -5.805 | 0.45 | 0.893 |
| | 167 | Y | 0.566 ± 0.061 | 12.785 ± 1.054 | **0.992** | 7.470 ± 1.128 | 0.640 ± 0.117 | 0.989 | 29.241 ± 1.441 | -2.872 ± 0.320 | 0.45 | 0.884 |
| | | N | 0.631 | 28.729 | **0.998** | 2.814 | 0.748 | 0.997 | 40.609 | -4.726 | 0.45 | 0.775 |
| | 264 | Y | 0.633 ± 0.110 | 11.887 ± 3.762 | **0.973** | 8.876 ± 4.539 | 0.701 ± 0.240 | 0.973 | 29.819 ± 1.810 | -2.934 ± 0.390 | 0.45 | 0.882 |
| | | N | 0.684 | 32.349 | 0.996 | 2.306 | 0.869 | **0.998** | 47.703 | -5.245 | 0.45 | 0.894 |
| | 470 | Y | 0.564 ± 0.027 | 11.699 ± 1.426 | **0.989** | 8.320 ± 1.309 | 0.658 ± 0.088 | 0.986 | 28.321 ± 1.437 | -2.646 ± 0.163 | 0.45 | 0.892 |
| | | N | 0.656 | 28.884 | **0.999** | 2.785 | 0.779 | 0.998 | 35.867 | -3.943 | 0.45 | 0.902 |
| 7.4 | 39 | Y | 0.733 ± 0.149 | 4.430 ± 1.073 | **0.980** | 22.558 ± 7.707 | 0.753 ± 0.158 | 0.978 | 7.428 ± 1.882 | 1.729 ± 0.265 | 0.45 | 0.894 |
| | | N | 0.634 ± 0.097 | 27.238 ± 4.629 | 0.998 | 3.232 ± 0.657 | 0.711 ± 0.100 | **0.999** | 26.928 ± 3.780 | -3.024 ± 0.345 | 0.45 | 0.834 |
| | 167 | Y | 1.446 ± 0.139 | 2.475 ± 0.809 | **0.936** | 200.659 ± 257.356 | 2.347 ± 0.936 | 0.849 | 11.142 ± 1.660 | -0.838 ± 0.248 | 0.45 | 0.888 |
| | | N | 0.757 ± 0.214 | 40.154 ± 10.905 | 0.945 | 2.062 ± 0.923 | 0.910 ± 0.195 | **0.961** | 35.079 ± 9.876 | -3.975 ± 1.114 | 0.45 | 0.825 |
| | 264 | Y | 1.232 ± 0.128 | 3.274 ± 0.892 | 0.947 | 42.433 ± 15.576 | 1.528 ± 0.091 | **0.949** | 12.407 ± 2.216 | -0.943 ± 0.230 | 0.45 | 0.887 |
| | | N | 0.912 ± 0.082 | 24.936 ± 5.704 | **0.987** | 3.700 ± 0.939 | 0.967 ± 0.091 | 0.886 | 26.951 ± 1.511 | -2.843 ± 0.218 | 0.45 | 0.907 |
| | 470 | Y | 1.118 ± 0.425 | 4.156 ± 3.327 | 0.947 | 19.618 ± 14.641 | 0.735 ± 0.396 | **0.958** | 9.768 ± 3.232 | -0.856 ± 0.317 | 0.45 | 0.915 |
| | | N | 0.778 ± 0.106 | 16.539 ± 3.429 | 0.981 | 5.567 ± 1.180 | 0.861 ± 0.085 | **0.987** | 24.097 ± 3.908 | -2.406 ± 0.423 | 0.45 | 0.935 |

For pH 6.5, Korsmeyer-Peppas is the best fitting model, as it was mentioned before. In the case of freeze-dried Cs NP's *n* exponent value is similar for all molecular weights, being between 0.518 and 0.633. These values indicate that the release happened through a mixed Fickian and swelling mechanism. Compared to release in pH 4.5, these *n* values are quite lower, proving the differences of chitosan behaviour for different acidity of the medium. Observing the values for the other constant of this model, *k*, increasing the molecular weight leads to a decrease in its value, going from 15.918 to 11.699. This structure factor has similar values to the freeze-dried samples in pH 4.5. In the case of Weibull model results, the *b* constant is between 0.569 and 0.701, meaning that the release occurred through Fickian diffusion. This is contradictory to Korsmeyer-Peppas results, but there is no right explanation for this to happen, possibly due to some unknown effect that this pH gives to chitosan. Even though this contradiction and the small differences in the correlation coefficients of these two models, conclusions for release mechanism for these samples by Korsmeyer-Peppas model are the chosen ones, as it is the one that presents higher $R^2$. Which means it is considered a release through a combined mechanism of Fickian diffusion and case II transport.

As for the case of not freeze-dried chitosan nanoparticles, at pH 6.5, *n* exponent of Korsmeyer-Peppas is around 0.6, which also signifies that release happened through an anomalous non-Fickian mechanism. Weibull model results lead to a combined mechanism of Fickian and case II. Also no significant changes happened between molecular weights and in this pH, by applying this model, no difference in release mechanism between freeze-dried and not freeze-dried was verified. Comparing these results to the release graphics presented in subchapter 6.3, where there was a huge difference in the releasing curves of freeze-dried and non-freeze-dried Cs NP's, it can be concluded that even though it seemed a different release and it achieved different percentages, the mechanism of release was the same, if taking into account the best fit model. Looking for *b* value of Weibull model applied to non freeze-dried Cs NP's, it is between 0.748 and 0.869 which means that by this model it is a case of a mixed mechanism of Fickian diffusion and case II transport. Also in these results, no difference in release mechanism between molecular weights is noticed.

Finally, for the case of pH 7.4 the best fit is again Weibull model with its *b* constant with values between 0.861, for the highest molecular weight, and 2.347, for the lowest. It is visible in this case that increasing chitosan molecular weight increases *b* value and leads to different release mechanisms. For Cs 470 kDa release results from a combination between Fickian diffusion and case II relaxation transport, as *b* is between 0.75 and 1. As for the other three molecular weights it was a complex release mechanism, probably due to existence of different mechanisms at the same time, as *b* values were higher than 1. In the case of Korsmeyer-Peppas model applied to these data, for Cs 39 kDa n exponent is 0.733 and for the other molecular weights is higher than 1, which means anomalous release in the first one, and super case II for the others. As for the k constant, in this freeze-dried samples is around 2-4 for all molecular

weights, which is substantially lower than for the other pH. As for the non-lyophilized Cs NP's, at pH 7.4, for the Weibull model the results indicate a combined mechanism of Fickian diffusion and case II transport, related to relaxation of polymer chain, which is different from what is seen in the freeze-dried samples. As for Korsmeyer-Peppas model, *n* exponent indicate that release occurred through Fickian diffusion, as it is between 0.43 and 0.85, for all molecular weights except Cs 264 kDa. This is, once again, a contradiction of results between these two models.

Analysing now the results of modelling DOX release from freeze-dried *o*-HTCC nanoparticles, presented in table 6.10, Weibull model is the best fit for release in pH 4.5 and Korsmeyer-Peppas for the other two pH, although the differences in the correlation coefficient are almost insignificant. In these samples happened the same thing as for chitosan nanoparticles with Peppas-Sahlin model, as the *m* exponent obtained from the simulations was always 0.45 and should be closer to the *n* exponent of Korsmeyer-Peppas model. There is a huge difference between *k1* and *k2* constants, giving the possibility of a Fickian diffusion as mechanism of release, instead of being related to relaxation of polymer.

Observing the results for pH 4.5, in particular Weibull parameters, these values indicate that release happened by a combination of case II, related to polymer swelling, and Fickian diffusion, as they are all near 0.9. As for Korsmeyer-Peppas model, its *n* exponent is around 0.8 for the four molecular weights, which corresponds to an anomalous release, where there is a similarity in diffusion and relaxation rates. This is somehow consistent with the conclusions of Weibull model for these samples. It also complies with the results of DOX release from chitosan nanoparticles. Possibly this is due to the acidic medium, that causes the same changes in the polymers structure, with either chitosan or its derivative.

As for release in pH 6.5, n exponent values for Korsmeyer-Peppas model are around 0.6, meaning combination between Fickian diffusion and case II transport mechanism of release. In the case of Weibull model*, b* value is 0.850 for *o*-HTCC 268 kDa, which means that in this sample release happened through a mix between Fickian diffusion and case II. For the other molecular weights the *b* value is lower than 0.75, indicating that release happened through Fickian diffusion. There is no right explanation for this difference for the various molecular weights, as it is only different for an intermediate Mw. Also it has led to contradictory conclusions to Korsmeyer-Peppas, even though correlation coefficients have negligible differences between models. Curiously, the same was obtained and concluded in the case of DOX release from chitosan nanoparticles at this intermediate pH. Possibly this intermediate pH already dissolves chitosan, even though is a slightly high pH.

In the case of neutral pH, 7.4, the best fit is again Korsmeyer-Peppas model with *n* exponent values greater than 0.85 for all molecular weights of *o*-HTCC, which means a super case II mechanism of release. Observing Weibull results, it indicates that DOX release happened through a complex mechanism, due to *b* value always greater than 1. In this case both models

are in agreement. The exact same assumptions were made in the case of DOX release from chitosan nanoparticles at this pH.

Some other observations can be made about Korsmeyer-Peppas model, as the other constant *k*, related to shape and structure of the polymer, which decreases with increasing of pH, for all molecular weights. Also the a constant, time factor of Weibull model, increases with increasing the pH, possibly due to a slower release in the first ours in pH 7.4 and quicker in pH 4.5.

Observing now the modelling of release data from coated superparamagnetic iron oxide nanoparticles, presented in Table 6.7, the same thing that occurred in the other systems in the application of Peppas-Sahlin model happened here, as the *m* exponent is always the same for all samples and it is much different from *n* exponent of Korsmeyer-Peppas model. Again, it is concluded that this model was not applied correctly. In this way, again the results from the other two models are fully explained. As it happened for *o*-HTCC nanoparticles, the best fit in pH 4.5 is Weibull model and for pH 6.5 and 7.4 is Korsmeyer-Peppas the best model.

For pH 4.5, Weibull is the best fit and its *b* constant is greater than 1 in the case of chitosan coated SPION's, which indicates a complex release mechanism. As for *o*-HTCC coated SPION's b value is between 0.75 and 1 for the two molecular weights studied, meaning a combined mechanism of Fickian diffusion and case II transport. Comparing this with the results for only Cs NP's or *o*-HTCC NP's, the conclusions were exactly the same for this model, which indicate that in the case of coated SPION's DOX release happened through the same mechanism of its coating. This leads to the possible conclusion that the material used in coating influence and changes the mechanism of release. Observing now the results of Korsmeyer-Peppas model, as it correlation coefficient is not that different from Weibull one, it is also visible a difference between the values of chitosan and *o*-HTCC coated SPION's. For the case of Cs SPION's, the *n* exponent is around 0.9, which is in the range of values that corresponds to super case II transport. As for *o*-HTCC SPION's, the *n* values are slightly lower, around 0.7, meaning an anomalous mechanism, resultant a combination of Fickian diffusion and case II transport. This is in agreement with Weibull conclusions for this pH and also with the results for polymer nanoparticles by themselves.

In the case of pH 6.5, firstly looking at Korsmeyer-Peppas results, *n* exponent values are around the same (nearly 0.6) for both Cs and *o*-HTCC SPION's. This value indicates an anomalous release as a combination of Fickian diffusion and case II transport, related to polymer swelling. As for Weibull results, *b* value is around 0.7 for all the samples with Cs or *o*-HTCC as coating, which means that Fickian diffusion is the release mechanism. This is, once again, contradictory, as it had happened in this pH for the others nanocarriers. For this pH the values of $R^2$ are almost the same for both models, which gives the idea that both of them describe this release, whereas Korsmeyer-Peppas has $R^2$ values slightly higher.

**Table 6.7 - DOX release modelling from *o*-HTCC nanoparticles and from coated SPION's with Korsmeyer-Peppas, Weibull and Peppas Sahlin models.**

| pH | ***o*-HTCC Mw (kDa)** | | Korsmeyer-Peppas | | | Weibull | | | Peppas-Sahlin | | | |
|---|---|---|---|---|---|---|---|---|---|---|---|---|
| | | | *n* | *K* | $R^2$ | *a* | *b* | $R^2$ | *k1* | *k2* | *m* | $R^2$ |
| 4.5 | 48 | | 0.815 ± 0.017 | 13.921 ± 0.980 | 0.994 | 7.017 ± 0.794 | 0.994 ± 0.020 | **0.999** | 26.108 ± 3.376 | -2.458 ± 0.277 | 0.45 | 0.911 |
| | 166 | | 0.841 ± 0.046 | 12.468 ± 2.411 | 0.996 | 7.427 ± 1.451 | 0.909 ± 0.055 | **0.999** | 25.807 ± 4.280 | -2.270 ± 0.511 | 0.45 | 0.916 |
| | 292 | | 0.827 ± 0.078 | 14.770 ± 3.732 | 0.997 | 6.559 ± 1.409 | 0.978 ± 0.011 | **1.000** | 30.087 ± 3.217 | -2.550 ± 0.563 | 0.45 | 0.916 |
| | 470 | | 0.795 ± 0.047 | 17.510 ± 2.196 | 0.996 | 5.160 ± 0.416 | 0.906 ± 0.036 | **0.999** | 29.909 ± 1.167 | -2.862 ± 0.197 | 0.45 | 0.920 |
| 6.5 | 48 | | 0.646 ± 0.079 | 8.160 ± 0.929 | **0.997** | 11.913 ± 1.550 | 0.694 ± 0.087 | 0.996 | 12.807 ± 0.049 | -0.725 ± 0.054 | 0.45 | 0.973 |
| | 166 | | 0.697 ± 0.007 | 7.903 ± 0.589 | **0.989** | 11.402 ± 0.721 | 0.689 ± 0.066 | 0.981 | 12.955 ± 1.495 | -0.373 ± 0.283 | 0.45 | 0.960 |
| | 292 | | 0.716 ± 0.057 | 9.452 ± 1.310 | **0.994** | 10.659 ± 2.190 | 0.850 ± 0.090 | 0.990 | 17.205 ± 4.034 | -0.933 ± 0.553 | 0.45 | 0.952 |
| | 470 | | 0.679 ± 0.007 | 12.894 ± 0.856 | **0.990** | 7.089 ± 0.503 | 0.734 ± 0.008 | 0.985 | 24.403 ± 0.881 | -1.965 ± 0.236 | 0.45 | 0.926 |
| 7.4 | 48 | | 0.889 ± 0.160 | 3.623 ± 0.530 | **0.976** | 33.094 ± 5.924 | 1.138 ± 0.072 | 0.974 | 7.692 ± 0.767 | -0.623 ± 0.105 | 0.45 | 0.929 |
| | 166 | | 1.010 ± 0.136 | 3.324 ± 0.292 | **0.974** | 50.767 ± 11.975 | 1.427 ± 0.119 | 0.909 | 8.249 ± 0.463 | -0.647 ± 0.034 | 0.45 | 0.925 |
| | 292 | | 1.031 ± 0.037 | 4.931 ± 1.238 | **0.973** | 28.399 ± 1.910 | 1.282 ± 0.166 | 0.900 | 10.264 ± 1.436 | -0.927 ± 0.153 | 0.45 | 0.919 |
| | 470 | | 0.900 ± 0.239 | 5.834 ± 1.602 | **0.939** | 35.573 ± 19.751 | 1.474 ± 0.091 | 0.742 | 11.396 ± 0.929 | -1.145 ± 0.113 | 0.45 | 0.891 |
| | **SPION's coating** | | | | | | | | | | | |
| 4.5 | Cs (kDa) | 39 | 0.908 ± 0.114 | 7.759 ± 2.087 | 0.981 | 13.484 ± 4.147 | 1.008 ± 0.056 | **0.991** | 14.499 ± 4.695 | -0.821 ± 0.754 | 0.45 | 0.967 |
| | | 470 | 0.988 ± 0.108 | 6.647 ± 2.430 | 0.967 | 15.760 ± 6.446 | 1.026 ± 0.106 | **0.981** | 13.028 ± 3.515 | -0.833 ± 0.641 | 0.45 | 0.960 |
| | *o*-HTCC (kDa) | 48 | 0.770 ± 0.006 | 9.987 ± 0.994 | 0.968 | 9.317 ± 1.012 | 0.821 ± 0.11 | **0.981** | 15.855 ± 1.729 | -1.044 ± 0.187 | 0.45 | 0.978 |
| | | 470 | 0.750 ± 0.187 | 9.410 ± 2.836 | 0.963 | 12.567 ± 2.443 | 0.979 ± 0.027 | **0.978** | 15.523 ± 2.312 | -1.115 ± 0.261 | 0.45 | 0.959 |
| 6.5 | Cs (kDa) | 39 | 0.662 ± 0.019 | 10.066 ± 0.533 | **0.999** | 9.292 ± 0.550 | 0.701 ± 0.023 | 0.999 | 15.201 ± 1.318 | -1.345 ± 0.098 | 0.45 | 0.958 |
| | | 470 | 0.726 ± 0.068 | 8.719 ± 0.867 | **0.996** | 10.637 ± 1.040 | 0.730 ± 0.016 | 0.994 | 14.580 ± 1.111 | -1.245 ± 0.142 | 0.45 | 0.950 |
| | *o*-HTCC (kDa) | 48 | 0.662 ± 0.040 | 10.424 ± 0.615 | **0.999** | 8.914 ± 0.598 | 0.709 ± 0.047 | 0.997 | 16.847 ± 1.667 | -1.273 ± 0.109 | 0.45 | 0.964 |
| | | 470 | 0.636 ± 0.020 | 9.641 ± 1.430 | 0.996 | 9.841 ± 1.510 | 0.675 ± 0.021 | **0.997** | 15.067 ± 2.438 | -1.247 ± 0.296 | 0.45 | 0.958 |
| 7.4 | Cs (kDa) | 39 | 0.813 ± 0.067 | 2.932 ± 1.316 | **0.983** | 47.821 ± 22.607 | 1.053 ± 0.256 | 0.968 | 6.137 ± 1.738 | -0.521 ± 0.232 | 0.45 | 0.915 |
| | | 470 | 0.794 ± 0.307 | 3.180 ± 1.116 | **0.954** | 33.793 ± 15.018 | 0.774 ± 0.307 | 0.953 | 6.663 ± 1.445 | -0.543 ± 0.146 | 0.45 | 0.915 |
| | *o*-HTCC (kDa) | 48 | 0.716 ± 0.273 | 3.096 ± 1.098 | 0.935 | 37.534 ± 13.880 | 0.953 ± 0.079 | 0.927 | 5.384 ± 1.013 | -0.466 ± 0.126 | 0.45 | **0.950** |
| | | 470 | 0.659 ± 0.197 | 4.032 ± 2.164 | **0.916** | 64.606 ± 53.688 | 1.265 ± 0.478 | 0.851 | 5.935 ± 2.245 | -0.598 ± 0.233 | 0.45 | 0.910 |

Finally, for pH 7.4 is important to notice that correlation coefficient in this samples is lower than for all the others already analysed, especially for Weibull model applied to release from o-HTCC SPION's. Even though, the results for Korsmeyer-Peppas indicate that release happened through a combined mechanism of Fickian diffusion and case II transport, as *n* exponent is between 0.43 and 0.85 for all the samples with both polymers as coating. As for Weibull model, for chitosan coat there are differences in mechanism for each molecular weight studied. For the highest molecular weight *b* value is 0.774, indicating a release through Fickian diffusion and case II transport. As for SPION's coated with chitosan with the lowest molecular weight, *b* value is higher than 1, leading to a complex release mechanism. In the case of Weibull applied to *o*-HTCC SPION's with the lowest molecular weight it indicates a release through the anomalous combined mechanism and for the highest molecular weight it is a complex release mechanism. This is somehow in agreement with results for Cs NP's or *o*-HTCC NP's at this pH.

### 6.5 Cytotoxicity Assays

The cytotoxicity of the studied nanocarriers was evaluated through resazurin tests with each composite used, for different concentrations and for two cell lineages VERO, kidney mammalian cells, and SaOS, a lineage of osteoblasts.

Chitosan nanoparticles cytotoxicity assays were performed for both highest and lowest molecular weights and for concentrations between 0.04 mg/ml and 5 mg/ml. Cell viability results for Cs NP's are represented in Figure 6.25 and Figure 6.26 for VERO and SaOS, respectively. In VERO cells Cs NP's reveal to be slightly cytotoxic for the lowest molecular weight (Cs 39 kDa) and not cytotoxic for the highest molecular weight (Cs 470 kDa) for each concentration, except for 1.25 mg/ml, where cell viability was around 50%, which indicates severe cytotoxicity. This last result is not in accord with the rest, because it is the only one that is cytotoxic. This could be explained by some difficulties in the experimental procedures, as it is a thorough and sensitive type of work, and possibly the cell density was not the same in these wells, as it was in the others. As for SaOs cells, which were much more sensitive while doing the experiment, the results for each molecular weight are different, and in this case it is Cs with the lowest molecular weight that reveals no cytotoxicity for all concentrations tested. For Cs NP's with highest molecular weight cell viability is around 60-70% for intermediate concentrations, which has no scientific explanation. Possibly occurred due to some experimental errors, as this type of cells are really hard to work with and extremely sensitive.

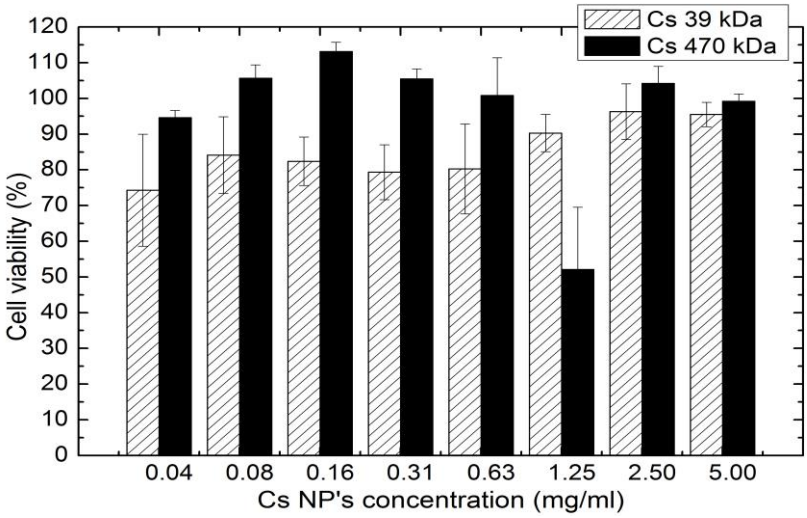


**Figure 6.25 - Cell viability for chitosan nanoparticles in VERO cells (24h trial).**

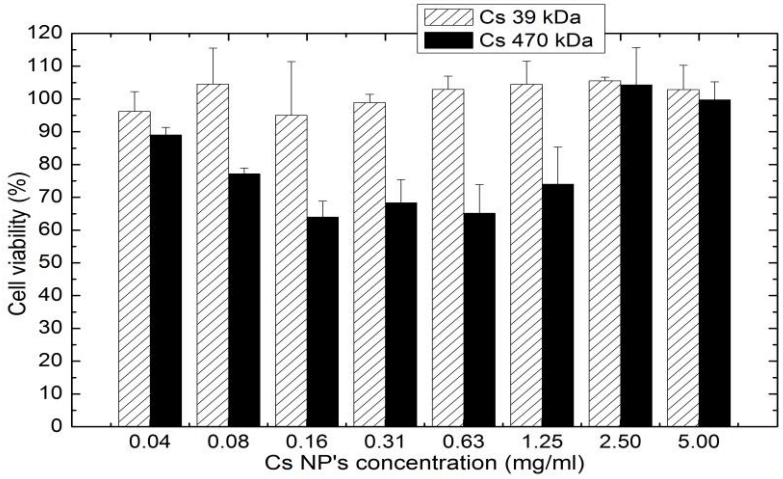


**Figure 6.26 - Cell viability for chitosan nanoparticles in SaOS cells (24h trial).**

In the case of nanoparticles of *o*-HTCC its cell viability is higher than 80% in VERO cells for both molecular weights and for all concentrations tested, as it is represented in Figure 6.27, which indicates that this nanocarrier is not cytotoxic in this type of cells. In SaOS cells, this nanocarrier behaved slightly different, as it can be seen in the results presented in Figure 6.28. It revealed to be not toxic for low concentrations until 1.25 mg/ml. For the case of *o*-HTCC 48 kDa it presented a considered cytotoxicity, with cell viability achieving 50% for a concentration of 5 mg/ml. As for *o*-HTCC with the highest molecular weight, it presents severe cytotoxicity for 2.5 and 5 mg/ml, which indicates that these two concentrations should be avoided when designing this type of nanocarrier for drug delivery.

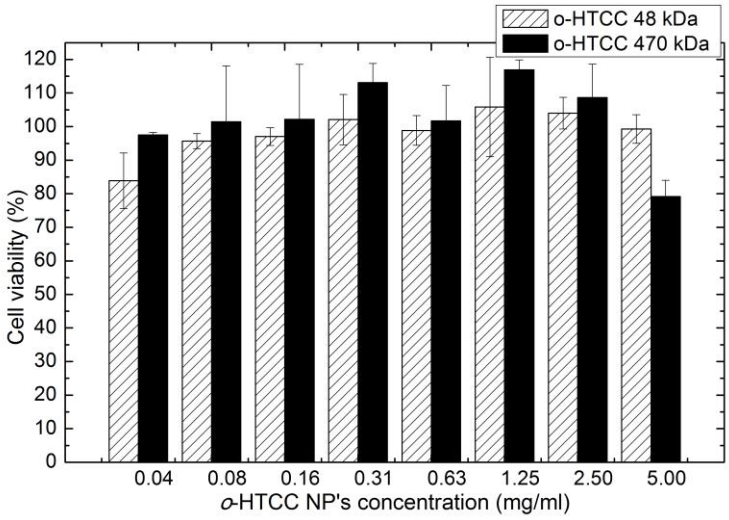


**Figure 6.27 - Cell viability of o-HTCC nanoparticles in VERO cells (24h trial).**

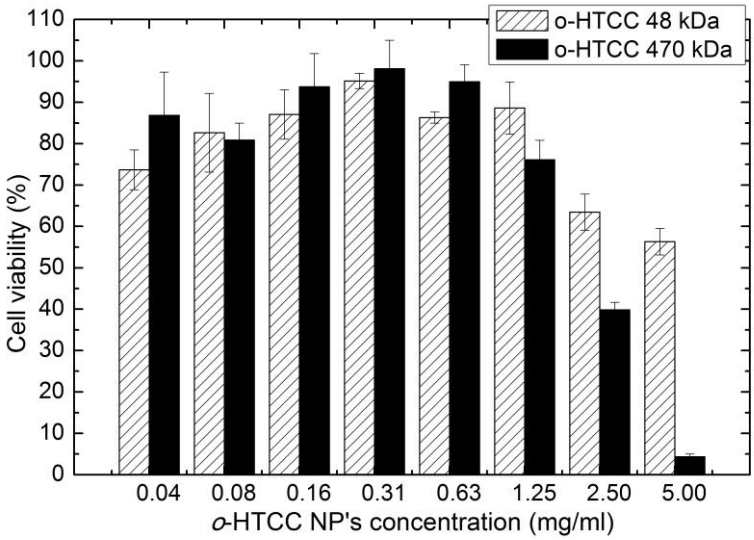


**Figure 6.28 - Cell viability of o-HTCC nanoparticles in SaOS cells (24h trial).**

Finally, cytotoxicity assays were performed for SPION's and coated SPION's with either chitosan or *o*-HTCC, both with the highest molecular weight in study. Observing the graphs presented in Figure 6.29, uncoated SPION's present severe cytotoxicity for concentrations higher than 1 mg/ml for both VERO and SaOS cells. This assay was performed for SPION's concentration between 0.06 and 2 mg/ml. In the case of coated SPION's, two parameters were varied: polymer and SPION's concentration. In order to be comparable to the results of only polymeric nanoparticles, it was tested coated SPION's in the same range of polymer concentration (from 0.04 to 5 mg/ml). As for SPION's concentration, the range is 0.005 – 0.145 mg/ml, in correspondence with polymer concentration, which means, e.g., that in a sample with 5 mg/ml of polymer were 0.145 mg/ml of SPION's. Extrapolating from the results of uncoated SPION's, it was

expected that in this concentrations, SPION's would not be cytotoxic, which was revealed for VERO cells, in Figure 6.30. Coating with both polymers, proved to be not toxic, except for chitosan at the highest concentration of the highest concentration levels.

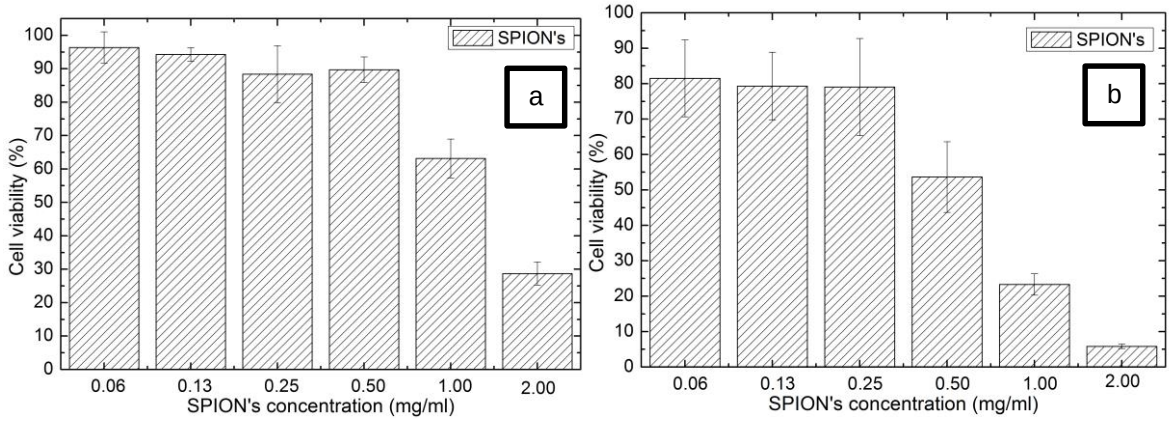


**Figure 6.29 - Cell viability of SPION's in (a) VERO cells and (b) SaOS cells (24h trial).**

As for SaOS cells, in the case of Cs SPION's the results, presented in Figure 6.31, indicate no cytotoxicity for all concentrations tested. As for o-HTCC SPION's the situation is different, as it present slight cytotoxicity or even severe, for most of the concentrations. Probably the combination of these two materials is not that appreciated for this type of cells, even in low concentrations.

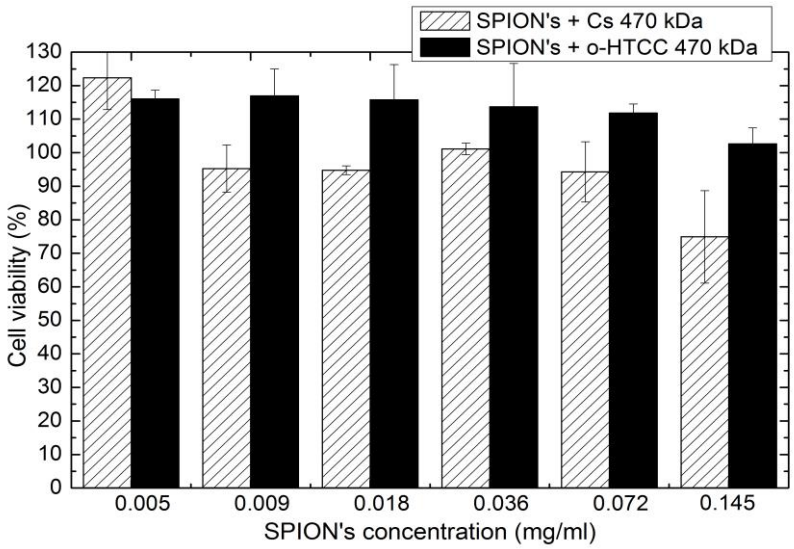


**Figure 6.30 - Cell viability of coated SPION's in VERO cells (24h trial).**

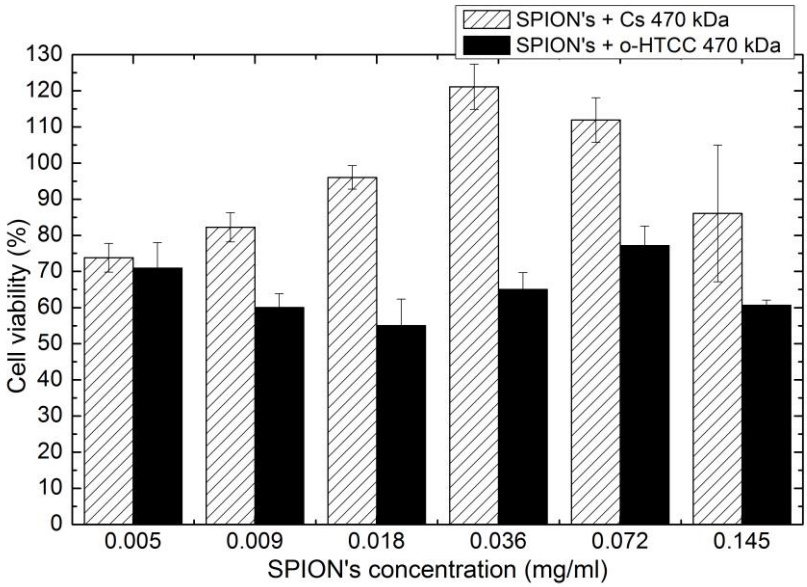


**Figure 6.31 - Cell viability of coated SPION's in SaOS cells (24h trial).**

# 7 Conclusions and future work

To achieve the main purposes of this dissertation, a study of DOX release profiles from Cs NP's, *o*-HTCC NP's and coated SPION's was performed and mathematical models were applied to better understand these release mechanisms. Some other procedures were done in order to characterize these nanocarriers and understand their properties so they can be used for targeted drug delivery systems.

In the case of nanoparticles size, it was concluded that polymer molecular weight has influence on its size and homogeneity. Nanoparticles ideal size should be around 100-200 nm [7], so that it could be accumulated in tumour areas. This size range was only achieved by chitosan and *o*-HTCC with the lowest molecular weight, which were 112 ± 12 nm and 115 ± 18 nm, respectively. For the highest molecular weight (470 kDa) of both polymers, Cs and *o*-HTCC, the obtained sizes were 303 ± 77 nm and 6086 ± 656 nm, respectively, which are higher as expected, staying out of the ideal sizes. This may lead to the conclusion that possibly nanoparticles with higher Mw will not be accumulated in the tumour environment. Some homogeneity issues are visible in this higher Mw, especially for *o*-HTCC NP's, as there is a high dispersion of sizes. Even though ionic crosslinking was the method used to produce these nanoparticles, as it is simple and not expensive it would be interesting to investigate how other methods could be used - such as spray drying or reverse micelle formation - in order to try to obtain more homogeneous nanoparticles solutions.

For all the other performed procedures, such as DOX encapsulation efficiency, DOX release studies or mathematical modelling, it is concluded that, in general, polymer molecular weight is not influent and the results are similar for the all molecular weights studied.

The studies of DOX encapsulation efficiency lead to the conclusion that the best parameters to obtain higher EE were higher ratios of crosslinking agent and polymer and higher DOX initial concentrations. For DOX release studies was chosen a ratio of TPP:polymer of 1:0.533 and an initial concentration of DOX of 1mg/ml, which are relatively good values taking into account these studies of encapsulation efficiency.

As for DOX release studies from chitosan nanoparticles, initially were performed with non-lyophilized samples, but when comparing to the freeze-dried ones, the latter are shown to have a more controlled release, which was one of the purposes of this work. It was verified that chitosan nanoparticles are pH-sensitive, as expected, by releasing higher percentages of DOX in more acidic mediums, indicating its potential use for targeted delivery systems. The same conclusions were obtained for both *o*-HTCC NP's and coated SPION's, where the same pH-sensitivity was observed. The next step in DOX release should be made in-vivo, by doing release experiments in either cells environment or even animals.

One of the main purposes of this work was the application of mathematical models used to describe drug release profiles. It was concluded that for the systems in study Korsmeyer-Peppas and Weibull are the models that best describe these mechanisms, with slight differences between their correlation coefficients. These models lead to concordant mechanism for the majority of the samples, indicating an anomalous or complex release in almost all of them, except for pH 6.5. These results are possibly due to swelling behaviour of chitosan and *o*-HTCC, a property that is not yet well described and explained in the known models. Further work could be done in order to better understand this DOX release from Cs NP's, o-HTCC NP's or coated SPION's in pH 6.5. Specifically, trying to find the transition pH where these polymers change their behaviour should be an important study, allowing a better understanding of this result for pH 6.5 and both chitosan and *o*-HTCC as materials, especially their swelling property.

In general, chitosan and *o*-HTCC nanoparticles appear to be non-toxic for all the concentrations tested and for both fibroblasts and osteoblast cells. In the future, cytotoxicity of these materials for higher concentrations could be tested, in order to find the concentration where it starts to be cytotoxic. As for coated SPION's they were not toxic for fibroblasts cells, but for osteoblasts they presented slight or severe cytotoxicity, especially with *o*-HTCC as coating. It should be interesting to study cellular internalization of DOX loaded in these nanocarriers, to better understand their behaviour in cellular environment and how they enter the cells. Also some investigation about cytotoxicity of the nanocarriers with DOX should be made, as it can give important information about the influence of the nanocarriers in overcoming cellular multidrug resistance, which is truly important for the use of these designed nanocarriers as therapeutic agents.

Superparamagnetic iron oxide nanoparticles produced by thermal decomposition revealed good stability, even though its synthesis produced low quantity of nanoparticles. The same study performed here of DOX release and its mathematical modulation should also be done for SPION's produced by other methods, e.g. chemical precipitation, in further investigations. Using these magnetic nanoparticles in hyperthermia should also be investigated, also with a study of DOX release after the application of hyperthermia, as this method is used to destroy cancer cells taking advantage of temperatures higher than the physiological one (37ºC). This could lead to the application of mathematical models and possibly different release mechanisms would happen, due to some changes in the nanoparticles properties.

In future work, all the nanocarriers studied in this dissertation could also be investigated as delivery systems for other drugs used in chemotherapy or as image contrast, in molecular imaging techniques, such as magnetic resonance.

# 8 Literature References


1. Boyle, P. and B. Levin, *World Cancer Report 2008: World Health Organization*. 2008.
2. Tan, M.L., P.F.M. Choong, and C.R. Dass, *Review: doxorubicin delivery systems based on chitosan for cancer therapy.* Journal of Pharmacy and Pharmacology, 2009. **61**: p. 131-142.
3. Soares, P., et al., *Doxorubicin vs. ladirubicin: methods for improving osteosarcoma treatment.* Mini-reviews in Medicinal Chemistry, 2012. **12**: p. 1239-1249.
4. Janes, K.A., et al., *Chitosan nanoparticles as delivery systems for doxorubicin.* Journal of Controlled Release, 2001. **73**: p. 255-267.
5. Aydin, R. and M. Pulat, *5-Fluorouracil Encapsulated Chitosan Nanoparticles for pH-Stimulated Drug Delivery: Evaluation of Controlled Release Kinetics.* Journal of Nanomaterials, 2012.
6. Kievit, F.M., et al., *Doxorubicin loaded iron oxide nanoparticles overcome multi drug resistance in cancer in vitro.* Journal of Controlled Release, 2011. **152**: p. 76-83.
7. Phillips, M.A., M.L. Gran, and N.A. Peppas, *Targeted nanodelivery of drugs and diagnostics.* Nanotoday, 2010. **5**: p. 143-159.
8. Jabr-Milane, L.S., et al., *Multi-functional nanocarriers to overcome tumor drug resistance.* Cancer Treatment Reviews, 2008. **34**: p. 592-602.
9. Gautier, J., et al., *Recent advances in theranostic nanocarriers of doxorubicin based on iron oxide and gold nanoparticles.* Journal of Controlled Release, 2013. **169**: p. 48-61.
10. Moghimi, S.M., A.C. Hunter, and J.C. Murray, *Nanomedicine: current status and future prospects.* The FASEB Journal, 2005. **19**: p. 311-330.
11. Essex, S. and V. Torchilin, *Liposomal formulations for focal and targeted drug delivery in cancer and other diseases*, in *Focal Controlled Drug Delivery, Advances in Delivery Science and Technology*, C.R. Society, Editor. 2014. p. 93-116.
12. Long, J., et al., *Anticancer drug-loaded multifunctional nanoparticles to enhance the chemotherapeutic efficacy in lung cancer metastasis.* Journal of Nanobiotechnology, 2014. **12**(37): p. 1-11.
13. Chouhan, R. and A. Bajpai, *Real time in vitro studies of doxorubicin release from PHEMA nanoparticles.* Journal of Nanobiotechnology, 2009. **7:5**.
14. Zou, P., et al., *Superparamagnetic iron oxide nanotheranostics for targeted cancer cell imaging and pH-dependent intracellular drug release.* Molecular Pharmaceutics, 2010. **7**(6): p. 1974-1984.
15. Yuan, Q., et al., *A stimulus-responsive magnetic nano particle drug carrier: Magnetite encapsulated by chitosan-grafted-copolymer.* Acta Biomaterialia, 2008. **4**: p. 1024-1037.
16. Ahmad, Z., et al., *Review: Polymeric micelles as drug delivery vehicles.* Royal Society of Chemistry Advances, 2014. **4**: p. 17028-17038.
17. Jain, S., et al., *Aquasomes: a novel drug carrier.* Journal of Applied Pharmaceutical Science, 2012. **2**(1): p. 184-192.
18. Umashankar, M., R. Sachdeva, and M. Gulati, *Aquasomes: a promising carrier for peptides and protein delivery.* Nanomedicine: Nanotechnology, Biology and Medicine, 2010. **6**: p. 419-426.
19. Swatantra, K., R. Awani, and S. Satyawan, *Chitosan: a platform for targeted drug delivery.* International Journal of PharmTech Research, 2010. **2**(4): p. 2271-2282.

20. Wu, Y., et al., *Chitosan nanoparticles as a novel delivery system for ammonium glycyrrhizinate.* International Journal of Pharmaceutics, 2005. **295**: p. 235-245.

21. Agrawal, P., G. Strijkers, and K. Nicolay, *Chitosan-based systems for molecular imaging.* Advanced Drug Delivery Reviews, 2010. **62**: p. 42-58.

22. Rinaudo, M., *Chitin and chitosan: properties and applications.* Progress in polymer science, 2006. **31**: p. 603-632.

23. Miao, Y. and S.N. Tan, *Amperometric hydrogen peroxide biosensor based on immobilization of peroxidase in chitosan matrix cross linked with glutaraldehyde.* The Analyst, 2000. **125**: p. 1591-1594.

24. Javid, A., et al., *Chitosan-coated Superparamagnetic Iron Oxide Nanoparticles for Doxorubicin Delivery: Synthesis and Anticancer Effect against Human Ovarian Cancer Cells.* Chemical Biology & Drug Design, 2013. **82**: p. 296-306.

25. Unsoy, G., et al., *Synthesis optimization and characterization of chitosan-coated iron oxide nanoparticles produced for biomedical applications.* Journal of Nanoparticle Research, 2012. **14**.

26. Gan, Q. and T. Wang, *Chitosan nanoparticle as protein delivery carrier - Systematic examination of fabrication conditions for efficient loading and release.* Colloids and Surfaces B: Biointerfaces, 2007. **59**: p. 24-34.

27. Agnihotri, S., N. Mallikarjuna, and T. Aminabhavi, *Recent advances on chitosan-based micro- and nanoparticles in drug delivery.* Journal of Controlled Release, 2004. **100**: p. 5-28.

28. Rampino, A., et al., *Chitosan nanoparticles: Preparation, size evolution and stability.* International Journal of Pharmaceutics, 2013. **455**: p. 219-228.

29. Berger, J., et al., *Structure and interactions in covalently and ionically cross linked chitosan hydrogels for biomedical applications.* European Journal of Pharmaceutics and Biopharmaceutics, 2004. **57**: p. 19-34.

30. Li, G., et al., *Preparation and properties of magnetic Fe3O4-chitosan nano particles.* Journal of Alloys and Compounds, 2008. **466**: p. 451-456.

31. Unsoy, G., et al., *Synthesis of Doxorubicin loaded magnetic chitosan nano particles for pH responsive targeted drug delivery.* European Journal of Pharmaceutical Sciences, 2014. **62**: p. 243-250.

32. Yuan, Q., et al., *Controlled and extended drug release behavior of chitosan-based nano particles carrier.* Acta Biomaterialia, 2010. **6**: p. 1140-1148.

33. Siepmann, J. and F. Siepmann, *Mathematical modeling of drug delivery.* International Journal of Pharmaceutics, 2008. **364**: p. 328-343.

34. Mitra, S., et al., *Tumour targeted delivery of encapsulated dextra-doxorubicin conjugate using chitosan nanoparticles as carrier.* Journal of Controlled Release, 2001. **74**: p. 317-323.

35. Sun, Y. and A. Wan, *Preparation of nanoparticles composed of chitosan and its derivatives as delivery systems for macromolecules.* Journal of Applied Polymer Science, 2007. **105**: p. 552-561.

36. Wan, A., et al., *Transmission Electron Microscopy and Electron Diffraction Study of BSA-Loaded Quaternized Chitosan Nanoparticles.* Journal of Biomedical Materials Research Part B: Applied Biomaterials, 2008. **86 B**: p. 197-207.

37. Wang, Y., C. Jou, and M. Yang, *Effect of quaternized chitosan on the fusion efficiency and cytocompatibility of liposomes.* Journal of Polymer Research, 2012. **19(1)**.

38. Fang, C., et al., *Fabrication of magnetic nanoparticles with controllable drug loading and release through a simple assembly approach.* Journal of Controlled Release, 2012. **162**: p. 233-241.

39. Alves, A., *Desenvolvimento de nanopartículas magnéticas para tratamento de cancro: estudo da síntese e estabilização das soluções colidais de $Fe_3O_4$*, in *Engenharia Biomédica*. 2012, FCT-UNL.

40. Gupta, A.K. and M. Gupta, *Synthesis and surface engineering of iron oxide nano particles for biomedical applications.* Biomaterials, 2005. **26**: p. 3995-4021.

41. Wan, J., et al., *Monodisperse water-soluble magnetite nanoparticles prepared by polyol process for high-performance magnetic resonance imaging.* Chemical communications, 2007: p. 5004-5006.

42. Maity, D., et al., *Studies of magnetite nano particles synthesized by thermal decomposition of iron (III) acetylacetonate in tri(ethylene glycol).* Journal of Magnetism and Magnetic Materials, 2009. **321**: p. 3093-3098.

43. Jarzyna, P., et al., *Iron oxide core oil-in-water emulsions as a multifunctional nanoparticle platform for tumour targeting and imaging.* Biomaterials, 2009. **30**(36): p. 6947-6954.

44. Ge, S., et al., *A facile hydrothermal synthesis of iron oxide nanoparticles with tunable magnetic properties.* Journal of Physical Chemistry C: Nanomaterials and interface, 2009. **113**(31): p. 13593-13599.

45. Soares, P., et al., *Effects of surfactants on the magnetic properties of iron oxide colloids.* Journal of Colloid and Interface Science, 2014. **419**: p. 46-51.

46. Higuchi, T., *Rate of release of medicaments from ointment bases containing drugs in suspension.* Journal of Pharmaceutical Sciences, 1961. **50**(10): p. 874-875.

47. Fu, Y. and W.J. Kao, *Drug Release Kinetics and Transport Mechanisms of Non-degradable and Degradable Polymeric Delivery Systems.* Expert Opin Drug Deliv., 2010. **7(4)**: p. 429-444.

48. Brazel, C. and N. Peppas, *Modeling of drug release from swellable polymers.* European Journal of Pharmaceutics and Biopharmaceutics, 2000. **49**: p. 47-58.

49. Costa, P. and J. Lobo, *Review: Modeling and comparison of dissolution profiles.* European Journal of Pharmaceutical Sciences, 2001. **13**: p. 123-133.

50. Dash, S., et al., *Review: Kinetic modeling on drug release from controlled drug delivery systems.* Acta Poloniae Pharmaceutica - Drug Release, 2010. **67**: p. 217-223.

51. Shaikh, H., R. Kshirsagar, and S. Patil, *Mathematical models for drug release characterization: a review.* World Journal of Pharmacy and Pharmaceutical Sciences, 2015. **4**(04): p. 324-338.

52. Lopes, C.M., J.M. Lobo, and P. Costa, *Formas farmacêuticas de liberação modificada: polímeros hidrifílicos.* 2005. **41**: p. 143-154.

53. Singhvi, G. and M. Singh, *Review: In-vitro drug release characterization models.* International Journal of Pharmaceutical Studies and Research, 2011: p. 77-84.

54. Mady, O., *Mechanisms and percent of drug release of each new mathematic approach.* International Reseach Journal of Pharmacy, 2013. **3**(6): p. 56-69.

55. Arifin, D.Y., L.Y. Lee, and C. Wang, *Mathematical modeling and simulation of drug release from microspheres: Implications to drug delivery systems.* Advanced Drug Delivery Reviews, 2006. **58**: p. 1274-1325.

56. Ritger, P. and N. Peppas, *A simple equation for description on solute release II. Fickian and anomalous release from swellable devices.* Journal of Controlled Release, 1987. **5**: p. 37-42.

57. Park, H., K. Park, and W. Shalaby, *Biodegradable Hydrogels for Drug Delivery*. 1993: Technomic Publishing Company.

58. Gierszewska-Druzynska, M. and J. Ostrowska-Czubenko, *Mechanism of water diffusion into non-crosslinked and ionically crosslinked chitosan membranes.* Progress on Chemistry and Application of Chitin and its Derivatives, 2012. **17**: p. 59-66.

59. Papadopoulou, V., et al., *On the use of the Weibull function for the discernment of drug release mechanisms.* International Journal of Pharmaceutics, 2006. **309**: p. 44-50.

60. Adams, E., et al., *Non-linear mixed effects models for the evaluation of dissolution profiles.* International Journal of Pharmaceutics, 2002. **240**: p. 37-53.

61. Gurny, R., E. Doelker, and N. Peppas, *Modelling of sustained release of water-soluble drugs from porous, hydrophobic polymers.* Biomaterials, 1982. **3**: p. 27-32.

62. Fu, Y. and W. Kao, *Drug Release Kinetics and Transport Mechanisms of Non-degradable and Degradable Polymeric Delivery Systems.* Expert Opinion on Drug Delivery, 2010. **7(4)**: p. 429-444.

63. Polli, J., et al., *Methods to compare dissolution profiles and a rationale for wide dissolution specifications for metoprolol tartrate tablets.* Journal of Pharmaceutical Sciences, 1997. **86**(6): p. 690-700.

64. Hixson, A. and J. Crowell, *Dependence of reaction velocity upon surface and agitation.* Industrial and engineering chemistry, 1931. **23**(8): p. 923-931.

65. Enscore, D., H. Hopfenberg, and V. Stannett, *Effect of particle size on the mechanism controlling n-hexane sorption in glassy polystyrene microspheres.* Polymer, 1977. **18**: p. 793-800.

66. Korsmeyer, R., et al., *Mechanisms of solute release from porous hydrophilic polymers.* International Journal of Pharmaceutics, 1983. **15**: p. 25-35.

67. Sathe, P., Y. Tsong, and V. Shah, *In-Vitro dissolution profile comparison: statistics and analysis, model dependent approach.* Pharmaceutical Research, 1996. **13**(12): p. 1799-1803.

68. Peppas, N. and J. Sahlin, *A simple equation for the description of solute release. III. Coupling of diffusion and relaxation.* International Journal of Pharmaceutics, 1989. **57**: p. 169-172.

69. Huang, M., E. Khor, and L. Lim, *Uptake and cytotoxicity of chitosan molecules and nanoparticles: Effects of molecular weight and degree of deacetylation.* Pharmaceutical Research, 2004. **21**: p. 344-353.

70. Loh, J., et al., *Spinning disc processing technology: Potential for large-scale manufacture of chitosan nanoparticles.* Journal of Pharmaceutical Sciences, 2012. **99 n 10**: p. 4326-4336.

71. Kasaai, M.R., *Calculation of Mark–Houwink–Sakurada (MHS) equation viscometric constants for chitosan in any solvent–temperature system using experimental reported viscometric constants data.* Carbohydr Polym, 2007. **68**(3): p. 477-488.

72. Lochte, F., *Controlled synthesis of magnetic nanoparticles: Magnetic and thermal characterisation for cancer theranostics*. 2014, TU Berlin and FCT-UNL.

73. Tatelli, M., et al., *Superparamagnetic iron oxide nanoparticles encapsulated in biodegradable thermosensitive polymeric micelles: toward a targeted nanomedicine suitable for image-guided drug delivery.* Langmuir, 2009. **25**: p. 2060-2067.

74. Calvo, P., et al., *Chitosan and chitosan/ethylene oxide-propylene oxide block copolymer nanoparticles as novel carriers for proteins and vaccines.* Journal of Pharmaceutical Research, 1997. **14**(10): p. 1431-1436.

75. Zhang, Y., et al., *DDSolver: An add-in program for modelling and comparison of drug dissolution profiles.* The American Association of Pharmaceutical Scientists, 2010. **12**(3): p. 263-271.

76. Borra, R., et al., *A simple method to measure cell viability in proliferation and cytotoxicity assays.* Brazilian Oral Research, 2009. **23**(3): p. 255-262.

77. Gierzewska-Druzynska, M. and J. Ostrowska-Czubenkio, *Influence of cross linking process conditions on molecular and super molecular structure of chitosan hydrogel membrane.* Progresse on chemistry and application of chitin and its derivatives, 2011. **16**: p. 15-22.

# Appendix

## A – Additional graphs of DOX release

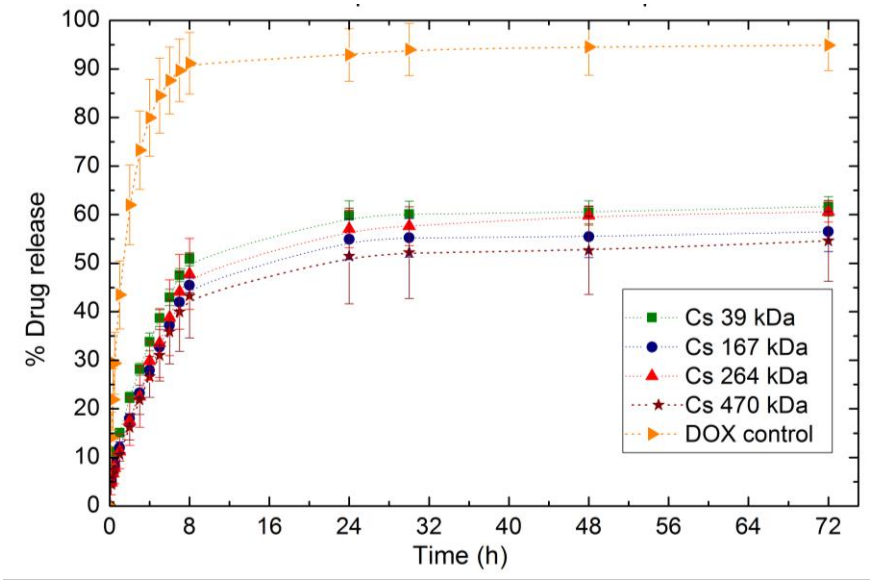


**Figure 0.1 - DOX release profile from Cs NP's at pH 6.5 for different molecular weights.**

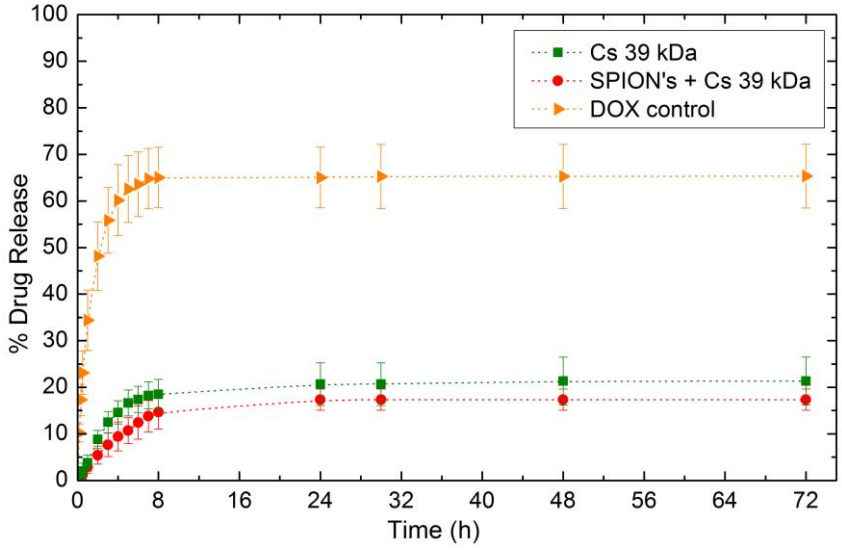


**Figure 0.2 - Comparison of DOX release from Cs NP's and Cs SPION's with 39 kDa at pH 7.4.**

## B – DDSolver menus

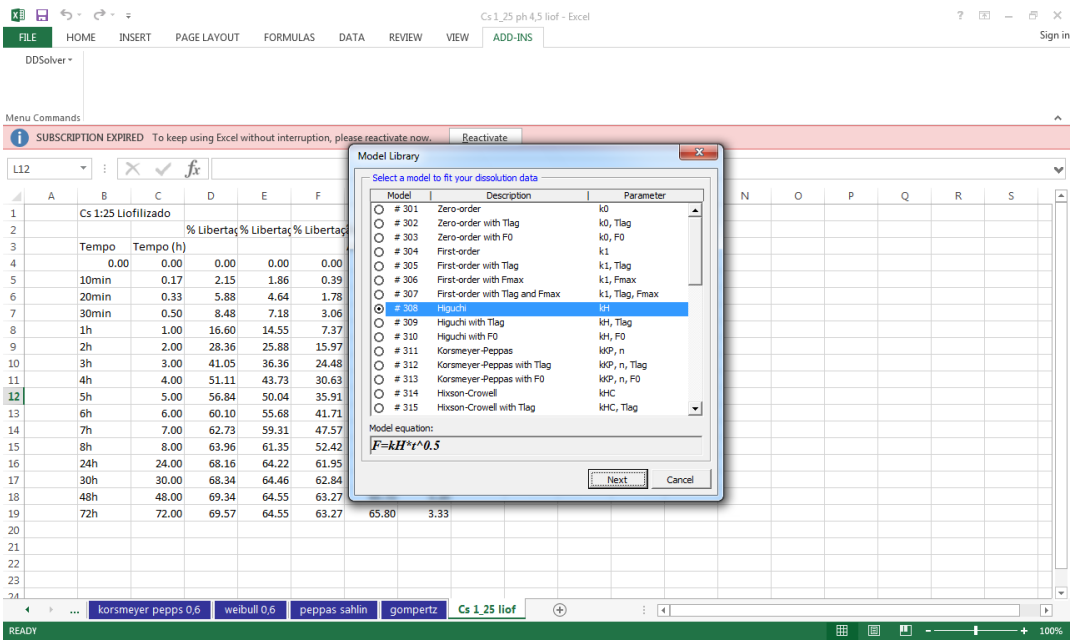


**Figure 0.3 - DDSolver menu where is chosen the model to apply to data.**

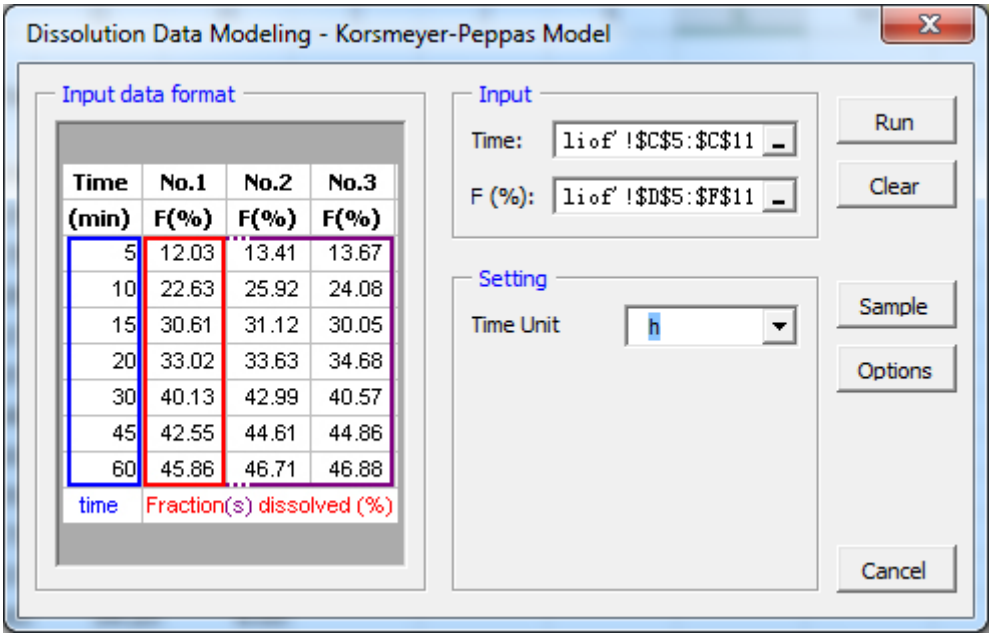


**Figure 0.4 - DDSolver menu where data is selected.**

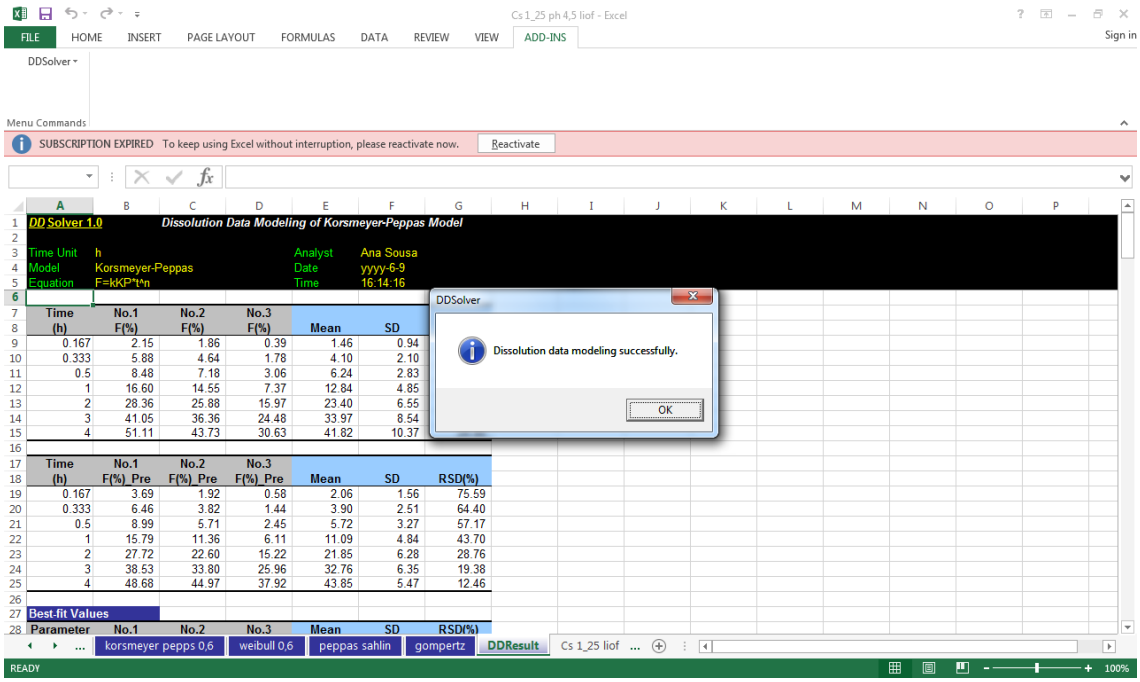


**Figure 0.5 - Example of DDSolver final result.**